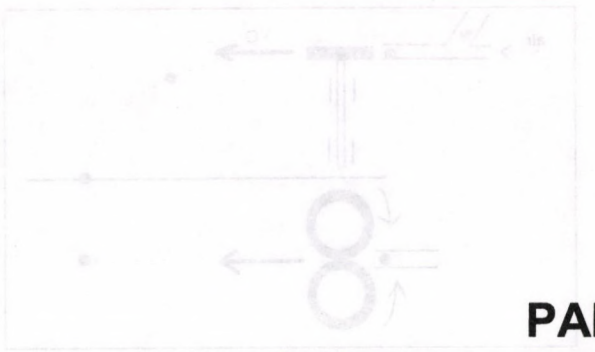

PART II.

SELECTED SCIENTIFIC PAPERS

TAJECTORY OF PARTICLES SUBJECTED TO GRAVITATIONAL FORCE AND AIR RESISTANCE

Dr. P. Soós - Dr. Zs. Szüle - Dr. I. Fülöp
University of Agricultural Sciences, Gödöllő

The incentive of carrying out the experiments was given by the need of the education where several times occurred the motion of fertiliser particle, wheat grain, spray droplet. One was not capable to calculate the cast distance, the instant velocity and the time of falling. The reason was that the literature gives the air resistance and drag coefficients in a wide range. Some textbooks gives 0.4-0.5 range of the air resistance (shape) coefficients for spherical body while some others give 0.7. It causes large uncertainty in calculations. The question has arisen which value should be used for example with peas without coating and what is the air resistance coefficient of non-spherical seeds like maize, sunflower, etc.

The relationships calculated with evacuated space for velocities and cast distances can be informative, however, they are far from the reality. The difference is especially large in the case of air velocities above 20-25 m/s.

In some textbooks the cast distance of the particle shot horizontally only the horizontal directional air resistance is considered. The vertical motion of particle is considered as if it would fall in evacuated space. This solution was certainly chosen by the authors, because the differential equation of motion was much simpler and the problem could be solved in an exact way.

It is true that the ballistics is taught in detail with mathematical background and they have also measuring results concerning the effective range of bullets in the Department of Armament of the home military college. Nonetheless the air resistance of bullet, fertiliser particle and sowing seed are certainly different, so that this way cannot be followed by us.

The relationships of the horizontal cast are developed in detail in the chapter titled „Mass point motion subjected to gravitational force and air resistance (external problem of ballistics)" of the textbook *Kármán Tódor - Maurice A. Biot: Methods of mathematics* (1967, in Hungarian). Our study started from there.

The goal of the experiment

Taking into account all of this the determination of air resistance coefficient of a few solid particle and seed. Having the air resistance coefficient the cast distance and some other characteristics of the motion can be calculated. To carry out the calculations, however, one have to solve the integrals in the relationships describing the ballistic curves of the motion.

As an initial step those questions were planned to be answered. The concrete aim of the experiment was the determination of cast distance of fertiliser particles and different grains, such as wheat, corn, sugarbeet, pea, etc., and steel ball. The values measured with steel ball serves as base data because its physical characteristics can be relatively well determined.

Expansion and methodology of the examinations

In order to sense the effect of the resistance on the motion of a grain a rather high initial velocity should be used. Taking this into account a particle shooting equipment was constructed and manufactured in the laboratory of the Institute. Its shooting velocity can be adjusted from 0 to 30 m/s.

The work consisted of four main parts, such as:

1. elaboration of the theoretical relationships
2. making computer codes
3. carrying out the measurements
4. evaluation of data

The particle shooting device

The equipment was planned by Kostyál Endre fifth year student as a diploma assignment (tutor: dr. Petróczki Károly). He also take part in the manufacturing. The operational scheme is shown in *figure 1.*

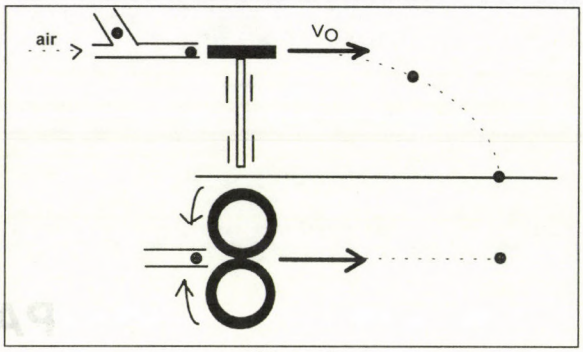

Figure 1
The operational scheme of the particle shooting device

The essence of the device is two rubber covered discs driven by an adjustable revolution electric motor. The discs contact at their edge in order to be able to grasp the particles fed between them. The particles accelerated to the circumferential velocity are cast away. The revolution speed and the direction of cast - i.e. the angle of the initial velocity to the horizontal can be adjusted.

The diameter of the discs are 240 mm, while the distance of shafts is 235 mm, as the rubber is deformed, which helps the firm grip of the grain blown between them through the feeding tube by air. The value of the initial velocity is between 0 and 30 m/s.

Theoretical relationships

In the calculations existing known relationships were used partly and they were developed and a new calculation method was used.

The differential equation of motion of the horizontally cast particle can be produced on the basis of the forces acting on the particle (*figure 2*).

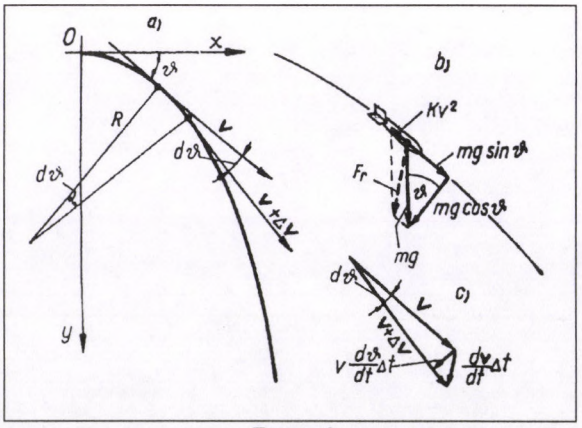

Figure 2
Trajectory (a) of the mass moving in the air, the schemes of forces (b) and accelerations (c).

The equilibrium of the forces in the line of motion direction is expressed by

$$m\frac{\mathrm{d}v}{\mathrm{d}\vartheta}\frac{g}{v}\cos\vartheta = mg\sin\vartheta - kv^2$$

and arranged

$$\frac{\mathrm{d}v}{\mathrm{d}\vartheta}\cos\vartheta - v\sin\vartheta = -\frac{k}{mg}v^3$$

As one can see in the figure, ϑ is the angle made by the instant tangent of the trajectory and the x axis. The velocity of the particle is tangential to the trajectory.

Without the details the solution to this equation is

$$v_x = v_{0x} f(\vartheta),$$

$$v_y = v_x \operatorname{tg}\vartheta = v_{0x} f(\vartheta)\operatorname{tg}\vartheta \qquad (1)$$

The expression of calculating the time is

$$t = \frac{v_{0x}}{g}\int\frac{f(\vartheta)\mathrm{d}\alpha}{\cos^2\vartheta} \qquad (2)$$

The x and y co-ordinates are calculated by the formulae

$$x = \int_0^t v_x\,\mathrm{d}t = \frac{v_0^2}{g}\int\frac{[f(\vartheta)]^2\,\mathrm{d}\vartheta}{\cos^2\vartheta}$$

$$x = \int_0^t v_y\,\mathrm{d}t = \frac{v_0^2}{g}\int\frac{[f(\vartheta)]^2\sin\vartheta\,\mathrm{d}\vartheta}{\cos^3\vartheta} \qquad (3)$$

In the case of horizontal cast, one must substitute the function

$$f(\vartheta) = \frac{1}{\sqrt{1+\frac{kv_0^2}{mg}\left(\ln\frac{1+\sin\vartheta}{\cos\vartheta}+\frac{\sin\vartheta}{\cos^2\vartheta}\right)}} \qquad (4)$$

which was determined by the authors in the mentioned paper from the boundary conditions.

$f(\vartheta)$ was not expressed for inclined throw, therefore it was carried out by ourselves. The result is

$$f(\vartheta) = \frac{1}{\sqrt{1+\frac{v_{0x}^2 k}{mg}\left[\frac{\sin\alpha}{\cos^2\alpha}-\frac{\sin\alpha_0}{\cos^2\alpha_0}+\ln\left(\frac{1+\sin\alpha}{\cos\alpha}\right)+\ln\left(\frac{1+\sin\alpha_0}{\cos\alpha_0}\right)\right]}} \qquad (5)$$

One can see that substituting the (4) and (5) formulae of $f(\vartheta)$ in (2) and (3) leads to very complicated equations for ϑ, which can be integrated exactly in a lengthy and cumbersome way, thus we made no attempt. By the help of computer techniques, numerical method the integration was made by a computer program developed by us.

For computing the following constant data are needed:

ρ_l - density of air (1.2 kg/m^3 value was used)
v_0 - initial velocity of shoot
α_0 - angle made by the initial velocity and the x axis
d - *diameter of the particle*
$a \times b \times c$ - width depth height of particle
κ - drag coefficient (air resistance shape coefficient, values given by textbooks are 0.4-0.5 and 0.7)

If all these parameters are known the time of motion (t), the velocities (v_x, v_y), the displacement co-ordinates (x, y) belonging to any ϑ tangent angle can be computed by equations (1), (2) and (3). Therefore the variable is ϑ.

If the velocity components are known one can draw the velocity hodograph of horizontal throw (*figure 3*).

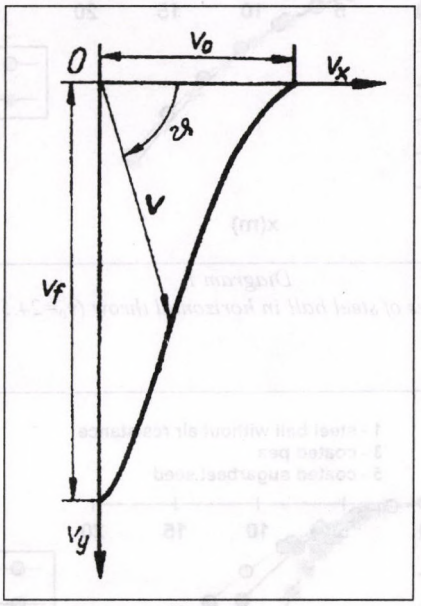

Figure 3
Hodograph of horizontal throw

From the cast distance measured in the laboratory the air resistance coefficients of the particles was calculated by a reverse computation.

7. Evaluation

1. Utilising the expressions found in the textbook *Kármán Tódor - Maurice A. Biot: Methods of mathematics* (1967, in Hungarian) theoretical expressions for inclined throw in air were elaborated.
2. A method of numerical solution of complicated integrals corresponding to the differential equation of ballistic carves was elaborated. To calculate the points of curves a QuickBasic programme was coded. This programme solves numerically the integrals in the formulae. It was needed because the mentioned scientists only produced the expressions without solution.
3. Throwing experiments were conducted in the laboratory. For this purpose a particle shooting device was manufactured. The experimental object particles were steel ball, coated pea, pea without coating, maize, sunflower and wheat seeds and fertiliser particle. The shooting velocity value was 24.5 m/s in each case. Based on the measured data the air resistance coefficients of particles was determined. The coincidence of the computed and measured values can be examined by measuring the throw distance. The measurement gives also the possibility to calculate the air resistance coefficient of any thrown particle and to obtain unknown or replace inaccurate values which are given in a wide range.
4. The material applied to computer can be built into the education in the corresponding version. The measuring data makes possible to make programmes concerning calculations of ballistics and graphic and diagram drawing modules can be connected. They all can be utilised in the education to facilitate the thorough studying of the topic and what is the most important, they highlights the practical use of theoretical relationships.

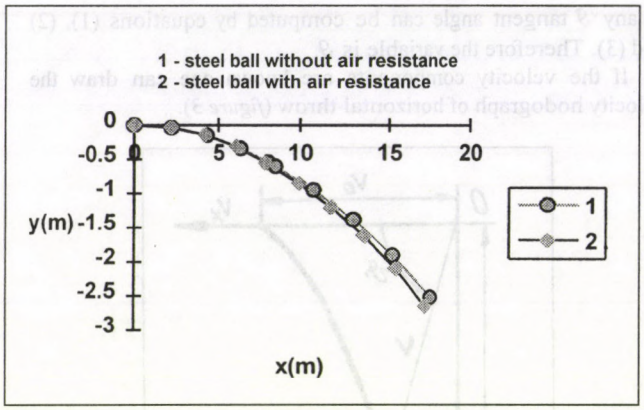

Diagram 1
Trajectories of steel ball in horizontal throw (v_0=24.5 m/s)

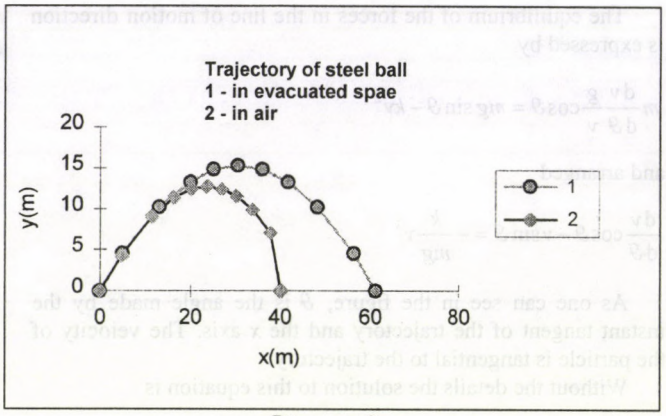

Diagram 2
Trajectories of steel ball in inclined throw (v_0=24.5 m/s, α_0=45°)

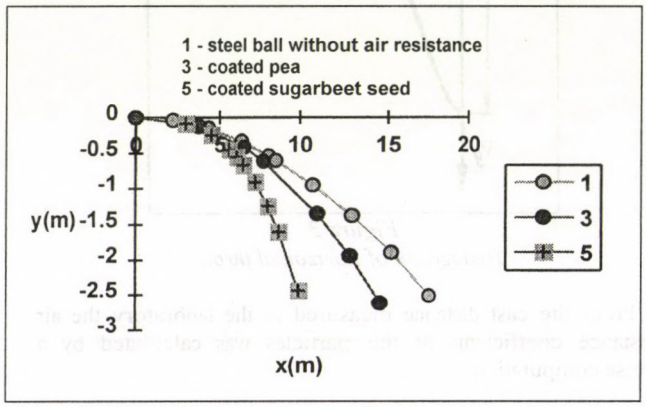

Diagram 3
Trajectories of steel ball and sowing seeds in horizontal throw (v_0=24.5 m/s)

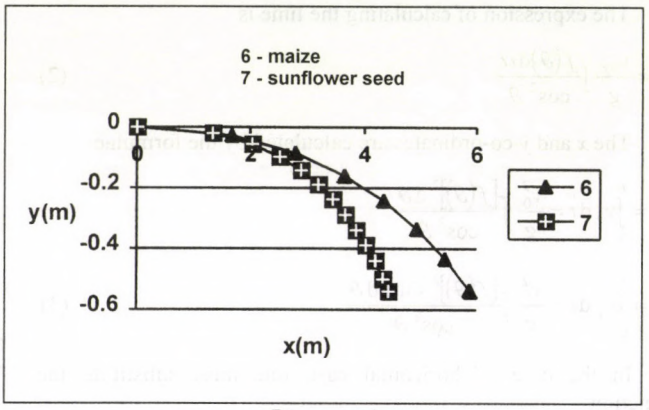

Diagram 4
Trajectories of maize and sunflower seed in horizontal throw (v_0=24.5 m/s)

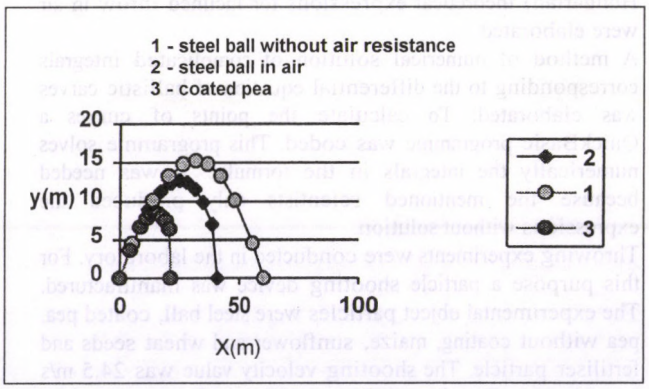

Diagram 5
Trajectories in inclined throw (α_0=45°, v_0=24.5 m/s)

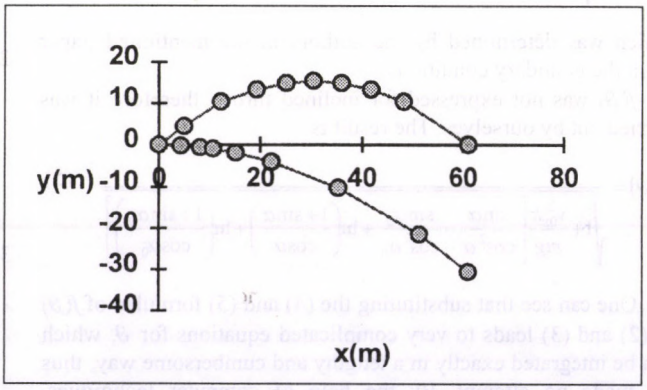

Diagram 6
Inclined and horizontal cast of steel ball in evacuated space (v_0=24.5 m/s, α_1=45°,α_2=0°)

DESCRIBING AUGER OPERATION BY MEANS OF DIMENSION ANALYSIS

Dr. J. Benkő
University of Agricultural Sciences, Gödöllő

The dimension analysis is not a new approach to the research on the design and operation of auger. Publications concerning the application appeared already in the sixties abroad. According to the experiences the moment requirement and the transport rate can be calculated from empirical equations containing dimensionless numbers set up using dimension analysis [3]. Unfortunately the method did not spread in the home research and design in spite of its several advantages. This effective method makes possible to take into account such characteristics an variables in the description of transport augers which can not be examined in mere theoretical approaches [2].

The analysis of dimensions is based on the conclusion of the similarity theory that the solution to the mathematical model of a phenomenon can be given as function relationships of dimensionless numbers called also dependent and independent invariant numbers. All the phenomena which are described by the same dimensionless equation make a **class** of the similar phenomena. Among them the **group** of similar phenomena are formed by those phenomena for which values of the independent invariant numbers in the unicity conditions i.e. of similarity criteria are identical [4].

An advantage of using dimension analysis is that the operational parameters (expected output rate, power need, etc.) of transport augers belonging to the same group can be estimated even in the design period having the measuring data for the group.

Another advantage rises up at the investigation of the apparatuses. The measuring results in the form of charts, diagrams or functions for more than 2 or 3 variables become not clear-cut. With the help of dimension analysis one can have a picture of the phenomena in the form of relationship of much less dimensionless numbers than the actual number of variables.

Dimensionless numbers of the transport auger

The first step of the dimension analysis is the determination of the dimensionless numbers (i.e. dependent and independent similarity invariant numbers) of the phenomenon examined which is a routine process if the variables are known. The complete success of the analysis depends on the correct selection of the variables describing the phenomenon. Unfortunately there is no rule of judging which variables are important or negligible, one can recline only on the anticipation and experience. That is why the selection of the variables needs thorough analysis and attention.

In case of transport augers the output rate and the moment requirement are considered as dependent variables. The reachable transport capacity - as it is know - is a function of the geometry dimensions and the rotational velocity, so that one should decide in the initial stage of the designing how much output rate should be produced. At the same time the output rate will determine the application possibility, too. For example, if a transport auger are to be fitted in a transport aggregate, that is selected on the basis of transport capacity expressed by the value of the transported volume or mass rate. Similarly, the driving moment requirement is also an important characteristic. During the designing the drive and the motor are selected on the basis of driving moment need and the revolution speed. The operator is interested in values for the assurance of the electric power needed by the driving.

The parameters influencing the operation of the auger can be put into three groups, such as geometric (design) variables, operational variables and material characteristics. The variables necessary to produce the dimension analysis or dimension matrix are summarised in *table 1*.

Table 1

Variable	Notation	Unit	Dimension
Geometry variables			
angle of transport	δ	°	-
diameter of auger wing	D	m	L
length of inlet port	Z	m	L
length of auger wing	L	m	L
diameter of auger shaft	d	m	L
inside diameter of auger house	D_{cs}	m	L
auger pitch	s	m	L
Operational variables			
revolution	n	1/s	T^{-1}
gravitational acceleration	g	m/s^2	LT^{-2}
moment need	M	Nm	ML^2T^{-2}
volumetric output rate	Q	m^3/s	L^3T^{-1}
Material characteristics			
moisture content	W	%	-
bulk density	ρ	kg/m^3	ML^{-3}

The dimensions of the variables can be written as the multiplication of the powers of the dimensions of the basic units (in a given system of units). The SI system dimensions of the characteristic variables are given in the last column of *table 1*. The basic units of SI are the length (L), mass (M) and the time (T). The dimension matrix constructed from them is shown in *table 2*, where the variables are arranged such way which helps the determination of dimensionless numbers because the first three rows makes a rectangular partition of non-singular matrix. In addition for simplicity, the logarithm of the dimensions of variables and the logarithm of the dimensions of the basic units are denoted by y_i (i=1,2,...,13), and z_j (j=1,2,3), respectively.

Table 2

		ln(L)	ln(M)	ln(T)
		z_1	z_2	z_3
$\ln(D)$	y_1	1	0	0
$\ln(\rho)$	y_2	-3	1	0
$\ln(g)$	y_3	1	0	-2
$\ln(\delta)$	y_4	0	0	0
$\ln(Z)$	y_5	1	0	0
$\ln(L)$	y_6	1	0	0
$\ln(d)$	y_7	1	0	0
$\ln(D_{cs})$	y_8	1	0	0
$\ln(s)$	y_9	1	0	0
$\ln(n)$	y_{10}	0	0	-1
$\ln(Q)$	y_{11}	3	0	-1
$\ln(W)$	y_{12}	0	0	0
$\ln(M)$	y_{13}	2	1	-2

There are several type method of determining dimensionless number. One of the most effective among them is the so called base factor method [1]. Its essence is the decomposition of the dimension matrix into base factors i.e. the multiplication of two matrices the first the second of which contains linearly independent columns and rows, respectively. Then the base elements of physical quantities can be determined from the base factors. The decomposition to factors usually can be avoid if one manages to write the matrix such way that the first rectangular

partition is non-singular, lower triangular matrix. In the case the procedure is as follows.

From the first three equations

$$z_1 = y_1,$$

$$z_2 = y_2 + 3z_1 = 3y_1 + 3y_2,$$

$$z_3 = \frac{1}{2}(z_2 - y_3) = \frac{y_1}{2} - \frac{y_3}{2}.$$

Substituting z_1, z_2 and z_3 values in the further equations

$$y_1 - y_5 = 0,$$
$$y_1 - y_6 = 0,$$
$$y_1 - y_7 = 0,$$
$$y_1 - y_8 = 0,$$
$$y_1 - y_9 = 0,$$
$$y_1 - y_3 + 2y_{10} = 0,$$
$$5y_1 + y_3 - 2y_{11} = 0,$$
$$4y_1 + y_2 + y_3 - y_{13} = 0.$$

And returned to the original notations

$$\ln(D) - \ln(Z) = 0,$$
$$\ln(D) - \ln(L) = 0,$$
$$\ln(D) - \ln(d) = 0,$$
$$\ln(D) - \ln(D_{cs}) = 0,$$
$$\ln(D) - \ln(s) = 0,$$
$$\ln(D) - \ln(g) + 2\ln(n) = 0,$$
$$5\ln(D) + \ln(g) - 2\ln(Q) = 0,$$
$$4\ln(D) + \ln(\rho) + \ln(g) - \ln(M) = 0.$$

The invariant numbers formed from the above equations are

$$P_1 = \frac{M}{D^4 \rho g},\ P_2 = \frac{Q^2}{D^5 g},\ P_3 = \frac{Dn^2}{g},\ P_4 = \frac{s}{D},\ P_5 = \frac{D_{cs}}{D},$$

$$P_6 = \frac{d}{D},\ P_7 = \frac{L}{D},\ P_4 = \frac{Z}{D},$$

which are completed by adding $P_9 = \delta$ and $P_{10} = W$.

The application of the method

Let us consider *figures 1* and *2* to demonstrate the applicability of the method which represent the partial results of the experiments on autumn barley with auger of parameters given in *table 3*. The parameters are not detailed here.

Table 3

Description of variable	Notation	Unit	Adjusted value
angle of transport	δ	°	10,20,30
diameter of auger wing	D	m	0,130
length of inlet port	Z	m	0,295
length of auger wing	L	m	2,0
diameter of auger shaft	d	m	0,027
inside diameter of auger house	D_{cs}	m	0,152
auger pitch	s	m	0,133
revolution	n	1/min	300-1000
moisture content	W	%	9-12

In the *figure 1* one can recognise the variation of the so called **capacity-characteristic number** (P_2) as function of **revolution characteristic number** (P_3) and the angle of transport (P_9), all the other invariant numbers are constant. In the *figure 2* the **moment-characteristic number** measured simultaneously with the capacity number is demonstrated. One can easily see that the figures contain information not only for the transport capacity and moment need of the D=130 mm diameter auger applied in the experiment but they describe the variation of all augers which have identical independent invariant numbers. It means that it is enough to manufacture and measure only one single experimental equipment to estimate the expectable transport capacity and driving moment need of different size transport augers.

References

1. BALOGH, L.-NÉ – BÉKÉSSY, A. – FÁY, GY.: Megjegyzések a dimenzióanalízis alkalmazásához. Energia és Atomtechnika. XV.,1962. (*Notes to the application of dimension analysis*, in Hungarian
2. BENKŐ, J.: Particle model for description of operation of screw conveyors. Buletin of the University of Agricultural Sciences, Volume 1, Gödöllõ,1995-1996.
3. REHKUGLER, G., E. - BOYD, L., L.: Dimensional analysis of auger conveyor operation. For Presentation at the 1961 Annual Meeting ASAE, Iowa State University.
4. SZŰCS, E.: Hasonlóság és modell. Műszaki Könyvkiadó, Bp. 1972.
5. (*Similarity and model,* in Hungarian)

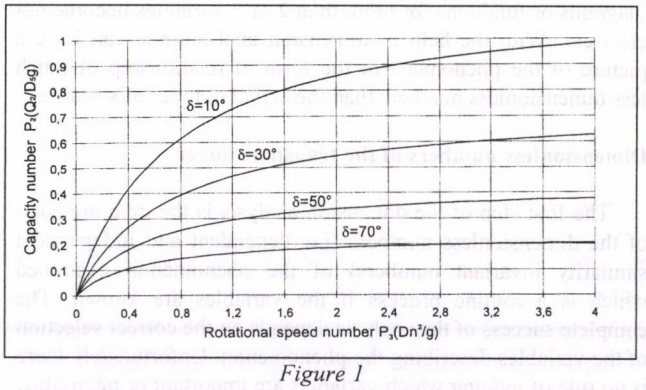

Figure 1
Capacity number as a function of rotation speed number

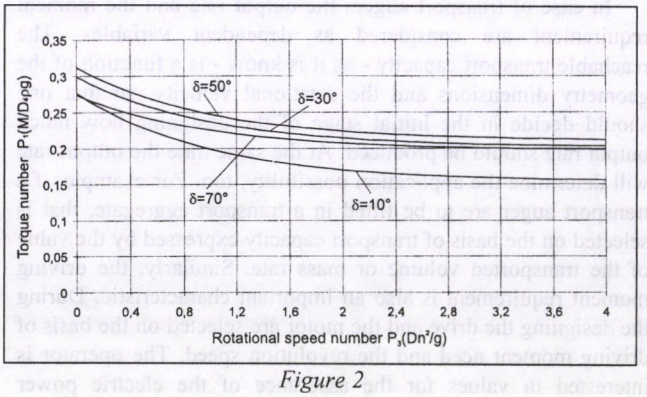

Figure 2
Torque number as a function of rotation speed number

RADIATION OF SOWING-SEEDS IN ELECTROMAGNETIC DISCHARGE SPACE

Dr. P. Szendrő - Dr. J. Koltay - Dr. Gy. Vincze
University of Agricultural Sciences, Gödöllő

Introduction

The study deals with those effects of physics, what influence the individual grains of material bulk of sowing-seeds in a zero mean value asymmetric electromagnetic space excited by high voltage series of impulses. The experimental model pilot apparatus is being outlined also. One effect discovered by the authors is that if a negative corona discharge is superposed on the above characterised electromagnetic space then the individual grains in the aggregation will be filled up according to their permettivity, so that they are effected by different magnitude and direction electromagnetic force. Based on the effect the grain bulk can be separated to its components. A utilisation of the effect is the sowing-seed cleaning. Further application possibilities are separation according to thousand grain mass and germination ability. The effect of surface discharge occurring to the individual grains is well utilisable. The treatment can significantly improve the germination ability and vigour of the low germination ability seeds.

This research was made with the support of OTKA 1522 and OMFB.

The simplifield theory of the effect of discharge space

1. Severalising effect In the followings the simplified theory of an effect of discharge space is discussed. The presentation is begun with the corona charge process based as shown in *figure 1*. The electrode on the figure is supplied with large amplitude alternate current which changes according to the diagram of *figure 2*.

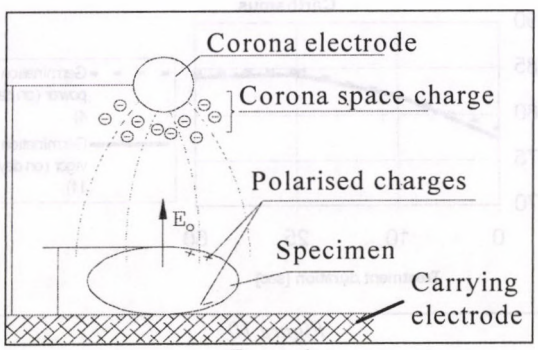

Figure 1

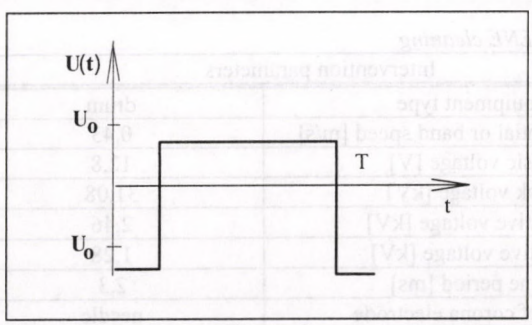

Figure 2

One can see in the figure that the voltage is lower in the positive half period and higher than the limit start voltage U_0 of the corona discharge in the negative one. At first the seed in the discharge space is polarised as determined by its transient permettivity in the negative half period of electrode voltage, then it attracts the negative ions of the discharge and starts to charge. Since the electrode voltage is lower than the discharge limit value in the positive halfperiod, the seed gets no additional charge. Its existing charge is slowly conducted to its carrying surface. this the discharge process the time coefficient of which is determined by the electric resistance between the carrying surface and the seed. After all the electric force acting on the seed is given by

$$F_a = \frac{1}{T}\int_0^{\tau} Q(t)E(t)dt = \frac{1}{T}Q_{ch\,a}\int_0^{\tau} E(t)dt + \frac{1}{T}Q_{da}\int_0^{\tau} E(t)dt ,$$

using the notation of *figure 2*, and $Q_{ch\,a}$ and Q_{da} are the average charges in the charging and the discharging processes, respectively. As the electrodes are supplied with alternate current, it holds that

$$\int_0^{\tau} E(t)dt = -\int_0^{\tau} E(t)dt ,$$

by which the preceding equation will result in

$$F_a = \frac{1}{T}(Q_{ch\,a} - Q_{da})\int_0^{\tau} E(t)dt ,$$

One can seen that i) the seed is attracted when $Q_{ch\,a} < Q_{da}$ and repulsed when $Q_{ch\,a} > Q_{da}$; ii) the electric force is determined by the transient electric permettivity of seed and the reduced resistance.

2. Stimulation effect In 1967 Mattews and Bradnock proposed a method to determine the germinating power which is based on the measurement of electric resistance. According to their investigation those effects of physics which deviate the moisture content, homogeneity and diffusion coefficient of their membranes modify their germination vigour, too. Some of them are presented here.

Respiration effect The plant origin material absorbs oxygen and emits carbon dioxide. In the effect applied by us corona discharge happens during what flood of electrons starts which is are bound by the oxygen molecules due to their negative charge. Such way negative oxygen ions are formed which move along the line of forces toward the seeds placed on other electrode.

Mechanical effect of the electric discharge The seeds treated in the experimental apparatus fits to the electrode with swept-in air gap due to their morphology. The signal shape of the applied electrode voltage is greatly steep both at the increasing and the decreasing sessions as shown in *figure 2*. The value of dU/dt is very high so that significant displacement current will flow in the space between the electrodes. The dD/dt density of the displacement current will be constant inside the seed and in the air at the air contacting part of the seed. Since $D = \varepsilon E$, the field intensity will be higher with same D if ε is lower i.e in the air. If the value exceeds the electric strength of the air, then electric discharge starts near the grain surface which makes microscopic size pores on the bounding membrane and the mass transfer become easier.

Homogenising effect It is well known that the mass transfer equilibrium is characterised by the independence of the μ chemical potential on the location in a thermodynamically a static system. The electric component of the chemical potential will change to the effect of radiation which generates transport processes inside the seed.

The experimental apparatus

The main parts of the equipment are: *mechanical part* with moving carrying surface, vibration feeder and divided collecting blade; *electric part* with corona electrode, high voltage power supply, discharge brush and direct current driving. *Figure 5.* a shows the separation equipment while the apparatus in *figure 5.b* is the stimulation one. The vibration feeder (a) spreads the grains on the moving carrying surface. The earthed moving part (b) is covered by thin insulation layer. The guide plate (c) directs the seeds separated from the drum to a cell of the collecting bin (d). The scheme of the electric part is shown in *figure 6.* The corona electrode (a) is connected to the secondary side of the high voltage transformer (b). The primary coil is feeded by the alternate current power supply (d). The rotator is driven by a direct current motor (e) the rotational speed of which is adjusted by the control unit (f).

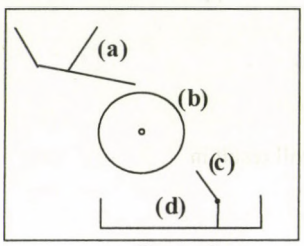

Figure 5.a

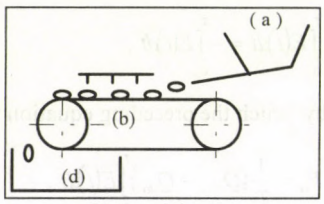

Figure 5.b

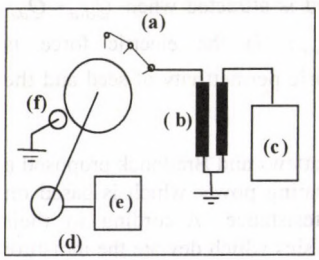

Figure 6

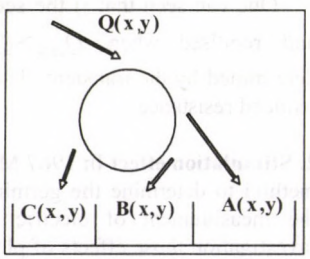

Figure 7

Results, conclusions

Using the equipment as a separator several sowing seed bulk were graded. Some results concerning sowing seed cleaning is shown in *table 1.* The meaning of the characteristics in the table can be found in *figure 7.* In separator operation mode it is possible to separate according to the germination power. An example id shown in figure 8 which exposes the separation of absinthe according to the germinating ability. The figure shows that the original congeries of seeds of 32.6 % germinating power become a more the 37 % germinating power aggregation by separating fractions 1, 6 and 7. The *figures 9 and 10* show the germination changes of the tobacco and carthamus seeds concerning germinating ability and vigour as functions of the treatment time.

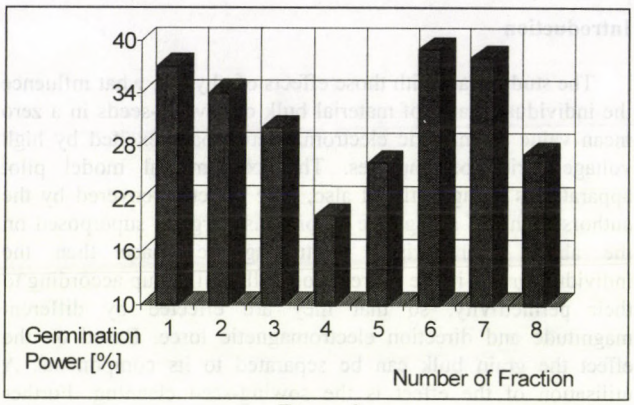

Figure 8

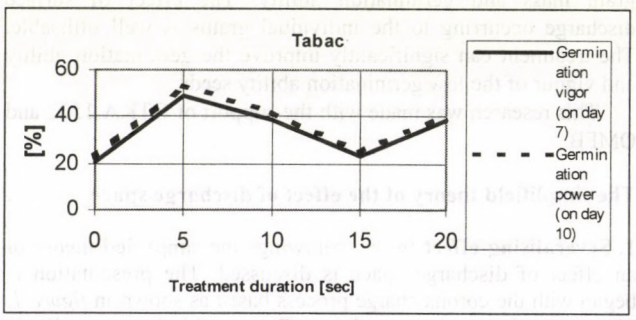

Figure 9

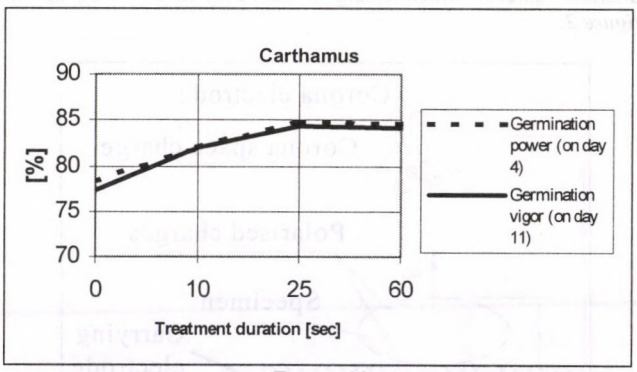

Figure 10

Table 1

The operational quality characteristics of grading at HELIANTHUS ACHENE cleaning

Material characteristics		Intervention parameters	
Measurement identification	1991.11.28/4	Equipment type	drum
Initial material marked	NET	Circumferential or band speed [m/s]	0,43
- moisture content [%]	8,2	Basic voltage [V]	12,8
- place of origin	BNR	Peak voltage [kV]	31,08
Components		Negative voltage [kV]	2,46
- basic material (x)	sunflower seed (achene)	Positive voltage [kV]	1,28
- contamination (y)	selerocium	Time period [ms]	2,3
- contamination (z)	-	Type of corona electrode	needle
Identification of clean fraction:	C	Time period of positive voltage [ms]	1,2
Number of treatment	1	Pre-cleaning with traditional equipment (yes/no)	yes

Faction		
Sign	Mass [g]	Distribution [%]
A	99,6	30,99
B	36,9	11,48
C	184,85	57,52
Q	321,35	100

Distribution of faction (cleaning and pollution) [%]			
Sign	x	y	z
A	85,34	14,66	0
B	98,64	1,36	0
C	99,59	0,41	0
Q	95,07	4,93	0

Sign of faction	Output rate ε [%]		
	x	y	z
A	27,82	92,11	-
B	11,91	3,15	-
C	60,26	4,73	-

Cleaning efficiency η [%]		
for y	for z	for y+z
91,0	-	-
Application degree of grading		
excellent	-	-

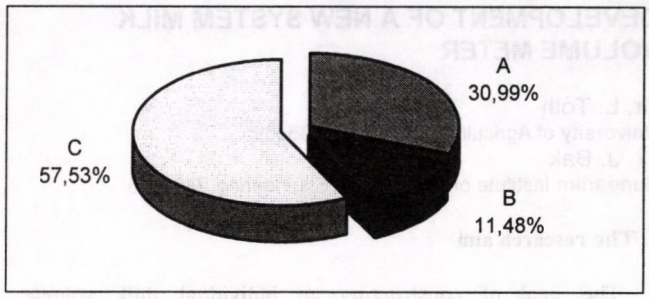

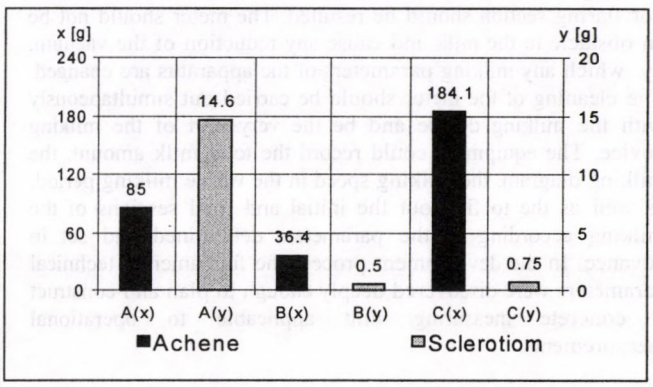

DEVELOPMENT OF A NEW SYSTEM MILK VOLUME METER

Dr. L. Tóth
University of Agricultural Sciences, Gödöllő
Dr. J. Bak
Hungarian Institute of Agricultural Engineering, Gödöllő

1. The research aim

The goal of constructing an individual milk volume measuring unit was established. The device should not alter the parameters of milking device at all and should be connectable to the long milk tube of the milking device where neither restrictor nor flaring section should be resulted. The meter should not be an obstacle to the milk and cause any reduction of the vacuum, by which any milking parameters of the apparatus are changed. The cleaning of the meter should be carried out simultaneously with the milking device and be the very part of the milking device. The equipment could record the total milk amount, the milking diagram, the milking speed in the whole milking period, as well as the to find out the initial and final sessions of the milking according to the parameters determined and set in advance. In the development process the fundamental technical parameters were discovered deeply enough to plan and construct a concrete measuring unit applicable to operational measurements.

2. Description of the problem

The individual milk quantity measuring units known so far apply mass or volume measurement principles. The mass measurements are usually based on gauge technique.

The measuring technique has favourable accuracy, but the temporary milk storage needs large containers which are ample and expensive to be made. At the same time because of the divergent section the need for cleaning agents quality and quantity is higher. It is difficult and involved to locate them in the milking device due to the considerable need for room. The volumetric principle systems have the same problem, the large inner volume of theirs and the complicated chambers necessary for this type of measurements. In consequence of large flow cross section differences their cleaning is rather involved. Their accuracy always depend on the extent of milk churning. Those measuring units are completed by electronics also in the past years and the microprocessor control offered the possibility to rise their accuracy to a proper level by correction. Recently practically all the measuring devices meet the requirements already.

The traditional volumetric measuring apparatuses, such as propeller or oval wheel solutions are not applicable, because the milk is randomly mixed with air and the velocity and direction of the mixture flow changes continuously.

3. The solution of the problem

The researches connecting machine milking and milk properties drew the attention to the fact that the electric conduction and the dielectric coefficient changes as functions of the cross sectional overflow and flow composition. Their continuous determination gives possibility to know the milk quantity with great approximation in a given instance, in a given tube session.

The sensor unit is built in the long milk tube - some 50 cm behind the collector, with 5 to 10° inclination in the milking platform of the lower milk pipeline milking equipments (see *figure 2*).

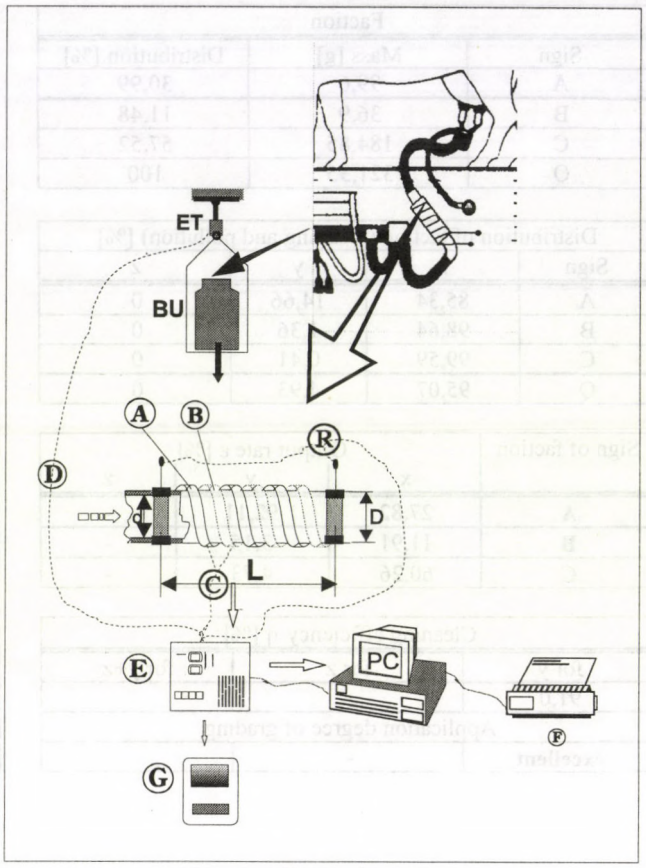

Figure 1
Principle of measuring
A and B spiral shaped capacitor arming, C - capacity change input, D - mass measurement device connection, E - A/D converter, PC - personal computer, F - printer, ET - measuring-sensing element, BU - milking pail (the latter two are necessary only for the experiments).

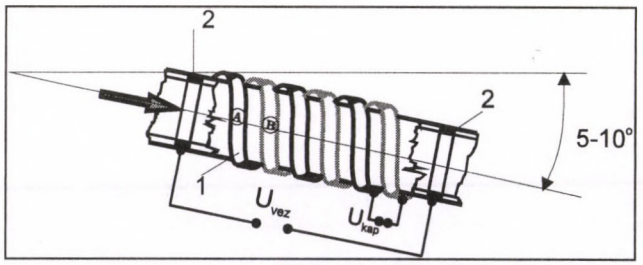

Figure 2
Set-up of the measuring sensor
1-A and B spiral capacitor arming
2 - ring for measuring electric conductivity

The sensor unit connects to the long milk tube of milking device by two rings what are the two pieces of sensor connectors for measuring electric conduction of milk. Between the two sensors the capacitor faces are bobbined in spiral shape (A and B). In the experiments 2 to 10 complete turns were used. The solution is analogous to the double thread. The wires connecting to the two rings (R and C) and the opposite armings of the capacitor leaded to the A/D converter (E) preceding the computer.

The direct current connected to the capacitor armings forming measuring bridge and the sensor rings will be changed by the milk flowing through. In the case of the capacitor the voltage will increase proportionally to the quantity of milk

flowing between the spiral armings as the dielectric coefficient of the system increases. At the same time the milk flowing between the two rings makes short circuit and the voltage between the two points decreases depending on the quantity flowing through. Those modifications of the voltage are scanned by the computer through the analogue to digital converter.

To process the signals a software has been compiled making possible to display the voltage changes on the vertical axis and the time on the horizontal axis on the monitor screen.

In the experiments the milk quantity flown through the milking device was collected in a milking pail which was placed on a gauge operated scale. The analogous signal of the gauge scale was connected to the third connecting pair of the A/D converter.

Such way three different signals were displayed on the computer screen: the change of electric capacity, the electric resistance changing and the modification of the milk quantity.

Those are shown in *figure 3.*

The measurements showed that the intensity of the changes in the voltage are in close correlation with the changes of the quantity flowing through. After accomplished the proper number of measurements the concrete relationship could be determined. Based on the formula a basic integration instrument was made which determines even the time-rated area changes of the three curves and the total area changes.

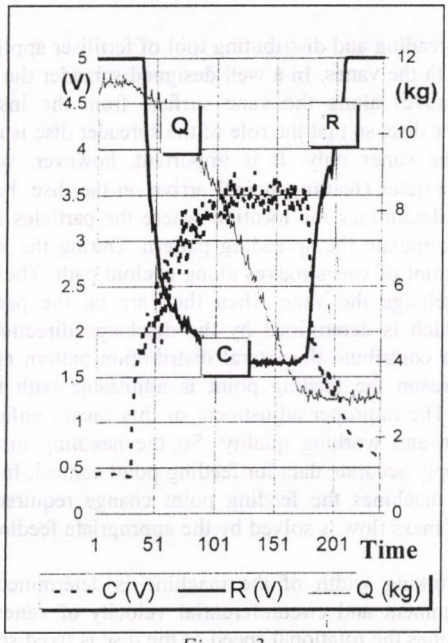

Figure 3

The change of the voltage and the milk quantity during the measurement (4-5 kg/min maximum milking rate)

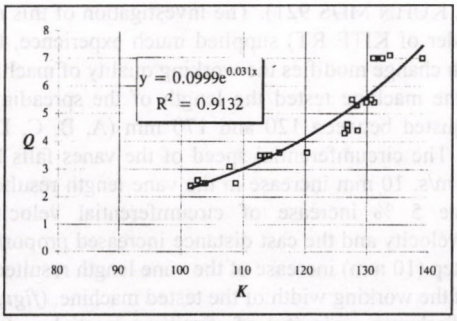

Figure 4

The change of the K value and the milk quantity (Q) during the measurement (2-6 kg/min maximum milking rate)

4. The relationship

*Determining **K** in the experiments*:

$$\frac{Q}{\frac{C_n + R_n}{n}} = K_n$$

*In the practice **Q** is the unknown:*

$$Q = ae^{bK}$$

where

Q	is the quantity of milk (kg)
C_n	the voltage change characteristic to the total capacity change (in Volt)
R_n	the voltage change characteristic to the total electric resistance change (in Volt)
K_n	the value characteristic to the measurement
a-b	the constants values of the instrument
n	number of measurements.

A great number of measurements were accomplished in practical conditions based on which the mathematical relationships was determined between the final three variables.

Simplifying the problems significantly for the easier demonstration: the characteristic integrated value of the voltage changing curve for the sensor rings are given by a single value R. And the same is applied to the capacity and the milk quantity variation. The values are then divided by the number of measurements to give an average value. That value is divided by the milk quantity determined in kilogram, so the resulted *K* will be the value of the instrument. As the milk quantity measurement is intended to be accomplish on basis of the first two parameters, the practical instrument measures *R* and *C* values which are multiplied by the constant will give the actual milk quantity.

The sampling frequency of the measurement is 20 ms. Therefore in the case of a complete six minute milking the number of samples is 50×60×6=18000. The limit value of the evaluation is adjustable by jumper so that the wetness the inner surface and the spraylike milk below 2 kg/hour value would not be measured by the instrument. In the future the sampling frequency of the practical instrument can be raised and the ±3% accuracy can be also improved.

5. Abstract

During the last 30 years, improvements of many variations of milk quantity recorders have been completed by the specialists of the R + D teams in research institutes and the factories. Because the milk is quite a heterogeneous material with respect to its flowing during the milking, the measuring devices got complicate equipment. The biggest problem of their use is the cross section area increased in comparison with the milk tubes or pipes and because of that, the flow intensity of the cleaning liquid decreases and it can be compensated only with use of extra energy (heat and detergent). A combined sensing process depending on the filling ratio was chosen which was suitable to perceive the changing in conductivity and permettivity (dielectric constant) of the liquid and this made unnecessary to alter the cross section area of tube even in the lowest measure. Conclusively, the milk quantity flowing through is measured by quasi external sensors assembled into (onto) the long milk tube section and its displaying, summarising and registrating is solved with the help of the connected PC. During the research. the basic parameters of a construction were determined which can be manufactured in the industrial practice.

DESIGN AND CONTROL QUESTIONS OF ROTARY DISC FERTILISER SPREADER MACHINES

Dr. Z. Csizmazia - I. Polyák
University of Agricultural Sciences, Debrecen

The fundamental question of the design and operation of rotary disc fertiliser spreader machines is the optimum working quality of the machines. Determination of the factors influencing the cross directional distribution of fertiliser is the most important to ensure this. Especially those affecting the motion of the fertiliser grains on the disc and those determining the discharge point, discharge velocity and discharge direction are the most important. Taking into account that the fertilisers applied have different characteristics the spreader should be designed to meet different fertiliser types with optimum working quality.

To utilise nutritive materials reasonably it is equally important to moderate the production cost, to improve the quality of work and to save the environment. In the countries having developed industry and agriculture one can experience an effort to apply the nutritive evenly distributed. The application machines are mounted such type of machines which makes possible to control the dose within certain limits even in operation. Up-to-date spinning disc broadcasters have been developed which are able to apply the alimentary substances with appropriate even distribution and changeable working width.

There are being widely conducted field experiments with land maps and positioning to accomplish the nutritive application which fits the demand of the plants the best.

The home development which followed the European norms earlier has stopped. The fertiliser usage has been reduced to minimum by the companies suffering from the lack of the money, and this is almost restricted to nitrate fertilisers. This was also accompanied by the wrecking of the application technique. The home developed fertiliser machines, which should be still developed, has worn out and their quality has been reduced. The replace them a great number of low quality imported machine came to this country, which were not even suitable enough to be sold in western countries. This situation is partly due to the abolishment of the compulsory machine qualification. At the same time several home company began to manufacture fertiliser spreader machines without any experimental and theoretical background which do not meet the agricultural and engineering conditions. Their design does not ensure the adjustment of the prescribed dose, the spreading evenness or width. Those spreader devices are not reliable considering spreading uniformity and width. Using this machines leads to uncontrolled, uneven, ineffective application of fertiliser and more amount of fertiliser is necessary to obtain the same result which causes extra cost, reduces the quality of produce, pollutes the environment. The luck of skill results in irresponsible manufacture and trade of machines. Those severe problems could be abolished by the obligatory machine investigation. For this purposes only the initial steps has been made even in the Western-European countries although the situation is more favourable there. The users customs have been formed by which the farmers buy such machines which have working qualities guaranteed by qualifying institutions and so the manufacturing companies are interested in qualifying their machines. Until these problems will be solved the attention of the users and dealers can only be directed to some questions considered important. Now a few significant characteristics of design, operation and machine selection are highlighted.

1. Conditions of the even feeding

Most of the recent fertiliser spreader machines are suspended constructions with gravitation feeding and orifice controlled. They work properly only with dry, clog free, grainy materials. That is why they need **admitting grid**.

The fertiliser tend to vault easily in conical containers - mainly as a consequence of absorbing humidity. This spoils the continuous fertiliser flow and feeding evenness. So that oscillating or rotating **anti-blockage device** is necessary to use above the feeding orifice. An ill-constructed anti-blockage device can be a source of several defects. The fertiliser particles sensitive to impact may be disintegrated by the anti-blocking element resulting in narrower spreading width and worse distribution evenness. So that only slowly rotating or oscillating tools are suitable. The adequate anti-blockage device has a rotational speed of 100-120 rpm. Such a device fixed to the spreading disc and rotating with the same speed does not meet the requirements.

The feeding evenness depends on the design of the feeding device. The shape of the suitable feeding orifice is near the optimal flow section (circle, rectangle, lozenge). for any dose.

The **dose table** should contain at least 50 values and a relevant material table should be available, too.

2. Conditions of the even distribution of fertiliser

The spreading and distributing tool of fertiliser application is the disc with the vanes. In a well designed spreader the fertiliser particles moves along the vane surface from the instance of reaching the disc, so that the role of the spreader disc is restricted to carry the vanes only. It is important, however, where the fertiliser particles (**feeding point**) arrive on the disc, because is decisively determines the location where the particles leave the disc and formulate the spreading pattern. During the spreading the outer point of vanes moves along cycloid path. The particles should discharge the vane when they are on the part of the cycloid which is determined by the discharge direction of the particles to contribute the lateral distribution pattern optimally. For this reason the feeding point is adjustable with the most machines. The improper adjustment of this causes unfavourable distribution and working quality. So the handling instructions should supply accurate data for feeding point control. In the case of certain machines the feeding point change required by the changes of mass flow is solved by the appropriate feeding orifice design.

The working width of the machine is determined by the shape, alignment and circumferential velocity of vanes. In the most machines the rotational speed of the disc is fixed so that the circumferential velocity of the vanes can be increased only by increasing the vane length. This can be made by the replacement of the vane or disc (e. g. AMAZONE) or changeable length vanes (e.g. KUHN MDS 921). The investigation of this machine (on the order of KITE RT) supplied much experience, how the vane length change modifies the working quality of machines.

With the machine tested the length of the spreading vanes can be adjusted between 120 and 170 mm (A, B, C, D and E positions). The circumferential speed of the vanes falls between 17 and 22 m/s. 10 mm increase in the vane length resulted in an approximate 5 % increase of circumferential velocity. The discharge velocity and the cast distance increased proportionally, too. One step (10 mm) increase of the vane length resulted in 2 m increase of the working width of the tested machine. (*figure 1, 2*)

The discharge velocity of fertiliser particles (v_0), the discharge direction (γ) to the disc tangent and so the contribution

to the distribution pattern are highly influenced by the alignment angle (β) of the spreading vanes (*figure 3*).

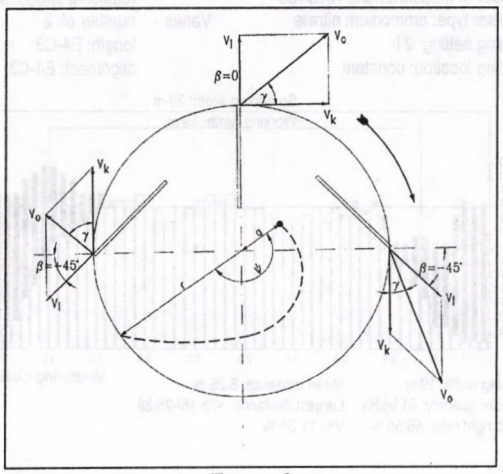

Figure 3
Velocities of the fertiliser particle discharging the disc

With constant circumferential velocity (v_k) the magnitude and direction of the discharge velocity depend on the magnitude and direction of velocity along the vane (v_l). The velocity tangential to the vane is determined by the forces acting on the fertiliser particle: the centrifugal force $F_{cf} = mr\omega^2$, the friction force $F_{CS} = 2mv\omega\mu$ from Coriolis force ($F_C = 2mv\omega$) as well as the friction force due to the weight of the particle $F_S = mg\mu$.

Using the d'Alambert principle one can write the following expression:

$$mr\omega^2 - 2mv\omega\mu - mg\mu - ma = 0$$

Where

m - mass of particle
r - distance between the particle and the disc centre
ω - angle rotational velocity of disc
v - the relative velocity of the particle tangential to the vane
μ - friction coefficient between particle and the vane
a - acceleration of particle

The analysis of the relationship shows that the velocity of the particles along the vane depends mainly on size, shape, rotational speed and surface roughness of the vanes.

The **angles of the vanes to the radial direction** (1-6) influences significantly the magnitude and direction of the discharge velocity. The discharge angle has great effect on the particle position in the distribution pattern. The one step alignment of the angle of one vane increased the working width from 16 m to 19 m, while the spreading unevenness increased by 2 % and the largest deviation increased by more than 10 %. (*figure 4, 5*). Therefore the wrong alignment of vane angles may result in a considerable reduction of the working quality. Although the forward pitching of the vanes increases the working width significantly, because of their spreading unevenness increasing effect these days backward pitched vanes are usually used.

Thus, in short, it can be stated that the spreading structure of the spinning disc fertiliser broadcasters can be designed only using sufficient theoretical knowledge and suitable experimental background in order to meet the agricultural, environment protection and engineering requirements.

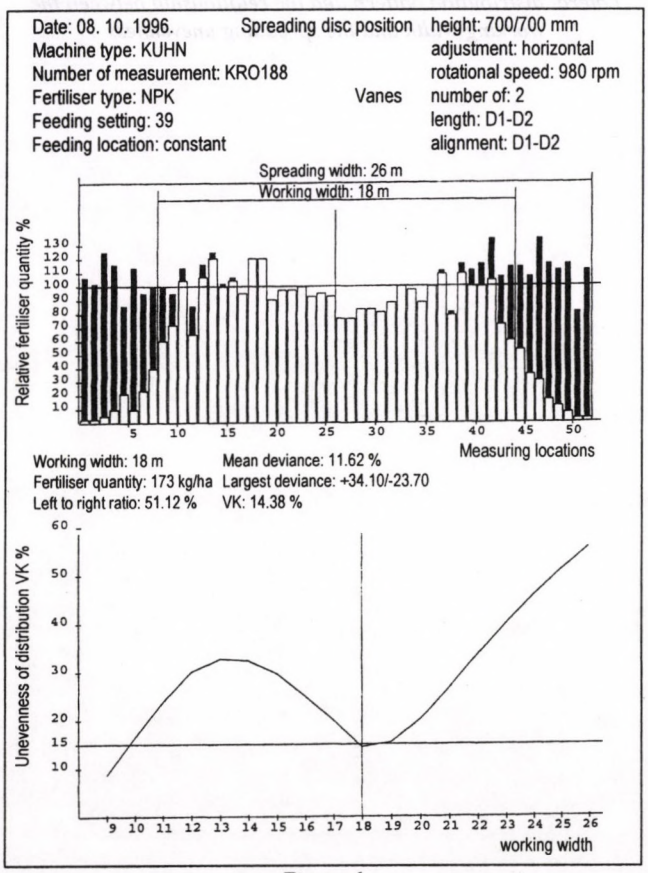

Figure 1
Lateral distribution pattern and the relationship between the working width and the spreading unevenness

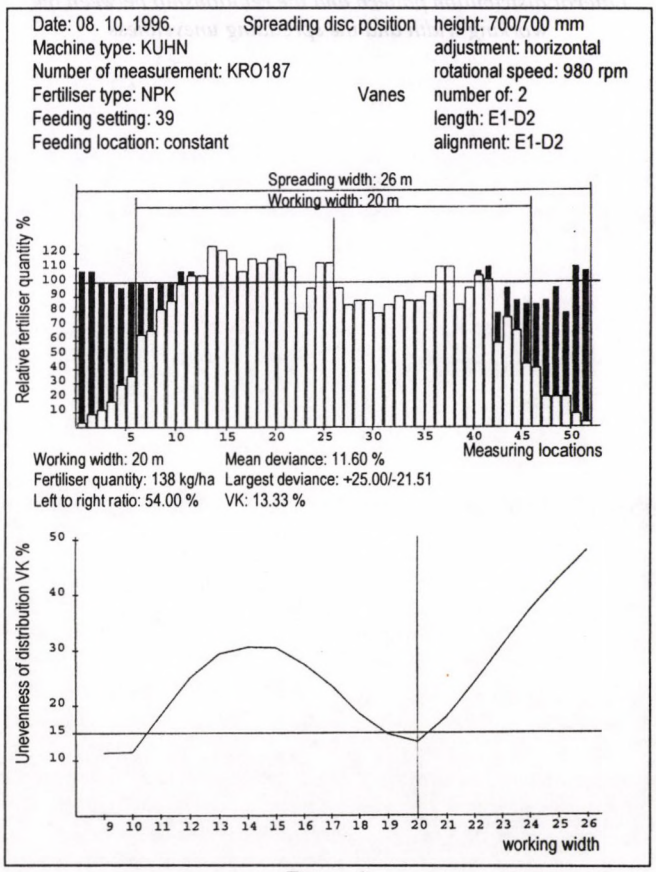

Figure 2
Lateral distribution pattern and the relationship between the working width and the spreading unevenness

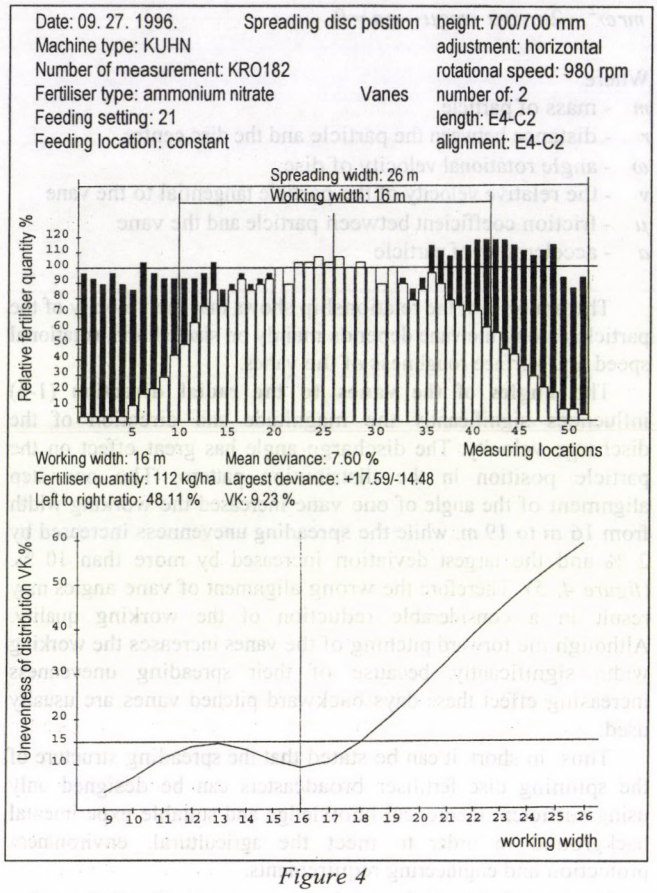

Figure 4

Lateral distribution pattern and the relationship between the working width and the spreading unevenness

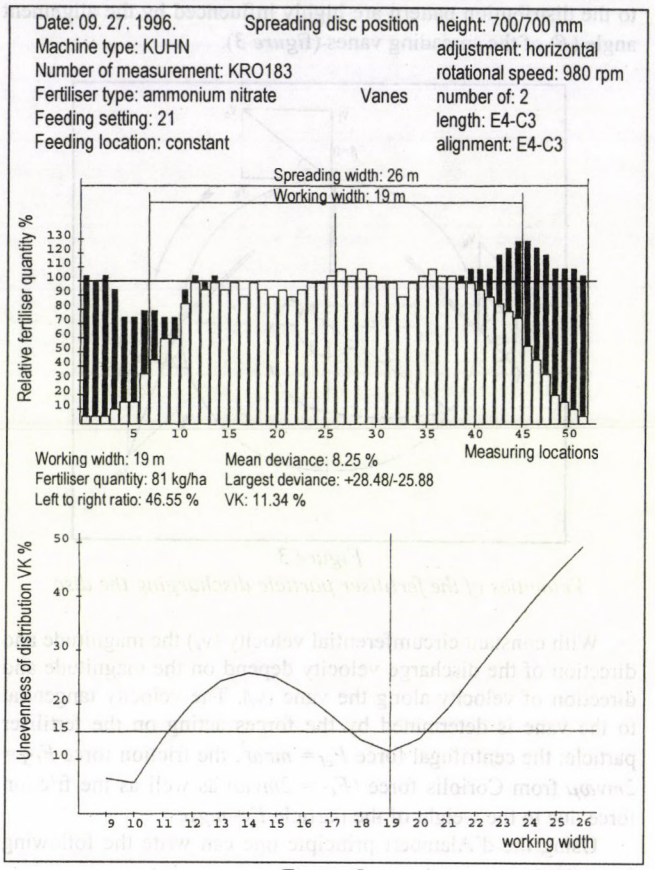

Figure 5

Lateral distribution pattern and the relationship between the working width and the spreading unevenness

DETERMINATION OF ENERGY BALANCE ON THE BASIS OF RHEOLOGICAL PARAMETERS

Dr. E. Gelencsér
University of Agricultural Sciences, Gödöllő

The time depending stress and deformation states are described by the discipline of rheology.
The linear models of rheology describe those states and can be successfully used for characterising stress and strain changes in agricultural materials. The introduction of stress rate and strain rate to the material equations makes possible to take the time factor into account. The general form of linear homogenous material model is

$$\Phi(\sigma, \varepsilon, \dot{\sigma}, \dot{\varepsilon}) = 0,$$

which already accounts for time depending creep and relaxation phenomena, too.

A possible form of this equation for uniaxial stress state is as follows

$$\sigma = a\,\varepsilon + b\,\dot{\varepsilon} + c\,\dot{\sigma},$$

where the notations are
σ the stress,
ε specific strain,
$\dot{\sigma}$ stress rate,
$\dot{\varepsilon}$ rate of specific strain and
a, b, c are material constants.

Provided that the materials in question follow the above relationship, the formula can be utilised in the determination of material characteristics. The complex viscoelastic material model corresponding to the equation may be built up from parallel and serial connections of the basic elements representing the elastic, viscous and plastic properties.

One of the basic elements is perfectly elastic, the force is proportional to the strain rate. The other basic element is for viscous liquid property producing a damping force proportional to the velocity. The plastic element restricts the stress level to plastic limit.

The solutions of the material equations describing the phenomena produce the characteristic constants of the material with the relevant boundary conditions.

The application of these equations reflects rather diverse approaches, moreover the selection of the models is not clear being random or uncompelled many times.

It is reasonable to examine the question of model selection first then to make the detailed analysis only after that. Using a few simple basic experiments one can find out which basic elements ought to be contained by the model and their ratios can be also determined.

The investigation made on the basis of energy conditions offers several advantages. Beyond the above mentioned model selection, it makes possible to determine the minimum energy loss of the process and energy saving can be achieved. The surplus calculations can be eliminated in a concrete solution.

One can find the solutions of the material *equations* for arbitrary stress and strain states in the literature.

It is not indifferent, however, if the desired state is achieved with minimal *energy* investment or what is the ratio of the energies invested and dissipated by the environment. This ration can be optimal but can mean excess energy. In certain cases the energy dissipated can be even harmful, mainly in the case of grain materials are subjected to such effects.

Material and energy equations

The solutions of the material equations are produced for uniaxial stress state. Assumed an arbitrary material law, the energy conveyed can be regained only partly because a portion will be dissipated. It is especially true for rheological models and for differential equations describing such kind of phenomena. The calculation for complicated complex models can be hardly made if at all, so that the number and types of the elements should be limited practically.
In the analysis three basic elements are used, such as
• elastic,
• damping and
• plastic elements

It is practical to describe separately in detail and then to build up their proper connections and combinations based on it.

Basic elements

Elastic element, HOOKE model.

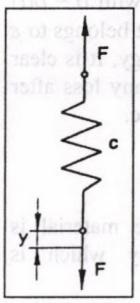

Figure 1
Hooke model

Its formula can be given in the form of

$$F = \frac{1}{c}\,y.$$

where:
F force [N],
c spring constant [mm/N],
y elongation [mm].

If the length of the element is L, the cross section of the rod is A, then one can change to the relationship between the stress and strain, by using the equation

$$\frac{1}{c} = \frac{AE}{L}$$

by which

$$\frac{F}{A} = \frac{1}{c}\frac{y}{A} = \frac{AE}{L}\frac{y}{A}\frac{L}{L} = \frac{AE}{L}\frac{L}{A}\frac{y}{L}$$

or

$$\sigma = E\,\varepsilon_H$$

The relationships containing the starting and the resulted characteristics are equivalent, only the force F and the y elongation are replaced by specific values of the σ stress and the ε strain, respectively.

Since a single elastic element shows up time independent behaviour the deformation versus time diagram is specified by the line ε_0 = constant and ε_0 and σ_0 initial values.

The energy is

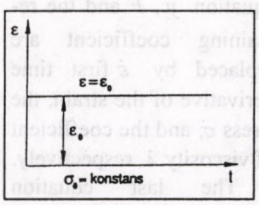

$$W_H = \int_0^{\varepsilon_H} \sigma \, d\varepsilon_H$$

Figure 2
ε-t diagram of elastic element

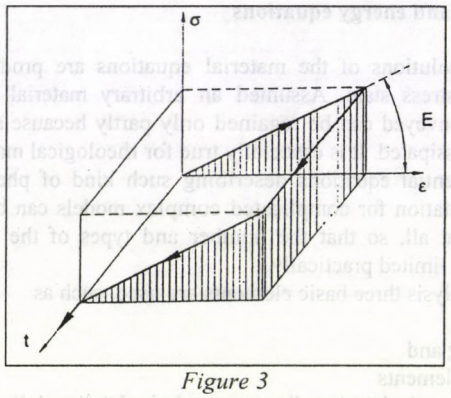

Figure 3
σ–ε–t diagram of Hooke model

Let us examine the phenomena for loading application and loading relief process.

With the Hooke-model one can arrive at the same result as the investigation of the time history of the phenomenon started from the σ_o = constant condition. So it is satisfied with $\sigma = \sigma(t)$ as the shape of the $\sigma = \sigma(t)$ diagram is the same if it belongs to ε = constant. By the analysis of the transmitted energy, it is clear that the invested energy can be regained without any loss after arbitrary t time. Such process is called reversible one.

Viscous element, NEWTON model

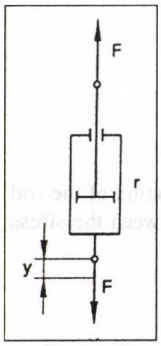

Figure 4
Newton model

The viscous property of the material is described by a damping body which is proportional to the velocity:

$$\frac{dy}{dt} = \dot{y} = \frac{F}{r}$$

where r is the damping coefficient [Ns/mm].

As done with the elastic element the specific quantities are introduced:

$$\frac{d}{dt}\left(\frac{y}{L}\right) = \frac{F}{Lr} = \frac{FA}{ALr},$$

i.e.

$$\frac{d\varepsilon}{dt} = \frac{\sigma}{\lambda};$$

and in the final form:

$$\sigma = \lambda \dot{\varepsilon}_N,$$

where

$$\lambda = \frac{L}{A} r$$

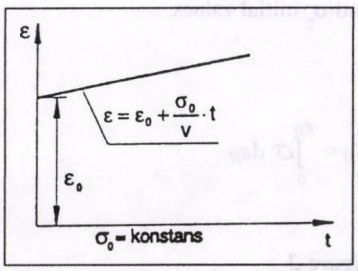

Figure 5
ε-t diagram of a viscous element

is the coefficient of viscosity [Ns/mm^2]. Differently from the starting equation $\dot{y}$, F and the remaining coefficient are replaced by $\dot{\varepsilon}$ first time derivative of the strain, the stress σ, and the coefficient of viscosity λ, respectively. The last equation already contains the time $\left(\frac{d\varepsilon}{dt}\right)$ and the deformation versus the time changes according to *figure 6* with ε_o and σ_o initial conditions.

The energy formula is

$$W_N = \int_0^t \lambda \, \dot{\varepsilon}_N^2 \, dt$$

The behaviour of the Newton model is quite different due to its viscous property. It can be well followed in the figure that the specific expansion is perfectly viscous and the total invested energy is dissipated and it can not be regained, i.e. the process is irreversible.

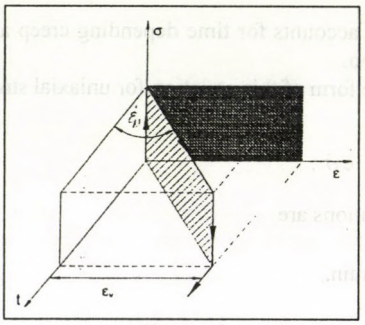

Figure 6
σ–ε–t diagram of Newton model

Plastic element or SAINT VENANT model

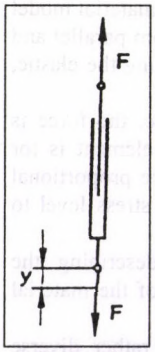

Figure 7
Saint Venant model

The plastic property of the material is practically described by a characteristic representing a limit value as internal friction property:

$$F_S = \mu_S F$$

where μ_S is the coefficient of the internal friction.

According to the previous fashion specific values are introduced as follows

$$\frac{F_S}{A} = \mu_S \frac{F}{A}$$

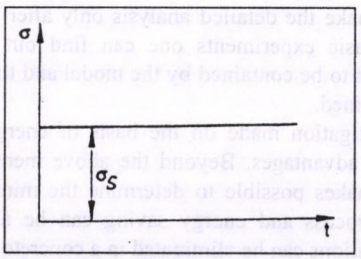

Figure 8
σ-t diagram of a plastic element

such way

$$\sigma_S = \mu_S \sigma.$$

where μ_S is the friction coefficient inside the material structure.

Strain is only produced if the $\sigma > \sigma_S$ condition is satisfied.

The energy is given by equations

$\sigma \leq \sigma_S, \quad \varepsilon = 0, \quad W_S = 0$

$\sigma > \sigma_S \quad \varepsilon \to \infty \quad W_S = \int_{\varepsilon_S}^{\varepsilon} \sigma_S \, d\varepsilon$

W_H stands for the elastic energy which is regained completely while W_N and W_S are dissipated representing the irreversible part of the process.

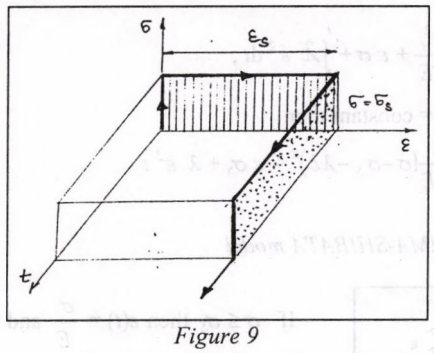

Figure 9
σ–ε–t diagram of the Saint Venant model

Two elements. Model of MAXWELL

The serial connection of elastic and viscous elements results in the Maxwell model. The total displacement is the sum of the displacements of the two components. Since both member is subjected to the same force by using the preceding results it can be written that

$$\sigma = \lambda\dot{\varepsilon} - R\dot{\sigma}$$

where

$$R = \frac{\lambda}{E}.$$

The accumulated energy is

$$W_M = W_H + W_N = \int_0^{\varepsilon_H} \sigma \, d\varepsilon_H + \int_0^{t} \lambda \, \dot{\varepsilon}_N^2 \, dt$$

$$W_M = \int_0^{\varepsilon_H} \sigma \, d\varepsilon_H + \int_0^{t} \lambda \left(\frac{\sigma}{\lambda}\right)^2 dt$$

$$W_M = \int_0^{\varepsilon_H} E \, \varepsilon_H \, d\varepsilon_H + \int_0^{t} \frac{1}{\lambda}[\sigma(t)]^2 \, dt$$

If $\sigma = \sigma_0 =$ constant, then

$$W_M = \frac{\sigma^2}{2E} + \frac{1}{\lambda}\sigma^2 t = \frac{\sigma^2}{2}\left(\frac{1}{E} + \frac{2t}{\lambda}\right)$$

The Maxwell model is a composite one, the strain changes with constant stress, by its nature.
One can easily follow that ratio of the reversible elastic and the irreversible absorbed, dissipated energy is determined by the ratio of the elastic and viscous energies. Such way an energy-dissipation efficiency factor is determined which can be written in the form of

$$\eta = W_N(t)/W_H(t)$$

KELVIN-VOIGT model

The model is composed by parallel connection of elastic and viscous elements. The stress and strain conditions are investigated using the same way as previously. The total load on the system is the sum of that on the elements. With small modifications the specific values are produced as

$$\sigma = E\varepsilon + \lambda\dot{\varepsilon}$$

which is the stress for the case of $\varepsilon = \varepsilon_0 =$ constant.

$$\sigma = E\varepsilon_0 = \text{ constant.}$$

The equation obeying the condition shows that the deformation reaches the value belonging to the given stress state with a time delay only. This phenomena is the creep explained with the internal friction of the material because it hinders the sudden change to a new equilibrium state.

The material equation is

$$\sigma = E\,\varepsilon_H + \lambda\,\dot{\varepsilon}_N$$

While the energy is

$$W_K = \int_{\varepsilon_0}^{\varepsilon_H} \sigma \, d\varepsilon_H + \int_0^{t} \lambda \, \dot{\varepsilon}_N^2 \, dt$$

$$W_K = \left[\frac{1}{2}E\varepsilon^2\right]_{\varepsilon_0}^{\varepsilon} + \int_0^{t} \lambda \left[\frac{E}{\lambda}\left(\frac{\sigma_0}{E} - \varepsilon_0\right)e^{-\frac{E}{\lambda}t}\right]^2 dt =$$

$$\frac{E}{2}\left[\frac{\sigma_0}{E}\left(\frac{\sigma_0}{E} - \varepsilon_0\right)\varepsilon^{-\frac{E}{\lambda}\tau}\right]^2 \frac{E\varepsilon_0^2}{2} + \left[-\frac{E}{2}\left(\frac{\sigma_0^2}{E^2} + \varepsilon_0^2 - 2\frac{\varepsilon_0\sigma_0}{E}\right)\varepsilon^{-\frac{2E}{\lambda}\tau}\right]_0^{\tau} =$$

$$\frac{E}{2}\left\{\left[\frac{\sigma_0}{E}\left(\frac{\sigma_0}{E} - \varepsilon_0\right)e^{\frac{E}{\lambda}t}\right]^2 - \left(\frac{\sigma_0^2}{E^2} + \varepsilon_0^2 - 2\frac{\varepsilon_0\sigma_0}{E}\right)e^{-\frac{2E}{\lambda}t} + \frac{\sigma_0^2}{E^2} + \varepsilon_0^2 - 2\frac{\varepsilon_0\sigma_0}{E}\right\}$$

In the case of Kelvin-Violet model it is again practicable to follow the procedure used formerly If the stress versus time function is known and constant according to the figure, the variation of the strain in time – the increase of the ε – is considerable i.e. creep is produced. While the load relief the inverse process called relaxation takes place. As a result of the load relief the initial situation is not restored. This is because the viscous element absorbs a part of the energy. This proportion of energy is represented by the prism bounded by the dashed line.

THREE ELEMENT MODELS

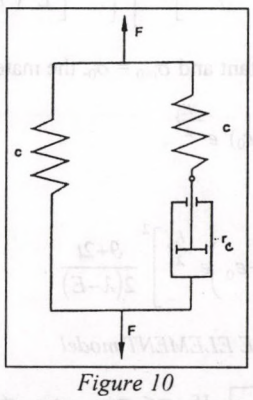

Figure 10
Poyinting-Thomson model

POYNTING-THOMSON model

In fact the model contains a Maxwell model and a parallel elastic element. In parallel elements the load on the system is the

sum of the loads in the parallel elements. Utilising the preceding results and introducing specific values one obtains the equation

$$\sigma = E\varepsilon + \lambda\dot{\varepsilon} - R\dot{\sigma}\,.$$

If $\varepsilon = \varepsilon_0$ = constant it changes to the form

$$\sigma = E\varepsilon_0 - R\dot{\sigma}$$

which differs from the Maxwell model only by the $E\,\varepsilon_0$.

The material equation is

$$\sigma = E\,\varepsilon + \lambda\,\dot{\varepsilon} + \vartheta\,\dot{\sigma}$$

The energy accumulated in the course of elongation is

$$W_{PT} = W_H + W_M = W_{H1} + W_{H2} + W_N$$

$$W_{PT} = \int_{\varepsilon_0}^{\varepsilon}\sigma_1\,d\varepsilon + \int_{\varepsilon_0}^{\varepsilon_2}\sigma_2\,d\varepsilon + \int_0^t \mu_2\,\dot{\varepsilon}_N^2\,dt$$

If $\sigma = \sigma_0$ = constant and $\varepsilon_{t=0} = \varepsilon_0$, then the energy W_{PT} is

$$W_{PT} = \int_{\varepsilon_0}^{\varepsilon}\sigma_1\,d\varepsilon + \frac{\sigma_2^2}{2c_2} + \frac{\sigma_2^2}{\mu_2}t =$$

$$= c_1\int_{\varepsilon_0}^{\varepsilon}\varepsilon\,d\varepsilon + \frac{(\sigma_0 - c_1\varepsilon)^2}{2c_2} + \frac{(\sigma_0 - c_1\varepsilon)^2}{\mu_2}t$$

$$= c_1\left[\frac{\varepsilon^2}{2}\right]_{\varepsilon_0}^{\varepsilon} + (\sigma_0 - c_1\varepsilon)^2\left(\frac{1}{2c_2} + \frac{t}{\mu_2}\varepsilon_0\right).$$

If $\sigma = \sigma_0$ = constant then

$$\varepsilon = \frac{\sigma_0}{E} - \left(\frac{\sigma_0}{E} - \varepsilon_0\right)e^{-\frac{E}{\lambda}t}$$

Substituting the material constants back one gets

$$c_1 = E, \qquad \left(1 + \frac{c_1}{c_2}\right)\mu_2 = \lambda\,, \qquad \frac{\mu_2}{c_2} = \vartheta\,,$$

and then using that the energy is expressed by

$$W_{PT} = \frac{E}{2}\left\{\left[\frac{\sigma_0}{E} - \left(\frac{\sigma_0}{E} - \varepsilon_0\right)e^{-\frac{E}{\lambda}t}\right]^2 - \varepsilon_0^2\right\} + \left\{\sigma_0 - E\left[\frac{\sigma_0}{E} - \left(\frac{\sigma_0}{E} - \varepsilon_0\right)e^{-\frac{E}{\lambda}t}\right]\right\}^2 \frac{\vartheta + 2t}{2(\lambda - E\vartheta)}$$

If $\varepsilon = \varepsilon_0$ = constant and $\sigma_{t=0} = \sigma_0$, the material equation is

$$\sigma = E\,\varepsilon_0 + (\sigma - E\,\varepsilon_0)\,e^{-\frac{E}{\lambda}t},$$

and the energy

$$W_{PT} = \frac{E\varepsilon_0^2}{2}\left[\left(\frac{\sigma_0}{E} - \varepsilon_0\right)e^{-\frac{E}{\lambda}t}\right]^2 \frac{\vartheta + 2t}{2(\lambda - E)}\,.$$

PARALLEL, THREE ELEMENT model

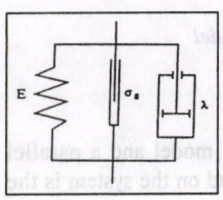

Figure 11
Parallel three element model

If $\sigma \le \sigma_S$, $\rightarrow$ $\varepsilon(t) = 0$, $\rightarrow$ $W_{P3} = 0$

If $\sigma > \sigma_S$ then the material equation is:

$$\varepsilon = \frac{\sigma - \sigma_S}{E}\left(1 - e^{-\frac{E}{\lambda}(t - t_0)}\right).$$

The energy

$$W_{P3} = W_H + W_S + W_N$$

$$W_{P3} = \frac{\sigma_H^2}{2E} + \varepsilon\,\sigma + \int_0^t \lambda\,\dot{\varepsilon}^2\,dt\,,$$

If $\dot{\varepsilon}$ = constant then

$$W_{P3} = \frac{1}{2E}(\sigma - \sigma_S - \lambda\dot{\varepsilon})^2 + \varepsilon\,\sigma_S + \lambda\,\dot{\varepsilon}^2\,t\,.$$

MURAYAMA-SHIBATA model

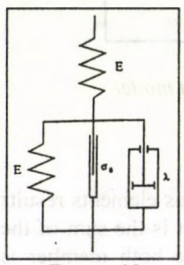

Figure 12
Murayama-Shibata model

If $\sigma \le \sigma_S$ then $\varepsilon(t) = \frac{\sigma}{E}$ and the material equation is given by the Hooke model simply.

$$\sigma = E_1\,\varepsilon_H$$

When the accumulated energy is

$$W_{MS} = W_H = \int_0^{\varepsilon_H}\sigma\,d\varepsilon_H.$$

If $\sigma > \sigma_S$ then the material equation is:

$$\varepsilon = \frac{\sigma}{E_1} + \frac{\sigma - \sigma_S}{E_2}\left(1 - e^{-\frac{E_2}{\lambda}(t - t_0)}\right).$$

The energy expression

$$W_{MS} = W_{H1} + W_{H2} + W_S + W_N$$

$$W_{MS} = \frac{\sigma^2}{2E_1} + \frac{(\sigma - \sigma_S)^2}{2E_2} + \varepsilon_2\,(\sigma - \sigma_S) + \int_0^t \lambda\,\dot{\varepsilon}_2^2\,dt\,,$$

If the speed of the specific expansion is constant, i.e. $\dot{\varepsilon}$ = constant, then

$$W_{MS} = \frac{\sigma^2}{2E_1} + \frac{(\sigma - \sigma_S)^2}{2E_2} + \varepsilon_2\,(\sigma - \sigma_S) + \lambda\,\dot{\varepsilon}_2^2\,t\,,$$

$$W_{MS} = \frac{\sigma^2}{2E_1} + \frac{\sigma - \sigma_S}{2E_2}[(\sigma - \sigma_S) + 2] + \lambda\,\dot{\varepsilon}_2^2\,t\,,$$

If $E = E_1 = E_2$ then

$$W_{MS} = \frac{1}{2E}\{\sigma^2 + (\sigma - \sigma_S)[(\sigma - \sigma_S) + 2]\} + \lambda\,\dot{\varepsilon}_2^2\,t\,,$$

The procedure applied herein utilises the independency principle of forces and compiles the energy balance based on the partial solution. Based on the detailed elaboration of the material equations of the basic elements and the two element basic models the previous results were only used to analyse energy conditions.

Now let us investigate the phenomena in the case of load application and the repeated load.

With Hooke model the result is the same as that of the basic element, since the time history is derivated from the condition σ_0 = constant. This is actually satisfied with $\sigma = \sigma(t)$ if ε = constant. When analysing the invested energy, one can see that the energy can be regained without loss after any t time, the process is reversible.

Built upon the simple basic cases the σ - ε - t functions can be produced for almost any type of model and fixing t = constant, σ - ε pairs are obtained so it is enough to fix those values. One should not forget about the aim of the process which is the determination of energy balance by analysing the effect and answer functions.

For a complete analysis it is necessary to know the material constants, but the determination of the material constants may be possible in an indirect way. The strain energy can be attached to any state using the absolute value or specific value belonging to unit volume or mass. The technique elaborated for the different elements is applicable to describe the density to time functions grain or stem material bulks in the case of single or repeated loads.

The physical meaning of the specific characteristics can be summarised as it follows

- $\sigma \rightarrow p$ the value of the stress σ is the vertical intensity of the distributed contact force system, one can consider it as an average pressure.
- $\dot{\sigma} \rightarrow$ gives the information how long the formulation $\sigma(p)$ takes and means the load application rate.
- $\varepsilon \rightarrow$ is the specific deformation or strain of the element given by the relevant model. Considering the whole region the surface is the important as the sink of this accounts for the volume decrement caused by the residual strain.
- $\dot{\varepsilon} \rightarrow$ is due to the intensity, efficiency or rate of the volume reduction
- $\sigma_S \rightarrow$ is the limit stress, above which residual strain is formed and energy loss will occur.

As the process is time dependent an effective compaction can be achieved if the value of σ stress or the proportional contact pressure is high enough i.e. the $\sigma > \sigma_S$ is satisfied. The process is relatively slow and one should allow enough time for the effect to spread vertically and sidewise to form favourable condition for compaction. In this case it is a natural goal to achieve as much dissipated energy as possible so that the dissipated energy part would ensure the appropriate compaction.

References

1. COOLIDGE : Proc. SESA 6 (1), 74, 1948.
2. GELENCSÉR, E.: Description of stress and strain condition on the basis of rheological models. Bulletin of the University of Agricultural Sciences Gödöllõ, 1986/1. 172 p. 149-160.p.
3. HUSZÁR, I. - GELENCSÉR, E.: Reológiai mérések optikai feszültségvizsgálattal. GÉP. XXVI, 1974/9. 332-338 p. (*Rheologycal measurements by means of photoelasticity*, in Hungarian)
4. HOFFMANN, H. - HUTH, H. V.: Zur Untersuchung des Spannungs-DeformationsVerhalten von Ackerböden, Agrartechnik,4.
5. MURAYAMA, S. - SHIBATA, T.: Flow and Stress Relaxation of Clays. Proc. of International Union on Theoretical and Applied Mechanics Rheology and Soil Mechanics. Grenoble 1964. Springer Verlag, 1966.
6. MYLONAS : Proc. 7th. Intern. Congr. Appl. Mech. 4. 1948. 165 p.
7. PINDERA : Remarks on Properties of Photoviscoelastic Model Materials. Experimental Mechanics 6 (7) 375-380, 1966.
8. REINER, M.: Rheologie. Handbuch der Physik. Band. VI. (Elastizität und Plastizität) Springer Verlag, Berlin 1958.7
9. THAMM, F.- LUDVIG, GY.- HUSZÁR, I.- SZÁNTÓ, I.: A szilárdságtan kísérleti módszerei. Műszaki Könyvkiadó, Budapest, 1968. (*Experimental methods of stress analysis*, in Hungarian)

CHANGING OF THE MOISTURE TRANSMITTING SURFACE OF ALFALFA STEMS DURING DRYING

Dr. K. Kacz - Dr. M. Neményi - T. Sándor
PANNON Agricultural University, Mosonmagyaróvár

Preliminaries

In 1994 thin layer scale-model experiments started in order to study the drying properties of alfalfa in the Department of Mechanization and Environmental Technology of the Mosonmagyaróvár Faculty of Agriculture, Pannon University of Agricultural Sciences.

The experiments were continued in 1995 and 1996.

It was found also in the thick layer alfalfa drying experiments, the chaff length influences the drying properties (**Kacz** 1983). The literature sources are deficient and are not uniform in judging it. It is well known that the leaves and stalks of the alfalfa dry in different ways. **Farkas** (1989) also dealt with the question without examining the effect of chaff length.

In the scale-model experiments the main track was on the drying of the different length parts. The aim was to derive the figures of the influence of chaff length, and to get familiar the basic parameters, which makes possible to model heat and material transport processes.

It is indispensable to know the mass flow density values for modelling heat and material transport. In order to determine them it was planned to examine the change of the size and the moisture transmitting surface in the 1996 year experiments.

Experiments, material and method

The experimental material was got from the Experimental Plant Production Court of the Faculty. The of the stem parts was chopped by a sharp tool. the investigated chaff length was 60, 30 and 15 mm.

In 1996 the experiments were made on 35-60 C temperature and with approximately identical initial moisture content. In the experiments alfalfa of unblown state and of rather ripen cellular structure stalks was used.

Drying experiments were made by an MB-200 type fast-determining moisture measuring apparatus. The measurement of the dry material content was made after 24 hours postdrying on 105 C. The accuracy of mass measurement was 0.01 g.

In order to determine the change of size and surface the major and minor diameters of the chopped stalks were measured using a calliper 0.02 mm accuracy. These data were used in the calculation of the mean diameter the lateral and the end surface areas. These measurements were carried out before and after the measurements, too.

An additional series of experiments were performed to find out how much the artificial vision may help recording the extent of the size and surface changes during moisture loss process. The experiments were conducted with the experimental apparatus assembled in the Department of Mechaniztion and Environmental Technology. The experimental measuring setup consists of a 486 CPU personal computer with VIDEO-BLASTER digital image processing card and a CCD industrial camera of type Hitachi KPC 550.

Video record of the specimens located separately on the drying plates was taken at the beginning of the experiments and during the experiments in every hours. To store and evaluate of the records a software called AGROPIC developed on the department was used. The software had the task to get and evaluate the digitised picture. It made possible to determine the main dimensions, such as length, width, projected area.

Results

The results of the investigations have been reported several times (**Kacz et. al.** 1995, **Neményi et. al.** 1996, **Kacz - Sándor** 1996). The results appertained mainly to narrow parameter domain and moisture transmitting surface assumed to be unchanged.

In the 1996 experiments the dimension and surface changes taken place during drying were also measured. Therefore it was possible to determine the specific fluid loss surfaces and the mass flow density values as functions of the moisture content.

The cross section of alfalfa stalks has usually elliptical cross sections thus both the major and minor diameters were measured and the average values were used with the individual specimens. The manual measurements performed before and after the experiments showed that not only shrinkage but flattening also took shape. The changes of the minor diameters exceeded tha of the major diameters by 10-15 % (*figure 1*). The scatter of the data can be explained by the aberrations in the stalk length, material quality and the starting moisture content. The alfalfa specimens in the experiments had 60, 30 and 15 stalk lengths, two different moisture states i.e. starting fluid content. (The mark 1 relates to more ripe, cellular plant while the mark to is for unblown alfalfa.)

The changes of the lateral and end surfaces versus moisture content is depicted in *figures 2* and *3*. The figures shows those values measured and determined by the method of artificial vision. The drying temperature of those experiments was 60 C. The shrinkage and surface degradation presents itself very strongly in the beginning of the drying process. Around w=20-30 % the material practically ceases to shrink.

The influence of the stalk length is experienced in a larger extent with the end surfaces and at higher moisture content. It is well recognisable in the *figure 4* for identical material qualities.

As for the comparison the dimension and surface change values obtained by artificial vision and manual methods a differences were found primarily at lower moisture content values and shorter stalk length. This is explained with the errors of the two dimensional measurements. In the course of shrinkage and flattening the straight and short stalk fragments can rotate, so that the projected are recorded by the camera may even increase in a small extent.

Figures 5 and 6 show the changes of the lateral and end surfaces related to the dry material based relative moisture content. At the cellular structure alfalfa the specific lateral surface should be treated separated while it is not necessary with the end surfaces. As the specific end surface changes in an inverse proportion to the stalk length, the general relationship was determined for values corrected to 30 mm length. At the different sizes it is necessary to multiply by the value 30/l.

The specific moisture loss (mass flow density) values were calculated by means of moisture loss and dry material mass values as well as the regression functions shown in *figures 5* and *6*. The changes in the mass flow density values of the lateral and the end surface mass flow are drawn in *figure 7* and *8*, respectively.

Conclusions

- During the drying of the alfalfa stalk considerable shrinkage and flattening is experienced due to the moisture loss. The lateral and the end surfaces was reduced to 70-80 % and to 50-65 % of the original values, respectively. In the case of lateral surface the cellular stalk alfalfa should be treated separately.

- The specific surface values of mass flow density related to 1 kg dry material mass can be well approximated by regression lines. The mass flow density value at the end surfaces is one order higher than that of the lateral surface.
- The method of two dimensional artificial vision can be used only with approximate accuracy. More accurate results are expected from the three dimensional measuring methods what are to be tried in this year.

The above results gives possibilities to simulate the process of alfalfa drying more accurately and to study the topic with finite element method.

References

1. FARKAS, I. (1989): The influence of the material properties on the drying process of crop. Polish Academian Sciences, Warsow,1989. No. 378. 29-34.p.
2. KACZ, K. (1983): Az előmelegített levegõs szellőztetéses lucernaszárítási modellkísérletek összefoglaló értékelése. Mosonmagyaróvári Mezõgazdaságtudományi Kar Közleményei, Vol. XXV. No.3.119-133.p. (*Summarising evaluation of preheated air ventilation alfalfa drying experiments*, in Hungarian)
3. KACZ K. - NEMÉNYI M. - CZABA I. (1995 A): A szecskahosszúság hatása a lucernaszár száradási tulajdonságaira. MTA-AMB Kutatási és Fejlesztési Tanácskozás. Gödöllő,1995. jan.17-18. 422-430.p. (*The effect of the chaff length on the drying properties of alfalfa stalk*, in Hungarian)
4. KACZ K. - SÁNDOR T. (1996): A lucernaszár száradási tulajdonságainak változása a vízleadás során. XXVI. Óvári Tudományos Napok. Mosonmagyaróvár,1996. szept. 25. 900-906.p. (*Changing of the drying properties of the alfalfa stalk during moisture loss*, in Hungarian)
5. KOVÁCS A. - JANCSÓK P. - NEMÉNYI M. (1995): Kukoricavonalak és hibridek száradási tulajdonságai. MTA-AMB Kutatási és Fejlesztési Tanácskozás. Gödõllõ,1995. jan.17-18. 296-308.p. (*Drying properties of maize types and hybrids*, in Hungarian)
6. NEMÉNYI M. - KACZ K. CZABA I. (1996): A lucerna szárítás hõ- és anyagtranszport folyamata. MTA-AMB Kutatási és Fejlesztési Tanácskozás. Gödöllõ,1996. jan.16-17. (*Mass and heat transport process of alfalfa drying*, in Hungarian)

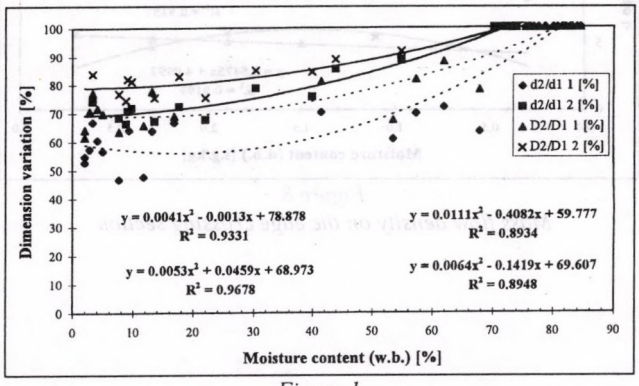

Figure 1
Variations of the Alfalfa stem diameter during drying (1. emptied stem)

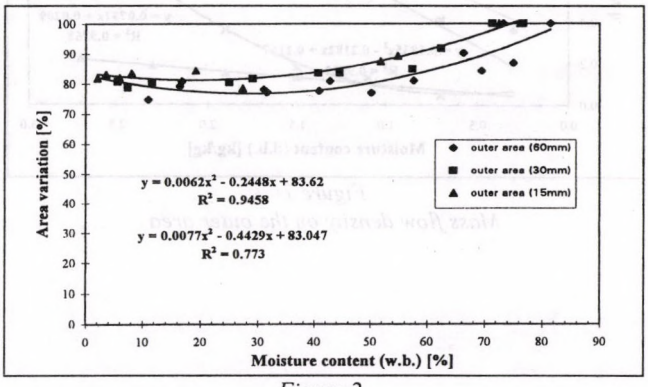

Figure 2
Outer area of stem during drying

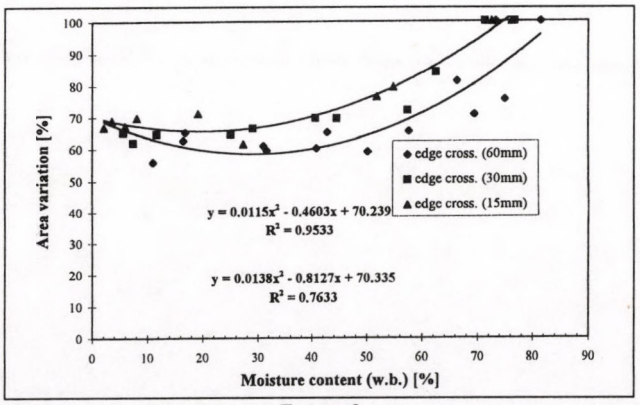

Figure 3
Edge crossing section variation during drying

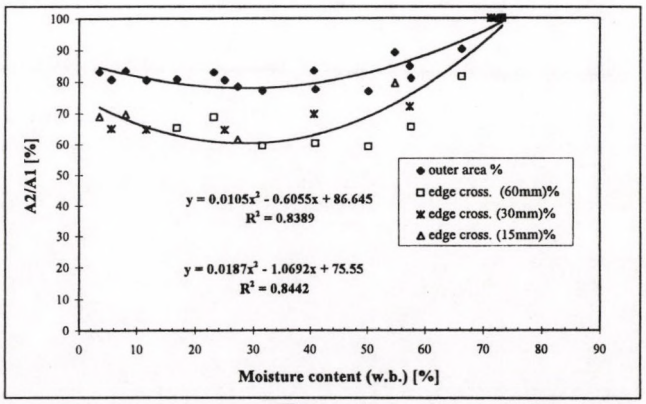

Figure 4
Edge crossing section change as a function of stem lenght

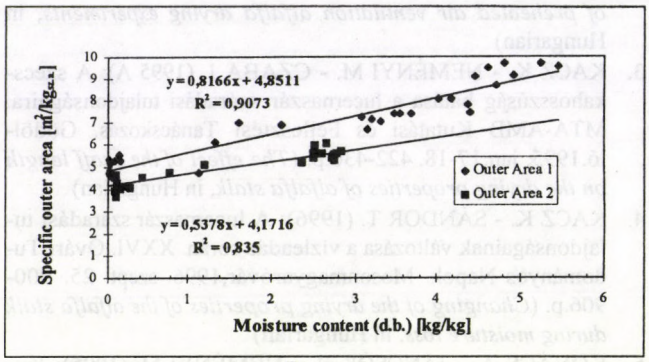

Figure 5
Decreasing of specific area of the edge cross section during drying (1. hollow stem)

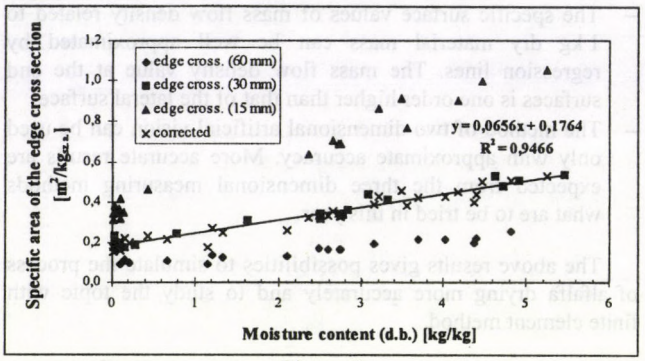

Figure 6
Decreasing of specific area of the edge cross section during drying

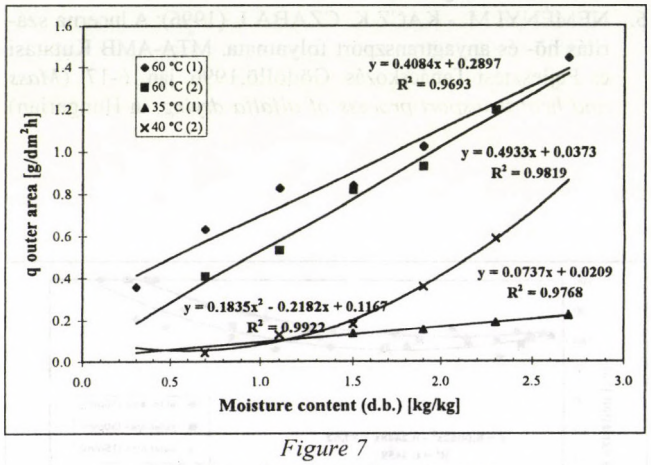

Figure 7
Mass flow density on the outer area

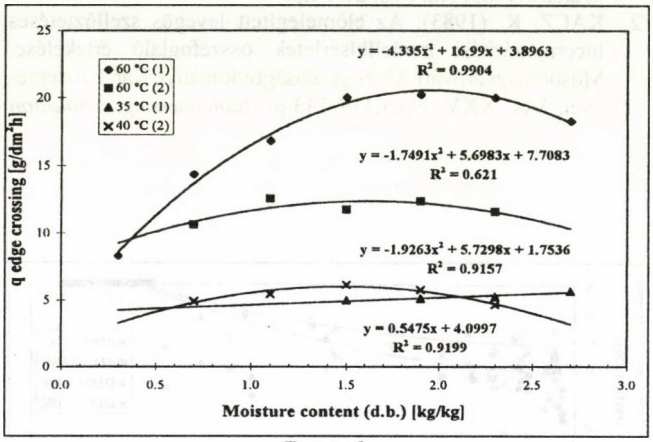

Figure 8
Mass flow density on the edge crossing section

EXAMINATIONS RELATED TO SOME IMPORTANT MECHANICAL CHARACTERISTICS OF THE FODDER PELLETS

Dr. J. Csermely - Gy. Komka - Dr. M. Herdovics – Dr. Z. Bellus
Hungarian Institute of Agricultural Engineering, Gödöllő

Goal of the research

In the course of the research work (OTKA: T 013144) fodder pellets, produced in the Fodder-Mixing Plant of the Bábolna Fodder-Insdustry Ltd. and in the laboratory of the HIAE, were tested in order to gain exact answers to those questions that had arisen connected with technologic and running of fodder production. In connection with the pellet producing there were two very important special subjects that we had to take into consideration, namely:
– rate of dust and chippings during the process, and
– stability of pellets produced.

Completing the examinations of the traditional pelleting process, research works were extended to the examination of the characteristics of the pellets produced from expanded basic material.

Material and method

There are more well known methods to determine the stability of shape of the pellets. Among them determination of shredding index is the most in general use because determination method of it can follow mostly the stress during transport. For the determination of the crumbling force a KAHL type measuring device was applied.

Abrasive resistance of the pellets is influencing by different factors. These factors can be divided into three main groups: characteristics of the fodder, - pelleting machine - and the technologic features of pelleting.

In the examinations BAA type layer compound feed was used. In addition to the essential components (wheat, corn, alfalfa meal, fodder lime and other supplements) this feed was differed from others as for the rate of wheat and corn in it. (*table 1*)

Table 1
Composition of the examined feed (%)

	Denomination of feed		
	Feed with higher % of wheat	Original	Feed with higher % of corn
Wheat	60.53	50.00	13.00
Corn	8.00	18.00	51.75
Soya flour (46 %)	11.80	22.00	17.10
Soya, Bolyi FF type	2.00	-	3.00
Alfalfa meal, 1.st class	2.50	4.50	2.50
Fodder lime	8.50	1.50	6.50
KBP 506-MN	4.00	4.00	4.00
RHODIMET 88	0.17	-	0.15
ZINC BACITRACIN	-	-	2.00
CEREASE	1.00	-	-
BIOLYSINE	0.50	-	-
Fat	1.00	-	-

From among the factors that influence the shredding and the resistance to rupture of the pellets the followings were determined:
– formation of the rate of chippings during pelleting process,
– influence of the composition of the mixed fodder,
– grain size of the mixed fodder,
– effect of change in pressure of the expander.

Beside the relation between the shredding index and the crumbling force according to the above mentioned variables, connections related to one another [K = f (PD)] also were determined.

Results

As it is known there is a connection between the **rate of chippings** during pelleting and the PD index. The goal was to point out the positive effect of the expanding pressure and this intention was successful as it shown in *figure 1*. As can be seen, the rate of chippings was considerable influenced by the composition of the feed and increasing the expanding pressure (from 0 bar to 30 bar) the rate of chippings could be decreased by 20-45 % respectively.

Analysing the connection between the **average grain size** *(figure 2)* and the expanding pressure [d_{50} = f (p)] it could be stated that increasing the pressure, the 8 mm of average grain size of the mixture at 0 bar would also be increased by 1.45-1.7 mm at 30 bar pressure

The **shredding index** increased in relation to the expanding pressure [D = f (p)]. Value of it was above 9,8 at the feed that contained higher percent of wheat. In the case of the feed with higher per cent of corn value of the PD index just reached the 8.0-8.5 limit value that could be declared as acceptable. Changes of the PD index can be followed in *figure 3*.

Connection between the **crumbling forces** that characterizes the **resistance to rupture** and the expanding pressure [K = f (p)] is shown in *figure 4*. This connection is probably found in home practice at first. It could be stated, just as in the case of the shredding index, that better results could be obtained using feed with higher per cent of wheat. Though the crumbling force increased by 1.7-2.0, some unfavourable features of feed based on corn were also noticable.

Searching for the connection between the crumbling force and the shredding index, two graphs were drawn. The mentioned features were plotted against the expanding pressure [K = f (PDp)] *(figure 5)* and the composition of the feed [K = f (PD;Ö)] *(figure 6)*. In the first case a considerable increasing in crumbling force could be observed by increasing the expanding pressure at the feed of higher per cent of wheat content in the range of PD 8-10 that was acceptable in practice. Increasing was the same at higher per cent of corn content but owing to the crumbling force of 55N, this kind of feed was ranked among the class of easily crumbling. In the second case, at a near constant 20-22 bar pressure, the tendency was the same. Crumbling force was characterized by 62-95N between the good PD index range of 8.5-9.2 and in relation to the kind of feed. Owing to the narrower PD index range a much steep increasing tendency was resulted in the connection.

Summary

On the basis of the examinations the following findings could be done:
– increasing in expanding pressure decreased the rate of chippings,
– suitable value of average grain size could be obtained at higher expanding pressure,
– increasing of expanding pressure resulted a favourable shredding index and higher crumbling force,
– increasing of crumbling force was directly proportional to the shredding index. This connection was more moderate in terms of expanding pressure than composition of the feed.

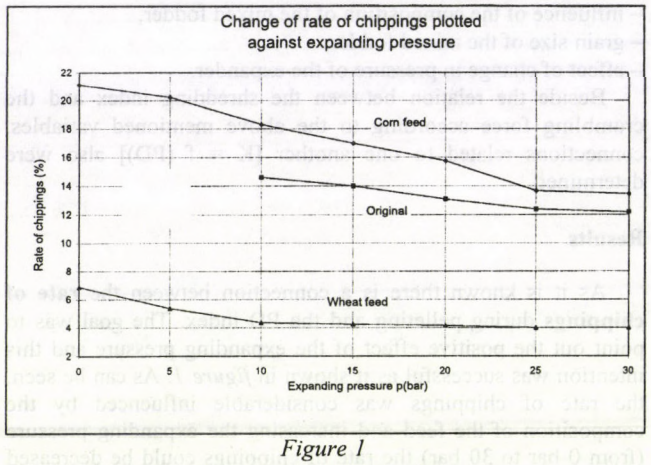

Figure 1
Expanding pressure p(bar)

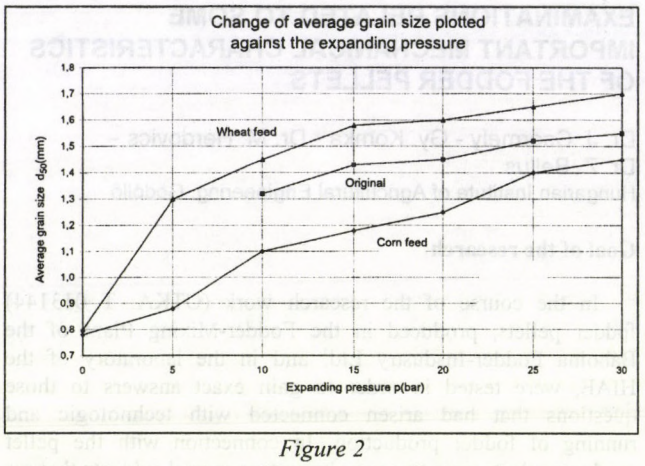

Figure 2
Expanding pressure p(bar)

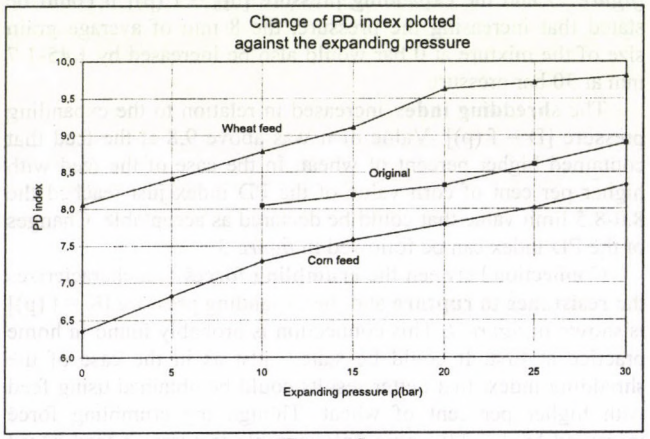

Figure 3
Expanding pressure p(bar)

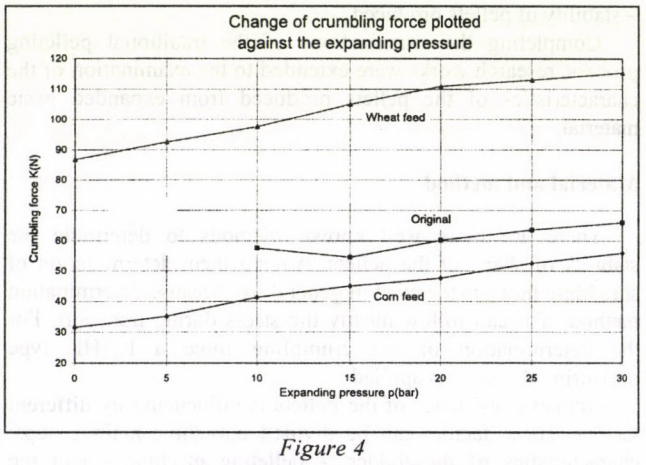

Figure 4
Expanding pressure p(bar)

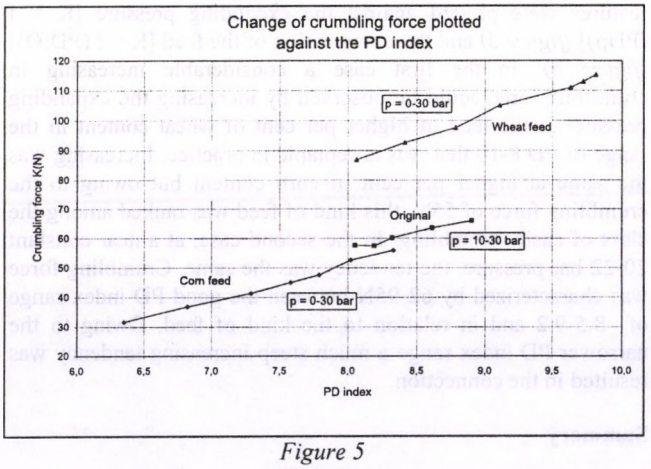

Figure 5
PD index

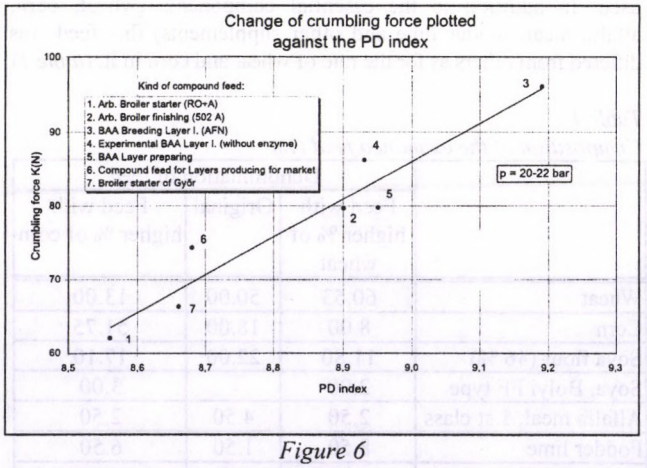

Figure 6
PD index

DIGITAL IMAGE PROCESSING FOR QUALIFYING CHOPPED PLANT BULKS

Dr. I. Szabó - L Kátai
University of Agricultural Sciences, Gödöllő

Introduction

With the wide spread of the high performance computers and the high quality video systems the Digital Image Processing (DIP) can be utilised even in such industry and economy fields were it seemed unimaginable earlier. The software and hardware tools what were only available in the military industry a few years ago, appear now in the civil utilisation and help the users at large (one can think of the evaluation of meteorology satellite photographs or the evaluation of quite sophisticated X-ray and tomograph pictures in the different therapies. In the special fields and processes the significance may differ but the application of DIP has the following advantages:

- high processing rate,
- elimination of subjective factors of natural vision of people (delusion, fatigue, etc.),
- higher resolution and sensitivity,
- theoretical possibility for automation of work elements that are hardly mechanizable.

At the same time from the aspect of economy, due to the high investment cost, the digital image processing can not be considered as a competitive solution in several low profitability industries. Description of chaffing quality with exact figures is extremely complex and complicated job, but it is very important for judging the operation from the aspect of processing and utilisation. The size (length and surface) distribution of chaff bulk is in the focus of attention.

How the composition, i.e. distribution of length and surface could be determined by means of image processing without individual manual measurements was the aim of the examination. The applicability can be evaluated by comparing to the results of traditional measuring method.

1. Principles, origination of the problem

One of the possible agricultural purpose applications is the determination of size distribution of chopped plant congregation. In the first step a photograph should be taken of the investigation objects and the picture obtained such way should be transformed in a form what the computer is able to process. The original analogue picture which can be treated as a continuous function $F(x,y)$. Using a sampling procedure a matrix

$$F(i, j)\ i,j=1, ..., n$$

where n is the number of points making the picture (pixels).

The individual pieces of the data in the matrix contain the colour codes (intensity parameters). In the case of monochrome pictures those values can contain the grey scale values, e.g. from 0 to 255 providing 8 bit digital storage capacity. On colour digitisation the codes are given by the three intensity values of the red, green and blue (RGB) colours (0-255 for red, 0-255 for green and 0-255 for blue). One can found out from the foregoing that a colour digitised picture needs three times larger storage capacity and a usual picture of 512 times 512 pixels with 3 times 8 bits colour capacity contains 800 kByte information.

The next and the most important step is the decomposition of this quite large set of data into two subsets of $F(i,j)$ pixels as they represent the background or a piece of chaff. In order to decompose the data matrix one should find such characteristics which makes possible to classify the points with the smallest error. If the background is practically chosen the objects can be simply separated on the basis of colours or grey scale.

2. Set up of the measuring device

The system is based on a 486 CPU IBM compatible personal computer which is able to accept video signal through its Video Blaster card. The shots are taken by VHS video camera. To achieve shadow-free pictures a bottom illumination object desk was used. The measuring setup is shown in *figure 1.*

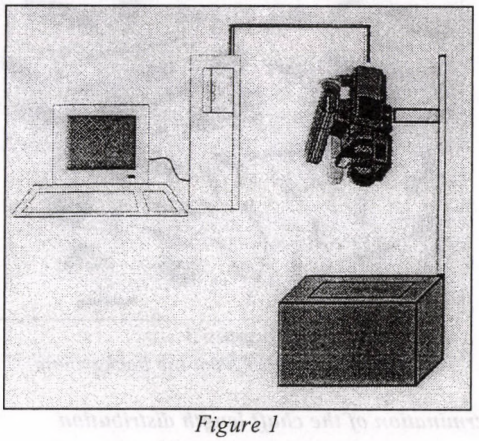

Figure 1
Measuring setup

3. Filling up the database

The first problem with the image processing occurs on the taking of the first picture. The chaff pieces should be put on the illuminated table in an order. They can not cover each other because the computer would handle them as single objects resulting in false values. The process is time consuming just as the manual measurement, but the lengthy operations of the manual measurement and classification are eliminated and the data will be available on magnetic storage device.

The steps of the measurements:

1. The picture of the arranged chaff samples is fixed, but for the later dimension reference the picture of a given length object should be also taken. This can be made with the chaff congregation or separately. The previous version was used by us and the reference was a paper strip of 20 mm length which can be well seen in *figure 2.* Such way it can be ensured that the same reference be used in the course of calculation independently of the actual camera alignment, focus distant which determines the apparent size of the object – chaff this case – on the picture.

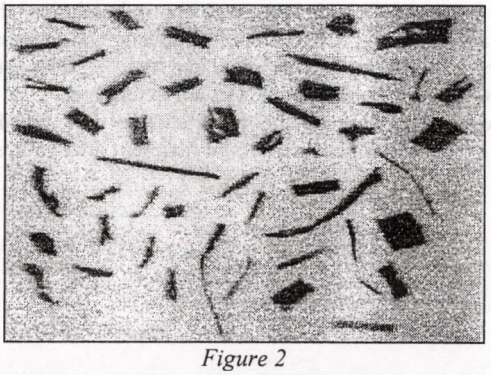

Figure 2
Image of the chaff sample

2. In the first stage the small contamination spots detected as objects but they do not belong to the chaff bulk (e.g. sand particles, small plant fragments) should be filtered out. The larger pieces what may be eliminated are filtered out in the calculations. After that the objects are separated from the background by the selection of the suitable threshold value. All after that the necessary measurements (largest distance between the two farthest point of object, circumference, area) can be carried out with the computer.

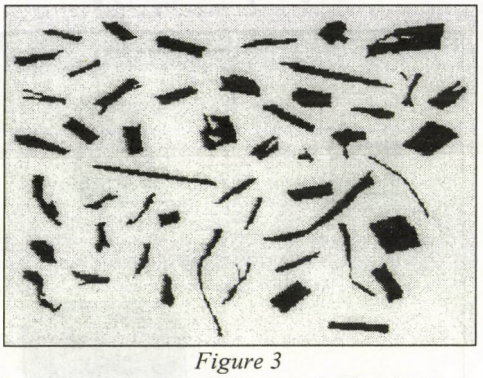

Figure 3
Objects separated from the background

4. Determination of the chaff length distribution

The largest distance of two points of object gives the length itself with a good approximation for thin chaff pieces, but for thicker rectangular shaped pieces it is larger. With some simplification the diagonal is measured. Provided in the following that the chaff elements are approximated by rectangles the diagonal dimension can be transformed to the longer size. It assumes the knowledge of the circumference of the object. Based on geometric considerations one can see, that if a circumscribed circle is fitted to the simplified chaff piece which has a radius equal to diagonal. And if the vertex of the rectangle is moved along the circle theoretically all the possible rectangle can be declared to the diagonal. Let the longer side of the rectangle b and the diameter of the circumscribed circle d and the angle made by them Having the values of diagonal length, circumference and angle α one can calculate the length of the rectangle (chaff):

$$K/2 = d(\cos\alpha + \sin\alpha) \Rightarrow \alpha$$

$$b = d\cos\alpha$$

As only the diagonal and the circumference is known an approximate calculation should be carried out for α and the value closest to the measured value should be chosen from the obtained half-circumferences. When α is known side length b can be calculated which is a good approximation of the chaff length according to the assumption. The length data transformed such way are arranged in histogram and by using the approach of Szendrõ the distribution parameters are determined.

The consideration of the chaff surface area failed in the length examination because lots of different area values can be ordered to a given length parameter (and vice versa), what makes the evaluation obscure or impossible.

On the other hand image processing offers rather good possibilities to examine the distribution of surface area, as accurate area calculation is possible which is rather cumbersome in other ways. The histogram of surface area distribution is similar to that of the length (*figure 4)* what brings up the demand of the independent utilisation.

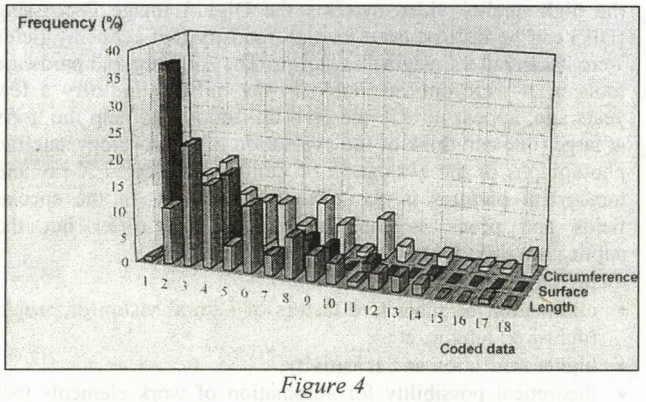

Figure 4
Comparison of length, surface area and circumference distributions of chaff congregation based on coded data

Summary

On the basis of experimental investigations it can be stated that the digital image processing is applicable to evaluate image information and it can supply reasonable results in agricultural circumstances, too.

As it is shown in *figure 5*, the data obtained by computer and manual processing can be compared and the distribution functions are very similar. It proves that the method is really applicable to qualify the bulk of plant eliminating the tiring work of manual selection and measurement. Moreover the evaluation is considerably sped up.

Although the tools improving the quality of processing significantly are rather expensive, the application shape and colour recognition – in general artificial vision – research in the agriculture is not questionable.

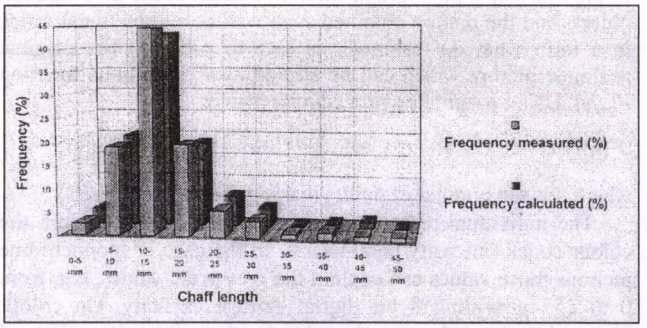

Figure 5
Function fitted to the length distribution of maize chaff

DEVELOPMENT AND INVESTIGATION OF VIBRATION CHAFFING DRUM

Dr. P. Szendrő - Dr. E Szabó - Dr. J Nagy
University of Agricultural Sciences, Gödöllő

1. Introduction

Seven million tons silage base material is made yearly in Hungary which uses 4,5 kg/t average amount of fuel oil, 31.500 ton total what is almost one half of the total fuel requirement of the all self-propelled machines, so that it is a significant factor of the agricultural energetics.

Theoretical research on the theory of self-propelled chaffing machines with special attention to the energetic conditions has been being conducted for several decades in the Institute of Machine Theory of Gödöllő University. The current experimental and product developing work is based on this.

work is based on this.

In the framework of the development the performance of the chaffing drum is intended to be reduced by using a new drum of vibration principle which applies sliding cut. During the chaffing process the blade moving along the edge penetrates easier into the green material which saves not only energy but the lifetime of the blade will also increase due to the reduced edge load.

In the development process the new principle experimental equipment was made. The drum dimensions of the most widely used chaffing machines even then. In the first stage of the development (1995) still the control of blade-holder elements was investigated. After the encouraging results in the second phase (1995) the new chaffing drum with blades was adapted to a widely used self-propelled chaffing machine (Claas Jaguar). The extensive laboratory examination is bieng made with this machine. This paper reports the results of the laboratory investigations achieved so far.

Szolnok Mezőgép Rt. the joint developer would like to supply the most significant self-propelled chaffing machine manufacturers with the product resulted by the development work.

2. Preliminaries, goals

The harvest and treatment of stem materials is a several decade highlighted area of the research on the Department of Agricultural Machine Theory. In the field of self-propelled chaffing machines already several patents, numerous publication and scientific thesis indicates the results. The theoretical bases to the current development are summarised in the following.

Theoretical considerations

According to the results discovered in the cutting energetic investigation of maize stalk:

„Based on the laboratory experiment of comminution by means of maize cutting pendulum, one can state the specific energy need of chaffing are mostly influenced by the cutting angle and the edge angle of cutting blade from the aspect of cutting edge design, by the inclination angle of stalk from the aspect of the relative position of the edges and the maize stalk, by the edge directional velocity component of cutting edge from the aspect of kinematics characteristic of cutting. By the practical selection of these characteristics there is a possibility to accomplish more economic energetic chaffing equipments."

The effect of the variation of the edge directional velocity component is shown in *figure 1*.

Independently of the cutting angle of the cutting blade the specific cutting energy makes a convex aggregate of curves in the function of. The minimum points of the curves are in the interval of 0.5-0.8 m/s interval of edge directional velocity component (while the average of the circumferential velocity of the cutting blade was 9 m/s).

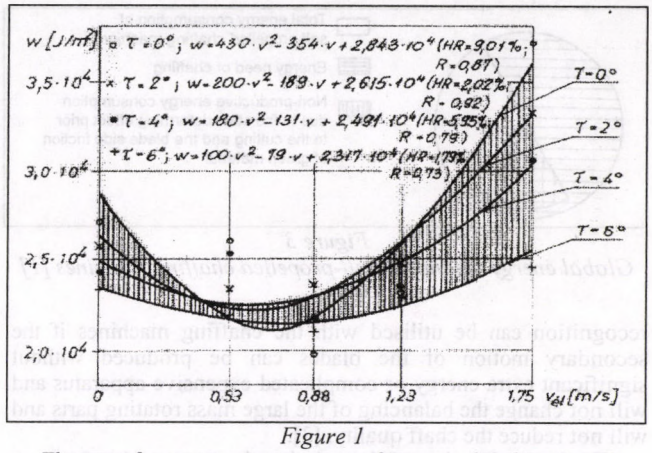

Figure 1

The specific energy requirement of versus edge directional velocity component for cutting blades adjusted in different cutting angles
*(τ - the cutting angle of cutting blade) [1]**

The explanation to the energetic phenomenon is that the friction coefficient of the contact surfaces exposes a decreasing tendency with increasing relative velocity between the surfaces (*figure 2*). A further reason for the reduced cutting energy need is that the cutting edge acts perpendicularly to the penetration direction against the friction resistance and so the preceding deformation is eliminated [1].

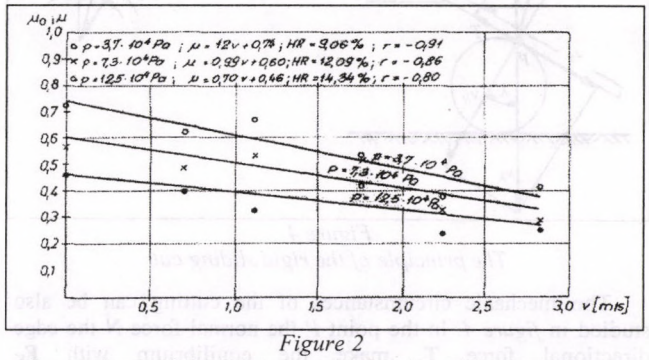

Figure 2

*The tendency of the friction coefficient (μ_0, μ) between the cut surface of maize stalk and steel plate as a function of the surface compression (p) and the displacement velocity [1]**

The machine design has already exhausted almost all the listed possibilities apart from the edge directional motion of the cutting blade, which is not a simple task in the case of large mass and high revolution chaffing drums. So all the modern chaffing machine applies slitting. It means that the blades mounted on the immovable and moving blades makes a favourable 8-15° angle during the cutting. However the thorough investigation of the slitting process shown that the energy loss is about 25-30% even in the case of the most favourable blade alignment what comes from the unnecessary compacting between the blades prior to the cutting and from the superfluous friction between the separated plant pieces and the side surfaces of blades. At the same time factually even the order of that non-productive energy is not indifferent, since the high mass flow (70-150 t/h) self-propelled chaffing machines require the application of very high power (150-250 kW) internal combustion engines with considerable fuel consumption. The specific energy need of the chaffing-depending on the construction of implement, fodder type and ripe state is 0.8-1.6 kWh/t.

Both the experimental and the practical experiences verified that slitting with the small extent edge directional motion of any blade will significantly reduce the superfluous energy consumption. Such a solution will also increase the useful lifetime of the blades due to reduced edge load. Of course, this

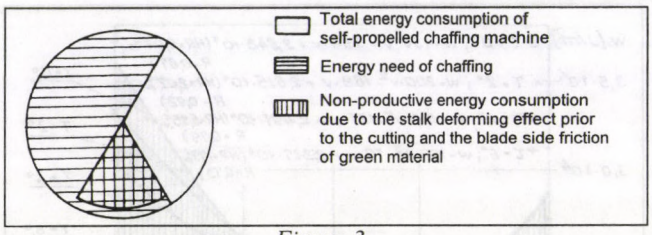

Figure 3
Global energy balance of self-propelled chaffing machines [1]

recognition can be utilised with the chaffing machines if the secondary motion of the blades can be produced without significant extra energy or complicated expensive apparatus and will not change the balancing of the large mass rotating parts and will not reduce the chaff quality. [3].

To the explanation of the solution, let us consider *figure 4.* The resultant $\bar{v}_K$ velocity of point P can be decomposed into two components such as $v_N = v_K \cos\lambda$ normal to the edge and $v_T = v_K \sin\lambda$ parallel to the edge which means that the blade moves relative to the material during cutting.

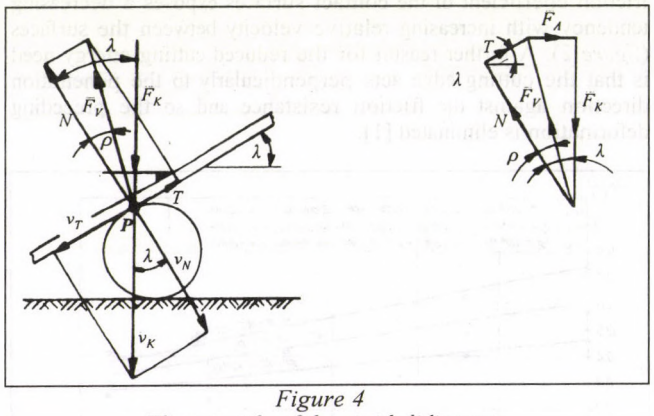

Figure 4
The principle of the rigid sliding cut

The mechanic circumstances of the cutting can be also studied in *figure 4.* In the point P the normal force **N** the edge directional force **T**, make the equilibrium with $\mathbf{F}_K$ circumferential and $\mathbf{F}_A$ support forces. The support force is produced by the bearing. On the basis of the vector polygon one can write $F_K = N\cos\lambda + T\sin\lambda$ .From the motion friction $T = \mu N$, $F_K = N(\cos\lambda + \mu\sin\lambda)$. Because λ=constant, the variation of the circumferential force depends only on the friction coefficient and the normal force. The evident advantage of this arrangement to the so called shear with edges penetrating toward each other keeping parallel that the cutting energy requirement is lower. Until slitting begins, however, the plant layer compacting energy consumption is considerable (26-30 % of the total cutting energy need) [4].

The energy need – as it was proved earlier [1] – can be also reduced by superposing small amplitude edge directional vibration motion. This idea was accomplished by the equipment developed by the Institute in the eighties.

The apparatus – called multicator – utilise the principle of vibration, but fundamentally differs from the preceding similar devices. In this equipment the edge directional vibration is generated by the more or less intermittent operation of the feeder equipment, the fluctuating flow of the produce and the changing chopping energy need. The present development is different, the blade motion is forced.

3. Operational principle of the equipment

As a result of the past two years development work the principle of the vibration chaffing drum has been developed from that theoretical perception by which the motion of the blades parallel to the edge is practical. That motion is parallel to the axis of the driving shaft in our implement. When the chaffing blades move parallel to the driving shaft one should consider the dynamic equilibration of the mass forces. The displacements are controlled by two control device located inside the drum for each half of the drum.

By the design the forced motion blade chaffing drum replaces the drum of a traditional self-propelled chaffing machine. Such way the possibilities were rather restricted due to the available space and the given connection dimensions.

For structural reasons and more favourable slitting circumstances the following conditions were met at the formulation of the control grooves:

- 7.5 mm blade travel for half drum,
- 0.5 m/s edge directional velocity in the middle session of the displacement and
- minimal acceleration at the reversion places.

4. Laboratory measurements

The experimental chaffing drum was built in the chaffing machine and driven by an electric motor during the measurements.

With instrumental examinations the following parameters were determined:

- revolution speed of the drum shaft,
- the electric power needed by driving the drum,
- axial travel of blades,
- axial velocity of blades
- axial acceleration of blades
- vibration characteristics of the drum and the housing,
- the torque input on the drum shaft,
- the output torque on the drum shaft transmitted to power take-off.

The total electric power consumption of the adjustable revolution three-phase electric motor was measured with different revolution per minute values of the chaffing drum driven by v-belt. By the separate measurement of the power loss in the inserted resistance for changing the revolution and by making the difference the specific energy needed by the drum driving was determined. The measurement served first of all the comparison to the measurement to drum without blades.

More and more accurate information is obtained by gauge torque measurements. The input and output power need and their changes became known with high precision.

Simultaneously the instant axial motion of the blade was also recorded (the sensor was connected on the left end surface of the half-drum. From this the axial velocity and the acceleration characteristic can be determined in a correct way by differentiating the displacement function once and twice. To determine loads on the plate walls (drum housing) carrying the drum support bearings vibration sensors were used.

5. Evaluation of results

Based on laboratory functional sense perception and measuring examination it could be stated already in 1995 that the developed „VIBRO CUT" experimental chaffing drum is able to produce the planned effect. After mounting the blade holders and the blades (in 1996) the sensitivity to the axial unbalancing has slightly increased. The reason is the inaccuracy of the manufacturing technology the correction of which is on the way after completing the experiments.

The operation of the chaffing drum is slightly noisier compared to the original one. That is due to the more rotating parts and the application of the alternating motion, but it does not excess the value expected at the construction plan and the phenomenon did not increased on the further building of the drum.

The axial travel, velocity and acceleration of the blades are shown in *figure 5*. The displacement graph is regular, the waving at the reversion places comes from the necessary play of the roller and the control groove.

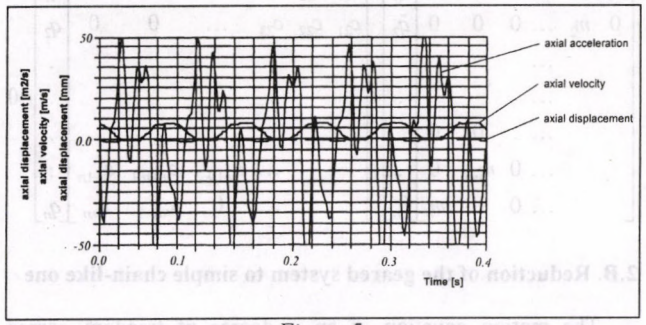

Figure 5
Measurement of „VIBRO CUT" chaffing drum

On the bases of the laboratory measurements one can state that the velocity maxima – of course in the changeover points – have 0.5-0.6 m/s positive and negative values. Those values are rather safe for the operation of the applied sliding and rolling parts and seals. At the same time it gives the necessary edge directional velocity which is necessary the desired sliding cut [1].

The idle power need dependence on the revolution speed is not a question. That is the information to the designer how mach power the control needs (of course, the vibration of the masses can not be solved without input power to them) and what is the estimated energy need compared to the total cutting energy balance.

Table 1
Idle operation power need of controlled chaffing drum

Measurement code	Revolution n [1/min]	Power consumption [W]
F1	27	2400
F2	97	2880
F3	372	3360
F4	571	4160
F5RR	760	5120

In the measurement near the operational revolution speed the increase is apparently considerable from 2.56 kW to 5.12 kW as it has doubled. Therefore power need of the control is below 3 kW according to the measurements.

Table 2
Idle operation power need of chaffing drum without control

Measurement code	Revolution n [1/min]	Power consumption [W]
F1D	262	2400
F2D	480	2400
F3D	675	2440
F4D	812	2440
F5D	880	5120

In the energy balance of the self-propelled chaffing machines of 200 kW driving engine the power need of the cutting drum may excess 80%. The power input increase of a few kW-s by the control is not significant to the expectable reduced power requirement achieved by the application of slitting-cut.

6. Summary, results

In the evaluation of the experimental results it could be stated that the intended operational principle could be accomplished with the equipment designed and already mounted with blades.

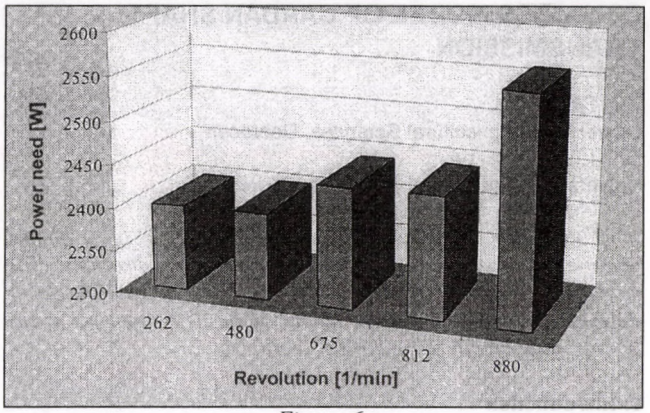

Figure 6
Idle operation power requirement of chaffing machine without control

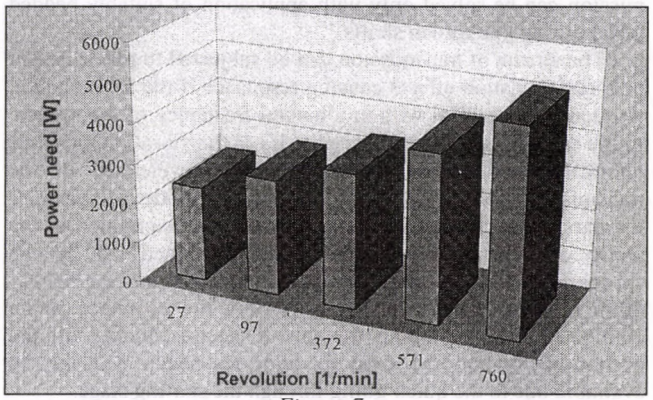

Figure 7
Idle operation power requirement of controlled chaffing machine

The planned construction can be accomplished and the manufacturing is not impossible and needs no extreme investments.

The investigation method has been formed which is applicable to determine the power requirement and the qualification of manufacture and assemblage.

It is considered our task to adapt the elaborated and applied examination method to plant tests.

Thus carrying out the further laboratory measurement examinations of the chaffing drum already mounted with blades is an outstanding job. It is also an intended aim to make possibilities to accomplish arable field test. Those chaffing experiments will be applicable to qualify the cutting work, in addition to the continuing the analysis of energy requirement and motion circumstances.

References

1. PÉTER SZENDRŐ: Driving element mainly for energy saving operation of agricultural cutting and threshing drums (with inventor associates). No. 177069, 1981. (In Hungarian)
2. PÉTER SZENDRŐ: Rotating drum cutting equipment, especially for stem fodder. (with inventor associates). No. 168907, 1977. (In Hungarian)
3. PÉTER SZENDRŐ: Analysis of the silage maize cutting process taking place in self-propelled chaffing machines Budapest, 1976. Akadémiai Kiadó. p. 83 (The scientific questions of the technical development of agriculture, 12) (In Hungarian)
4. PÉTER SZENDRŐ: Chaffing of fibrous green fodder plants. Akadémiai Kiadó. 1995. p. 157 (In Hungarian)

DYNAMICS MODEL OF CARDAN SHAFT TRANSMISSION

Zs. Tiba
University of Agricultural Sciences, Debrecen
Dr. J. Janik
University of Agricultural Sciences, Gödöllő

The paper presents the formulation steps of a model applicable to examine bending and torsion vibrations. The model concerns general arrangement of transmission. The paper deals with the determination of the natural frequencies of the driving referring to the technical literature.

1. Introduction

Very often the implement is operated far from the drive and due to the design of the machine structure the power transmission can be solved only with application of suitably bedded serial zigzag line cardan shafts.

The stream of transmission can be subjected to displacement or force excitation effects causing resonance if the an excitation frequency is identical with any natural frequency of the system. In the case of resonance the amplitudes of the vibration increases unlimited resulting in the breaking of an element of the transmission. By setting up the transmission model of dynamics the natural frequencies of the system can be determined in the phase of construction and they can be tuned off by the appropriate selection of the geometry dimensions and the rigidity of the bearings. Often in a steady operation the resonance can be eliminated only by tuning the lowest eigen-frequency off the excitation, so that the time to form resonance will not be available due to the quick going through the starting stage.

2. Transforming the driving arrangement to chain-like model.

The cardan shaft transmission in *figure 1* can be geared or branching type according to the type of drives. In the first case a geared transmission drive and in the second case multiple gear alternate transmission is applied. Determination of the eigen-frequencies of a chain-like model is relatively simple. Thus it can be practical to reduce and transform the general model to a chain-like model of the identical natural frequencies and to examine that instead of the direct investigation on the original one [1]. The branching system can be transformed to a chain-like one in two steps: the branching system is first transformed to a geared one and then to a chain-like one.

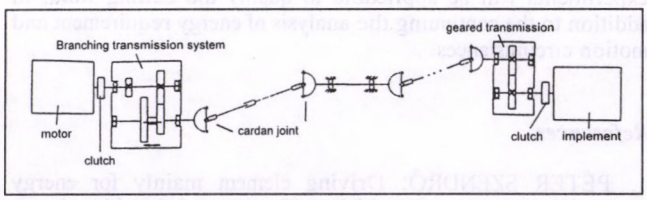

Figure 1

2.A. Characteristics of the moyiom equation of a simple chain-like system

The motion equation of a system of n degree of freedom is obtained by the Lagrange's equation:

$$m\ddot{q} + cq = 0 \qquad (1)$$

where M is the diagonal mass matrix while c is the tridiagonal spring matrix.

The sum of the spring matrix is zero, except when the first or last element of the chain is fixed to the wall. In this case the sum of the elements of the first or the last rows will not be zero.

$$\begin{bmatrix} m_1 & 0 & \dots & 0 & 0 & 0 \\ 0 & m_2 & \dots & 0 & 0 & 0 \\ & & \dots & & & \\ & & \dots & & & \\ & & \dots & 0 & 0 & \\ & & \dots & 0 & m_{n-1} & 0 \\ & & \dots & 0 & 0 & m_n \end{bmatrix} \begin{bmatrix} \ddot{q}_1 \\ \ddot{q}_2 \\ \cdot \\ \cdot \\ \cdot \\ \ddot{q}_n \end{bmatrix} + \begin{bmatrix} c_{11} & c_{12} & \cdot & \dots & 0 & 0 \\ c_{21} & c_{22} & c_{23} & \dots & 0 & 0 \\ & & \cdot & & & \\ & & \cdot & & & \\ & & \cdot & & & \\ & & \dots & c_{n-1,n-2} & c_{n-1,n-1} & c_{n-1,n} \\ & & \dots & 0 & c_{n,n-2} & c_{n,n} \end{bmatrix} \begin{bmatrix} q_1 \\ q_2 \\ \cdot \\ \cdot \\ \cdot \\ q_n \end{bmatrix} = 0$$

2.B. Reduction of the geared system to simple chain-like one

The motion equation of an n degree of freedom geared system is

$$M\dot{p} + Cp = 0 \qquad (2)$$

The mass matrix of the system M is diagonal, while the spring matrix C is also tridiagonal just like in the case of a simple chain-like transmission. Nonetheless the sum of the row elements of the matrix is not zero in at least two rows. It can be verified that there exist such a $S = s_1, s_2, \dots s_n$ matrix which transforms the above system to a chain-like one.

$m\ddot{q} + cq = 0$, where m=S*CS, c=CS and q=Sp.

The elements of the matrix S are determined by using the conditions that the sum of the row elements of the spring matrix should be 0. The value of s_1 can be chosen to be s_1=1.
Carrying out the matrix multiplication the first row will be

$$s_1 C_{11} s_1 + s_1 C_{12} s_2 = 0 \text{ and expressed } s_2 = -\frac{C_{11} s_1}{C_{12}}$$

All the elements of matrix S can be determined by expressing the unknown values s_i after each other.

2.C. Transforming the branching system to a geared one

The motion equation of an n degree of freedom branching system is

$$Nr + Qr = 0 \qquad (3)$$

There exist such a $T = \langle s_1, s_2, \dots s_n \rangle$ matrix which transforms the above system to a geared one.

$M\ddot{q} + C\ddot{q} = 0$, where $M = T^* NT$, $C = T^* QT$ and $p = Tr$.

The elements of the matrix T are determined from the condition that that matrix M required to be diagonal. The matrix T is produced in n steps by iteration [2]. Each step of the procedure gives one column of the matrix T. In the first step t_i can be chosen free, too: $t_1^* = [1,0,0,\dots,0]$.

The iteration results in

$$t_2 = -N^{-1} Q t_1 + t_1 \frac{t_1^* Q t_1}{t_1^* N t_1} \qquad (4)$$

$$t_i = -N^{-1} Q t_{i-1} + t_{i-1} \frac{t_{i-1}^* Q t_{i-1}}{t_{i-1}^* N t_{i-1}} + t_{i-2} \frac{t_{i-2}^* Q t_{i-2}}{t_{i-2}^* N t_{i-2}} \qquad (5)$$

where the last member of t_i is found in the case of $i \geq 3$.

3. Determination of the rigidity if the transmission bedding for rolling radial bearings

The rigidity of the bedding is determined by the rigidities of the bearing and the box together. If the rigidity of the box is one order higher than that of the bearing then the rigidity of the bearing can be considered the rigidity of the bedding in the range of elastic deformation. Further difficulties are caused by the non-linear characteristics of the bearings (*Figure 2)* meaning that the rigidity depends on the magnitude of the load.

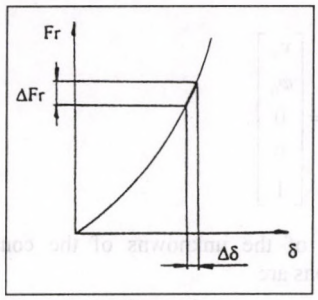

Figure 2

The rigidity/elastic properties of the rolling bearings can be originated from the Hertz theory of contact deformation and the rolling bear rigidity model of Sjövall [3]. To use the Sjövall rigidity model one should know the bearing geometry dimensions, bearing play and the loading. To determine the spring rigidity $\Delta\delta$ is determined for the 2 % increased and the 2 % decreased load.

$$s = \frac{\mathrm{d}\,Fr}{d\delta} = \frac{\Delta Fr}{\Delta\delta} \tag{6}$$

where s is the spring rigidity belonging to the given load.

4. Vibration theory examination of the transmission

The model already chain-like reduced having known spring rigidity bedding locations can be examined from vibration theory aspect. The unbalanced rotating shafts can generate excitation effect on the transmission and can cause bending vibration while the excitation effects of the built in cardan shafts may be dangerous for torsion vibration because their rotation varies. That is why the investigation of the bending and torsion vibration is necessary. The examination of the longitudinal vibrations is neglected here. In the vibration study the damping effects are also neglected because they do not influence the natural frequencies of the system significantly but the calculations are much simpler without them.

5. Determination of the eigen-frequencies of bending vibration of the transmission

The model describing the continuum vibration of bars can be used to examine the bending vibration of rotating shafts when the angular velocity is not high and the inertia moments of the discs mounted on the shafts are rather small [4]. In order to simplify the investigation, further assumptions and simplifications are applied:

- The principal moments of inertia should be the same in all the rotated angle position in order to eliminate the parametric bending vibration. Circular and ring cross section shafts meet those conditions.
- In the investigation the y directional displacement $q(z,t)$ is selected as general co-ordinate.
- In addition it is assumed that the cross sectional planes remain planes during the vibration and rotate only about axes parallel to x. (*figure 3*).

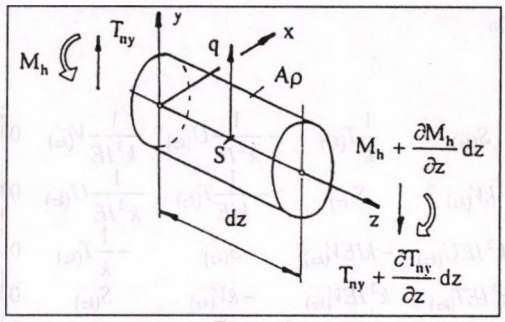

Figure 3

The force coming from the unbalanced mass is considered only with its y directional component. In accordance with it only the y directional load and the y directional spring rigidity is applied in the calculation. The equation of motion of a constant cross section part of rod can be described by a fourth order, linear, constant multiplier partial differential equation [5].

$$\rho\frac{\partial^2 q}{\partial t^2} + IE\frac{\partial^4 q}{\partial z^4} = 0 \tag{7}$$

The solution of the equation of motion is searched in the form of

$$q = v_z \cos(\alpha t + \varepsilon) \tag{8}$$

and using the substitution

$$k^4 = \alpha^2 \frac{a\rho}{IE} \tag{9}$$

the differential equation

$$v^{IV} - k^4 v = 0 \tag{10}$$

the basic system of which Krülov functions are practical to be selected.

The general solution to the differential equation is

$$v_z = D_1 S_{(kz)} + D_2 T_{(kz)} + D_3 U_{(kz)} + D_4 V_{(kz)} \tag{11}$$

Where D_1, D_2, D_3, D_4, multipliers can be determined from the boundary conditions. The ends of sessions can be chosen in the support points of cardan shaft transmission stream, in the place of cardan shafts and in the application points of excitation forces (*figure 4*).

The motion characteristics of the individual cross sections are described by the vectors of state:

$$n_i = \begin{bmatrix} v_i \\ \varphi_i \\ M_i \\ \overline{T}_i \\ 1 \end{bmatrix} \tag{12}$$

where

$v_{(z)}$ the displacement of the cross section

$\varphi_{(z)} = \dot{v}_{(z)}$ the rotation of the cross section

$M_{(z)} = -IEv''_{(z)}$ the bending moment in the cross section

$\overline{T}_{(z)} = -IEv'''_{(z)}$ the shear force in the cross section

The motion characteristics of an arbitrary section of the constant cross section rod session is determined from the matrix equation

$$\eta_1 = F\eta_0 \tag{13}$$

where

$$F = \begin{bmatrix} S_{(kz)} & \frac{1}{k}T_{(kz)} & -\frac{1}{k^2 IE}U_{(kz)} & \frac{1}{k^3 IE}V_{(kz)} & 0 \\ kV_{(kz)} & S_{(kz)} & -\frac{1}{kIE}T_{(kz)} & \frac{1}{k^2 IE}U_{(kz)} & 0 \\ -k^2 IEU_{(kz)} & -kIEV_{(kz)} & S_{(kz)} & -\frac{1}{k}T_{(kz)} & 0 \\ k^3 IET_{(kz)} & k^2 IEV_{(kz)} & -kV_{(kz)} & S_{(kz)} & 0 \\ 0 & 0 & 0 & 0 & 1 \end{bmatrix} \tag{14}$$

which is the session matrix or transfer matrix.

If the cross section of the rod varies, it has elastic support or it is loaded by external force, moment, the solutions valid for the individual sessions should be fitted. From the conditions of fitting which - two geometry conditions, the momentum equation and the law of moment of momentum - the point matrix P which is characteristic to the session borders. For example the following boundary conditions can be written for cardan joints [6]:

geometry conditions:

$$v_{j\ joint} = v_{b\ joint}$$

$$\varphi_{j\ joint} = \varphi_{b\ joint} + \Delta\beta$$

momentum law:

$$\overline{T}_{nyj\ joint} = \overline{T}_{nyb\ joint}$$

operation of cardan joint

$$M_{j\ joint} = M_{b\ joint} = 0$$

where the subscripts j and b indicates the cross sections to the left and to the right of the joint. $\Delta\beta$ is the angle in radian which stands for the angle elongation in operation state compared to the rest state of the shafts connected by the joint .So that if the mass of the joint and the moment of inertia are neglected the point matrix o the joint is as follows

$$P = \begin{bmatrix} 1 & 0 & 0 & 0 & 0 \\ 0 & 1 & 0 & 0 & 0 \\ 0 & 0 & 1 & 0 & \Delta\beta_i \\ 0 & 0 & 0 & 1 & 0 \\ 0 & 0 & 0 & 0 & 1 \end{bmatrix} \tag{15}$$

It is noted that the construction of the point matrix rises no problem even if the mass of the joint is not neglected. If the matrices F and P are determined to all the sessions and session ends of the model then the state matrix of the last cross section of the model is

$$\eta_n = P_n F_n P_{n-1} F_{n-1} \ldots P_1 F_1 \eta_0 \tag{16}$$

If the boundary conditions are applied to the state matrix, the problem exposes a linear, inhomogeneous system of equations to solve. The solution will supply the state vector η_0. Multiplying this vector with the corresponding session matrix will supply the characteristics of mechanics in arbitrary location of the transmission. For example in the case of free shaft end cross sections marked by 0 end n:

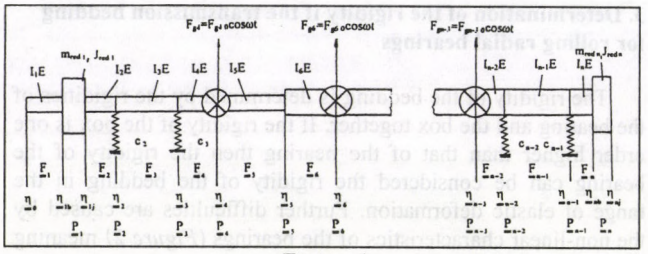

Figure 4

$$\eta_0 = \begin{bmatrix} v_0 \\ \varphi_0 \\ 0 \\ 0 \\ 1 \end{bmatrix}, \quad \eta_n = \begin{bmatrix} v_n \\ \varphi_n \\ 0 \\ 0 \\ 1 \end{bmatrix}. \tag{17,18}$$

The number of the unknowns of the constructed linear system of equations are

$v_0, \varphi_0, \Delta\beta_1, \Delta\beta_2, \ldots, \Delta\beta_k$, $2+k$ altogether.

The number of equations are

$M_n = 0, \overline{T}_n = 0, M_1 = M_2 = \ldots M_k = 0$, $2+k$ altogether.

k is the number of joints.

One can see that the system of equations can be solved. In general, it is not necessary to solve the system of equations if only the natural frequencies are searched. It can be proved that resonance occurs when the determinant of homogenous part of the system of equations is zero. The eigen-frequencies can be determined with arbitrary accuracy by using the method of residuals. After choosing any value of α eigen-frequency and calculating the determinant one can decide if Δ=0 is satisfied or not. If the signs of $\Delta_{(0)}$ and $\Delta_{(1)}$ are the same, $\alpha_{(0)} < \alpha_n < \alpha_{(1)}$ is true for the sought frequency (*figure 5*).

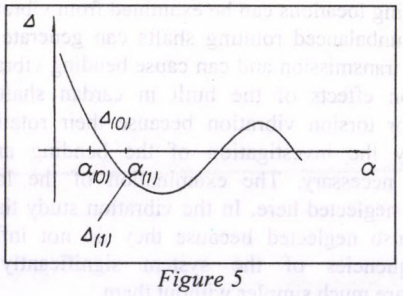

Figure 5

The chosen values of α is changed until Δ=0 is obeyed for α_n. By means of the method all the natural frequencies can be determined.

4.B. Examination of the torsion vibration

As it is known the cardan joint transmits the power with a changing angular velocity which depends on the angle position of the connected shafts. As one can see, the system of differential equations describing torsion motion of the transmission contain periodic varying multipliers. One can state in general, that the cardan shaft transmission is a parametric excited system even if the kinematics arrangement of the transmission assures the same rotation of the first and the last elements. The torsion examination is carried out with multiple mass, concentrated parameter spring model. In the formulation

of the model the inertia moments of the cardan shafts are taken into account by disc models of J moment of inertia. For simplifying the calculations the model is applicable under β=20° angle of shafts.

The general form of the Lagrange's equation of the second kind is [7]

$$\frac{\mathrm{d}}{\mathrm{d}t}\left(\frac{\partial E}{\partial \dot{q}}\right)-\frac{\partial \mathrm{E}}{\partial q}=Q \tag{19}$$

where

$$E=\sum E_i$$

The moment of the whole system,

$$Q=\sum Q_i$$

The rate of all the forces with unit co-ordinate velocity.

The Lagrange's equations of the second kind is written for the model shown in *figure 6*, where the chosen general co-ordinate is the angle rotation of the discs. Irt is produced

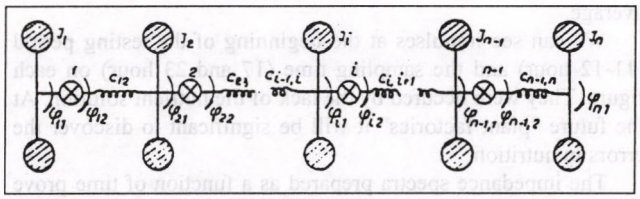

Figure 6

$$J_1\ddot{\varphi}_{11}-\frac{1}{c_{12}}(\varphi_{21}-\varphi_{12})\frac{\partial\varphi_{12}}{\partial\varphi_{11}}=0$$

$$J_1\ddot{\varphi}_{11}+\frac{1}{c_{12}}(\varphi_{21}-\varphi_{12})-\frac{1}{c_{23}}(\varphi_{31}-\varphi_{22})\frac{\partial\varphi_{22}}{\partial\varphi_{21}}=0 \tag{20}$$

$$J_n\ddot{\varphi}_{n1}-\frac{1}{c_{n-1,n}}(\varphi_{n1}-\varphi_{n-1,2})=0$$

where $\frac{\partial\varphi_{i2}}{\partial\varphi_{i1}}$ is the transfer coefficient of joint number i.

$$\frac{\partial\varphi_{i2}}{\partial\varphi_{i1}}=1+2\delta_i\cos 2\varphi_{i1} \tag{21}$$

and $\delta_i\cong\frac{\beta_i^2}{4}$, while β_i is the angle between shafts connected by the joint number i [8].

$$\varphi_{i+1,1}-\varphi_{i2}=X_i-\delta_i\sin 2\varphi_{i1} \tag{23}$$

is in the system of equations, where

$$X_i=\varphi_{i+1,1}-\varphi_{i1},\ i=1,2,...,n\text{-}1 \tag{24}$$

After substitution and performing the practical partitioning the following matrix equation is obtained

$$\ddot{X}+AX+BX2\cos\varphi+B\sin 2\varphi\cos 2\varphi=0 \tag{25}$$

A and C are tridiagonal matrices while B and D contain only diagonal elements and one single element to the right of the diagonal. The solution of the inhomogeneous system of equations represented by the matrix equation is searched in the form of $X=ye^{i\alpha t}$ which leads to

$$\ddot{X}=-\alpha^2X=a^2ye^{i\alpha t} \tag{26}$$

After substitution and simplification the determinant of the homogeneous part exposes tridiagonal form.

Those written at the investigation of bending vibration are valid here, too. The natural frequencies of the torsion system are found for the zero values of the determinant. The following boundary conditions are used to the solution: according to the built in position the angle orientations of the joints are determined relative to the first joint. If for example all the joints are built in a position rotated by 90° relative to the previous, the following boundary conditions can be written

$$\varphi_2=\varphi_1+90°$$

$$\varphi_3=\varphi_2+90°=\varphi_1+180°$$

$$\varphi_4=\varphi_3+90°=\varphi_1+270°$$

$$\varphi_n=\varphi_{n-1}+90°=\varphi_1+(n-1)90°$$

where n is the number of joints.

The variation of the rotation of shafts driven by the joints are expressed by $\varphi_2,\varphi_3,...,\varphi_n$ related to the shaft driven by the first joint. The frequency equation obtained by the development of the determinant contains periodic variation multipliers. As a consequence of this, one natural frequency $\alpha_1<\alpha_2<\alpha_3<...<\alpha_n$ belong to each φ_1 position of the transmission. If $\alpha_1<\alpha_2<\alpha_3<...<\alpha_n$ values are determined for the range $\varphi_1=0°-180°$, $\alpha_1(\varphi_1),\alpha_2(\varphi_1),...,\alpha_n(\varphi_1)$ function is achieved. The resonance can be eliminated, if the excitation frequency ω will not cross any $\alpha_i(\varphi_1)$ function graph in steady operation.

It can be stated finally, that the eigen-frequencies of the bending and torsion vibration of the transmission are functions of the geometry dimensions and the rigidity of bedding among others.

If the excitation frequencies are close to any eigen-frequency, resonance will occur. The natural frequencies can be tuned off by the suitable selection of geometry dimensions and the rigidity of bedding and the resonance can be eliminated.

The relevant PhD. study and research are supported by the „Magyar Tudományért" Fund.

References

1. DR. BOSZNAY ADÁM: Műszaki rezgéstan Műszaki Könyvkiadó, Budapest, 1962. (Technical vibration theory, in Hungarian)
2. Mechanikai Tanszék Munkaközössége: Dinamika V. Tankönyvkiadó, Budapest. 1981.
3. MOLNÁR - DR. VARGA: Gördülőcsapágyazások tervezése. Műszaki Könyvkiadó, Budapest, 1977. (Design of rolling bearings, in Hungarian)
4. SZ. D. PONOMARJOV: Szilárdsági számítások a gépészetben 6. Műszaki Könyvkiadó, Budapest,1966. (Strength calculations in the engineering, in Hungarian)
5. Singiresu S. Rao: Mechanical Vibrations. Addison - Wesley Publishing Company
6. DR. LUDVIG GYŐZŐ: Gépek dinamikája. Műszaki Könyvkiadó, Budapest, 1983. (Dynamics of machines, in Hungarian)
7. DR. SÁLYI ISTVÁN: Lengéstan I - XIII. fejezet. Tankönyvkiadó, Budapest. 1981. (Vibration Theory, in Hungarian)
8. DOZ. DR.-ING.FLOREA DUDITZA: Kardangetriebe und ihre Anwendungen. VDI-Verlag GmbH, Düsseldorf 1973.

EVALUATION OF THE NUTRIENT UPTAKE OF VEGETABLES BY BIOELECTRIC METHOD

P. László - J. Zana
University of Horticulture and Food Industry, Budapest
F. Kőrösi
University of Agricultural Sciences, Gödöllő

Materials and methods

We can build the low frequency alternating current model of plant tissue and organs with parallel connected RC circuit elements (*figure 1*).The admittance of the model:

$$Y = \frac{1}{Z} = \frac{1}{R} + i\frac{1}{X_C} = G + iB = G + i\omega C$$

The conductance (G) is in connection first of all with the structure of the cells. The susceptance (B) is a function of the permittivity by the frequency and the capacitance. The electric capacitance is in connection with the polarisation and the metabolism directly. The plant materials are considered as dielectric. The transports inside the plant manifested as the changes in the dielectric. The dielectric causes the change of the capacitance which can be measured on the plants. This way we can gain information about the present nutritive elements.

Basic claim is that during measuring, using an auxiliary electric power sources the cell building and nutrition should not be disturbed. This means that the plant can be influenced by the environmental circumstances, only. In the interests of the things mentioned above we evaluate the electric capacitance at a constant frequency (1 kHz) using low power (1 W) sine wave alternating current. The measurments were carried out by platinum needles attached to the plants.

As a result of the measurments we can get the digitalized capacitance values within 10 seconds. We used a computer for collecting and storing of the data. The auxiliary power was connected to the plants only during the measuring time.

In the experiments we tested a paprika variety *Fehérözön* and a bean variety *Echo Elit.* The paprika plants were raised in breeding containers and the bean plants were raised in nutrient solution. The environment characteristics were stabilized by a conditioned greenhouse modul. The phosphorus uptake was monitored during IO weeks including the three weeks period of flowering and fertilization.

The bean seedlings were grown up period among low salt concentration conditions (0.5 mM CaSO4) up to their primordial phenological stage, following this their phosphorus, potassium, calcium, magnesium and zinc uptake was monitored by computer aided capacitance measurement during the 72 hour nutrition period.

Results of experiments

The phosphoius content of the soil was 30, 60,120 and 240 mg/kg. We can see on the *figure 2* the results measured daily on four plants presenting the treatments. The figure shows an increasing capacitance in connection with an increasing phosphorus concentration. This increase is greater in the period of flowering the phosphorus intake influences the intensity of photosynthesis. We can see on the figure that there is practicalli no increas in the nutritient transport between 120 and 240 mg/kg, so 120 mg/kg is approximetly the saturation level.

Figure 3 shows two separated phases the pre-flowering and the flowering *stages.* Both of them are of a saturation type function independence of the phosphorus content. So we can evaluate that level of phosphorus content which is worth to apply to increase the yield.

We made a change in the concentration of the nutrient solution at the begining of the experünent. The solutions were the followings:

Salt	Concentration
Ca(N03)2.4 H20	5.00 mM
KH2PO4	6.80 mM
Mg504.7Hz0	2.38 mM
Mn504.4H20	10.00 mM
ZnSO4.7Hz0	10.00 mM

We monitored the solutions at 6,12,18, 24, 48 and 72 hour.

During changing of the solutions the plants were in the air for two minutes. The capacitance measuring was carried out in 20 minutes and the impedance spectrum was registered (figure 4) during 15 hours from the beginning of the experiment. Each treatment was applied on 3 plants. The *figure 4* consists of their average.

We can see impulses at the beginning of the testing period (11-12 hour) and the sampling time (17 and 23 hour) on each figure. They were occured by the lack of the nutrient solution. At the future "plant factories" it will be significant to discover the errors in nutrition.

The impedance spectra prepared as a function of time prove significant difference in electric capacitance in the effect of the macro and mesoelements K, P, Ca and Mg than the microelements Mn and Zn. We can calculate this effect using two sample t-test at the 95 % significance level. We think it is also important that the effect of macro and mesoelements is more longlasting against the behaviour of the microelements. So we can draw the conclusion that the microelement intake is finished in 15 hours but the transport of potassium, phosphorus and magnesium lasts more then 15 hours.

Conclusions

The metabolism of the physiological process of plants related to nutrition elements can be tested by in vivo taken spectra of electrical capacitance measured by alternating current. This method is useful to evaluate the nutritient uptake speed and nutritient concentration. So we have a method, with high precision of measurement, to apply our results for automaticated cultivation plants controlled by themselves.

This research activity was suspended by the Hungarian Scientifc Research Fund (OTKA, identificated as TO 16273, project leader Prof. István Farkas).

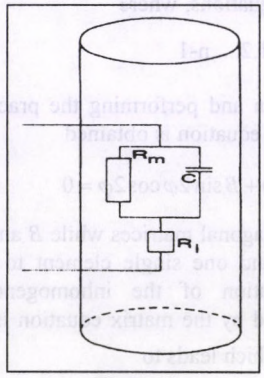

Figure 1
RC modell

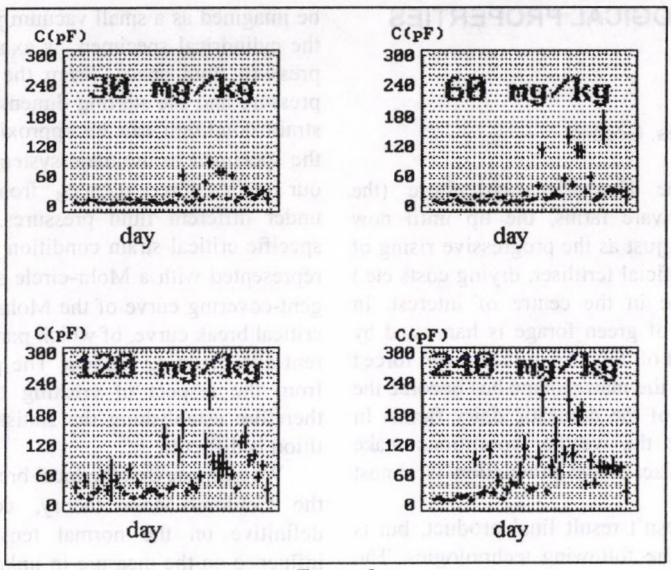

Figure 2
Effect of phosphorus content of soil

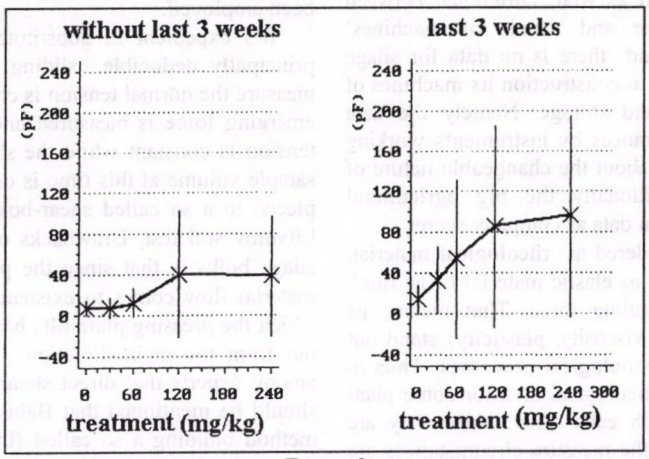

Figure 3
Effect of phosphorus content of soil before end during flowering

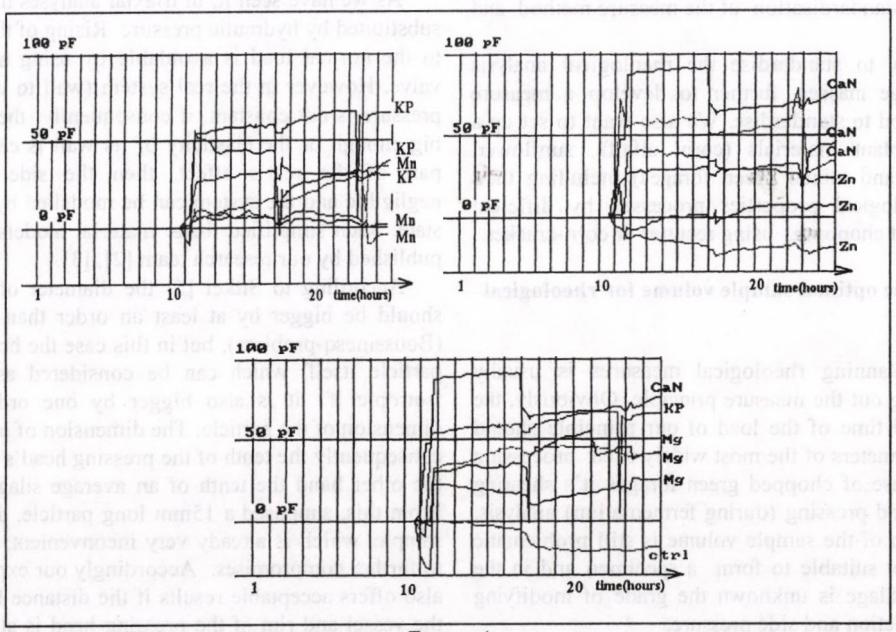

Figure 4
Changes in dielectric capacitance as effect by the uptake solutions

MEASURING OF RHEOLOGICAL PROPERTIES OF SILAGE

Dr. P. Szendrő - L. Bense
University of Agricultural Sciences, Gödöllő

The transformation of the Hungarian agriculture (the formation of capital-weak private farms, the up until now unfavourable credit conditions), just as the progressive rising of production costs of forages (artificial fertiliser, drying costs etc.) hold the chopped green forage in the centre of interest. In Hungary approx. 6-8 mill tons of green forage is harvested by chopping every year. Major part of this is silo-maize and forced chopped corn-maize. Nowadays the maize silage has become the most important forage source of the domestic dairy farms. In countries like Germany, where the weather conditions make unsure the growing of corn-maize, silage production is almost the only aim of maize growing.

In most cases chopping doesn't result final product, but is only the preparation phase of the following technologies. The size distribution of the cut up living material is essential in successful silage process, although the mechanical behaviour of the viscoelastic bulk is important as well. Difference between mechanical parameters of silage and metals of machines' mechanical parts are definitive and there is no data for silage which could be the starting point in construction its machines of transportation, further process and storage. Namely the data gathered under different circumstances by instruments working in different ways, to say nothing about the changeable nature of the biological material. Additionally the big agricultural machine factories handle their own data as company secret.

The silage mass can be considered as rheological material, since the way it behaves whether as elastic material or as fluid, depends on the speed of its loading force. That means, its rheological properties (elasticity, viscosity, plasticity) stand out in different extent during the technological processes. Thus in the literature scarcely emerging rheological data for some plant materials are not compatible with each other, since they are determined by many factors and the measure circumstances are not exactly given. From this point of view giving the exact measure- and evaluation conditions are fairly important as well as the unconditional standardisation of the measure method and instruments.

Our task is now to standardise the rheological analysis conditions for silage masses, further to develop a measure instrument and method to standardise. We also want to set up a table on different plant materials (corn, alfalfa, sunflower, sorghum, miscantus and mixed green forages) including their silage masses' rheological properties processed by different methods such as exact chopping, using recutter or corn-cracker.

How to determine the optimal sample volume for rheological analysis

Difficulties in planning rheological measures is usually caused not by picking out the measure principle. Obviously, the direction, weight and time of the load of our principle should follow the same parameters of the most widely used processing technology. In the case of chopped green forages it's shearing (during lumbering) and pressing (during fermentation) analysis. Yet the determination of the sample volume is still problematic since the silage is not suitable to form a specimen and in the case of containered silage is unknown the grade of modifying factors such as wallfriction and side pressure.

In triaxial measures a membrane-firmed sample can be used. The volume of the sample here is a couple of ccms, which could be imagined as a small vacuum packed column. During analysis the cylindrical specimen is axial pressed until break in a high pressure fluid space. From the measured loading force, fluid pressure and the starting dimension of the specimen the critical strain condition can be approximately determined. We loaded the specimen in the main system of axis, thus σ_1 derives from our loading force, $\sigma_2 = \sigma_3$ from the fluid pressure. Measuring under different fluid pressures, a material and conditions a specific critical strain condition set is obtainable, which can be represented with a Mohr-circle set on the σ, τ plane. The tangent-covering curve of the Mohr-circle set is the $\tau_{max}(\sigma) = \tau(\sigma)$ critical break curve, of which parameters are employed by different silo planning models. The procedure is fairly complicated from the respect of creating the high pressure fluid space, therefore establishing the statistically correct number of repetition is difficult.

We suppose that the local break starts with slide according to the Coulomb-Mohr theory, consequently the τ_{max} depend definitive on the normal tension, and as the membrane's influence on the measure in unknown just as the dependence of the deformation and the tension on the time is neglected, at first approach of analysing silage bulks the triaxial theory has not been employed.

It's expedient to substitute the triaxal measure with the principally deducible sliding analyse. (In short: in triaxial measure the normal tension is changed while in the sliding plane emerging force is measured and in sliding analyse the normal tension is constant while the shearing force is measured.) The sample volume at this time is only a some cdm and which then placed to a so called shear-box. The method resembles to the Litvinov soil test. Drawbacks of the method during measuring silage bulks is that since the particles grasp to each other , a material flow comes to existence in the measure space, due to which the pressing plate tilts back and the direction of load gets out from the main direction. On this basis is a view spread among experts that direct shear analyses are not reliable.(Here should be mentioned that Balassy[1] has developed further the method building a so called floating frame apparatus which is outstanding applicable for share analyses of corn bulks. However data for silage bulks are not published.)

As we have seen it, in triaxial analyses the silo pressure was substituted by hydraulic pressure. Rising of the side pressure due to the normal load is avoidable by using a pressure regulator valve. However in the real system (wall to wall silo) the inner pressure is not constant, if consequently the silage container is big enough or the elasticity of its wall is capable of acting the part of the rest's effect, then the side pressure becomes negligible and the system can be modelled by a one axis tension state. Such simplified linear material models have already been published by our research team [2], [3].

According to Sitkei [5] the diameter of the pressing head should be bigger by at least an order than the analysed body (Boussinesq-problem), but in this case the body is not the silage particle itself, which can be considered as homogenous and isotropic if it is also bigger by one order than the linear dimension of the particle. The dimension of optimal micro silo is consequently the tenth of the pressing head's diameter, which on the other hand the tenth of an average silage particle's length. From this, supposed a 15mm long particle, derives a 1.5m long sample, which is already very inconvenient, thus we are forced to further compromises. Accordingly our experiences, microsilo also offers acceptable results if the distance between the side of the vessel and rim of the pressing head is at least by one order bigger than the particle size. The vessel applied by us had a diameter of approx. 430mm and a volume of 54 cdm.

Rheological measures

Most widely used rheological methods are the tension-relaxation, creeping and dynamic analyses. Dynamic analyses worth to apply only in cases of materials with small rheological time constant. In creeping experiments the material is loaded for moments and the grade of it is held constant. The examined time dependent parameter is the deformation. The step function type load is problematic, if namely the loading is solved by "dropping", its dynamic consequences may false the measure results. Relaxation analyses are carried out with constant deformation while the time dependent parameter is the tension. The deformation should be established in a very short time, otherwise certain relaxation passes off during the loading process which is immeasurable. Instant load is practically very difficult to accomplish, however if the material's relaxation time is big enough, an instrument functioning with expediently big and constant deformation speed can be proper to make comparison measures. *Figure 1* illustrate the deformation speed's effect on the relaxation process.

Set-up of measure system

It comes from the theoretical explanation above, that an instrument is needed to be constructed which is highly adjustable in both the sample volume and in the loading force's grade and complexion (relaxation, viscosity, penetration measure), further is capable of measuring both the deformation and the loading force even together as well.

As most suitable for accomplishing all these seemed to be a device, functioning on the principle of bridge formed tear-machine and of which set-up is represented in *figure 2*. The apparatus is able to use different sized measure vessels to some extent. The R.P.M of the load producing asincron motor can be adjusted in two phases, but the deformation speed is grade-free adjustable within 0-60 mm/min by changing the transmission and adjusting the frequency. The loading body can be pistons of different diameters, cone and sphere. (The instrument can be considered as an adaptation of the Höppler viscosymeter in case of employment of sphere pressing body.)

Relaxation can be measured in the easiest way with the device. Then the vessel is risen by the jack at a costant rate, accomplishing certain deformation in the sample. After securing the jack the computer reads the force sensor's value at pre-programmed frequency. The measure can be continued until the total relaxation of the bulk, but it can also be automatically interrupted if a certain grade of force is reached or after passing certain time.

Creep measure needs a PC-labcard equipped with a relay-output. The sample is condensed by operating the jack until the prescribed loading force is reached and the force sensor's sign switches the electric motor off. At the bulk an instant relaxation happens, the measured force falls, therefore the electric motor shall be switched on again to hold the constant loading force. The value of force hysteresis at turning in and out should be determined in experimental way and need to be standardise among the measure's basis parameters.

Prescription of the experimental conditions

After picking out the measuring system and the sample volume the next problem is caused by giving the measure conditions. The temperature of the analysis can be for instance supplied unambiguously, while the moisture content is more difficult to tell. Most important in this is, that the natural (at harvest measured) moisture is occasionally changeable, the plant mustn't be redamped and the dried material is rheologically accounted already to another material. This dangers the data's reproductionability and the measure's authenticity, consequently the moisture content need to be supplied and standardised in the method. In *figure 3* the progress of a maize silage's relaxation can be traced during drying.

The stiffness of plant fibres depends not only on moisture content but also on ripeness of the plant which is difficult to express by numbers (e.g. it could be bound to the different colours of the plant in the different ripeness).

The orientation of the silage particles in the bulk has an effect as well on the bulk's mechanical properties. According to our experience, the spring stiffness of an organised bulk is always bigger. In case of small particle size it's impossible organising the particles therefore it is pratical to prescribe such a sample taking method which assures the random position of the particles in the bulk. Beyond that, it should be picked out such a sample-silo size that is bigger by orders than the length of silo particles, so can the bulk considered as homogenous and isotropic.

At last, the size distribution of the silo bulk is important as well, of which expression is already known [4]. An example for connection between the theoretical cut length and the tense-relaxation can be seen in *figure 4*.

Further aims

To fulfil the aims composed in the object of the research-utilising the possibilities of the more purpose rheological measure apparatus- the repetition of measures need to be determined by the means of statistics. Only on beware of the weight of different parameters might be made a proposal which method and which rheological measure apparatus for chopped green forage to standardise. Filling up the undertaken form can be started only if the applied method is already known, up to that time the gathered data due to the lack of possibility of comparing them, shall be considered as informal. Creating the database takes still probably years, taking into consideration that harvesting by chopping is season work. However by this database we working on, the exact characterisation of the silage will be possible and establishing the optimal values can help to improve the quality of the fodder quality.

References

1. BALÁSSY Z.: Correction of data measured in a shear box. Soil and Tillage Research, Elsevier, Amsterdam, 19 (1991) 2, 165-173 p.
2. SZENDRŐ P. - BENSE L.: Szecskázással nyert aprított növényi halmazokra kidolgozott kúszási modell. MTA Agrár-Műszaki Bizottság Kutatási és Fejlesztési Tanácskozása, Gödöllő, FM Műszaki Intézet, 1991. 2. kötet, 359–363.p.
3. SZENDRŐ P. - BENSE L.: Szecskázással nyert aprított növényi halmazokra kidolgozott relaxációs modell. MTA–MÉM AMB Kutatási és Fejlesztési Tanácskozás, Gödöllő, 1992., 38.p.
4. SZENDRŐ P.: Szálas zöldtakarmányok szecskázása. Akadémiai Kiadó, Budapest, 1995.15-73.p.
5. SITKEI GY.: A mezőgazdasági anyagok mechanikája. Akadémiai Kiadó, Budapest, 1981. 149-160 p.

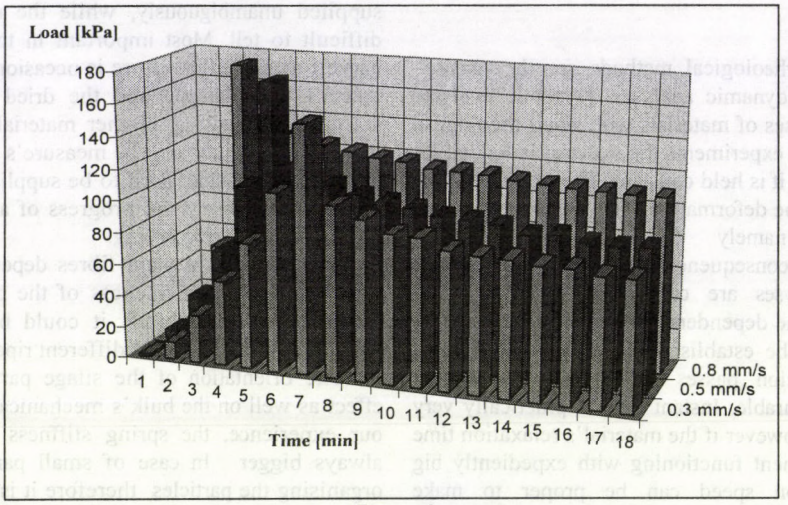

Figure 1
Deformation speed on relation of maize silage

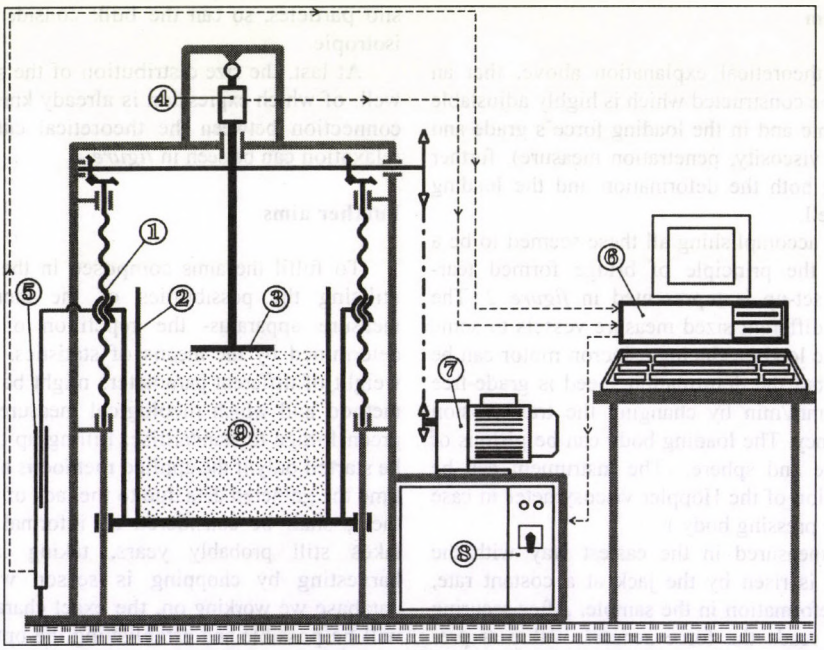

1. Screw jack, 2. Measuring vessel, 3. Loading body, 4. Force transducer, 5. Inductive displacement transducer, 6. Computer, 7. Asincron motor, 8. Control panel, 9. Sample

Figure 2
Measure device setup for rheological analyses

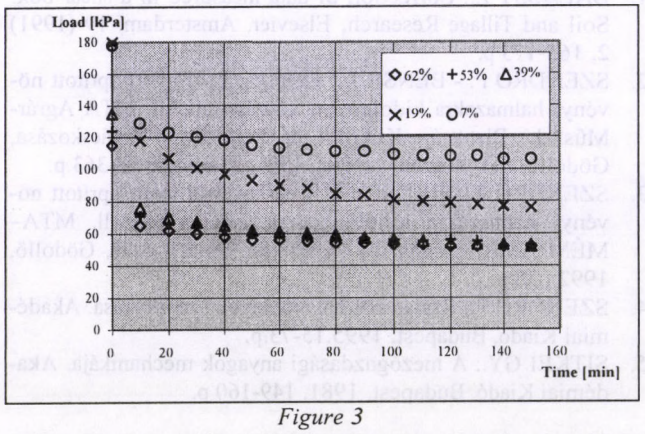

Figure 3
Effect of moisture (◊,+,Δ,X,O) on the relaxation of maize silage (Length of cut 17 mm, with corn-cracker)

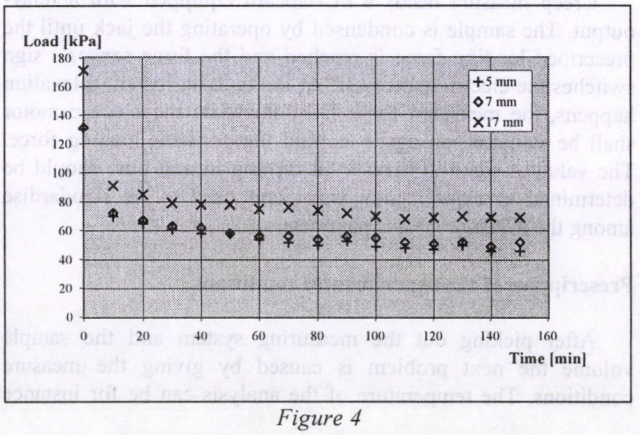

Figure 4
Effect of theorical length (+, ◊,X) of cut on the relaxation of maize silage (Moisture content 41.5%)

MATERIAL TRANSPORT OF THE SEED CORN DURING DRYING PROCESS

Dr. J. Csermely - Dr. Z. Bellus - Dr. M. Herdovics - Gy. Komka - Dr. L. Fenyvesi
Hungarian Institute of Agricultural Engineering, Gödöllő

1. Raising of the issue

Owing to the thick grain layer, the different parameters of the corn and cob, the alternating direction of the drying medium and its double using, the operational features of the drying process of the hybrid maize can only be determined by practical measurements.

Experiments were assisted by the National Scientific Research Fund (OTKA)

2. Methods and materials

Experiments were carried out by drying of KISKUN TC-361 sort of hybrid maize where the average moisture content of the harvested corn and cob was 30.1 % and 55.5 % respectively (ear: 36.5 %).

Experiments were accomplished in operative conditions using a CAMPBELL system chamber drier of series, arrangement with 2 x 4 elements, where the drying medium was inducted at the top and at the bottom of the drier. Temperature of the **primer** air flow was 46.5 °C with a relative humidity of 12.5 %, while the same features of the **secunder** air were 38.5 °C and 30.0 %. Because of the known difficulties of the sampling, samples were taken at 0.5 m height from the bottom and 0.5 m from the top of the grain bulk of 2.3 m height. The previous level was nominated as the **lower layer**, while the latter the **upper** one.

At the mathematical drafting of the drying process we have set out from the well-known connection using up the measured drying features. The applied method made possible to analyse the **1st** and **2nd stages** of the drying process. It was very important mainly in the case of the **upper layer**. There was also possible to study the process of the so called back-moistening.

3. Results and conclusions

a.) Material transport in the **lower layer** of the grain bulk can be considered the same process and can be well characterized by the relation of the *figure 1* because the 1st and 2nd stage of drying in the lower layer takes place by the help of air flow with temperature and relative himidity of near the same. Average drying rate of the corn in the two stages is 0.25 % water content per hour.

b.) Drying process of the hybrid maize in the **upper layer** is not suggested to describe by only one mathematical function, as it can be seen on *figure 2.* Separating the 1st and 2nd drying stages (T = 23h), the material transport can be followed by reassuringly exactly as it can be seen on *Figure 3.*

c.) Graph of the *figure 3* and the model equations describe the process of the heat and material transpsort of the **upper layer** faithfully. It is well perceptible that during the **1st stage** of the drying process (T = 0-23 h), mainly the **increasing** of the **heat content,** while during the **2nd stage** (T = 23-48 h) the **material transport** are the determining features. Drying rate of the corn during the two stages can be taken into consideration by on an average of 0.28-0.35 % water content per hour.

d.) On the basis of the measurements the **equation general** of the **material transport** is as follows:

$W_a = W_v + (W_k - W_v) \exp [-a(T_a - T_k)^n]$

where:

W_a = current moisture content (%)
W_k = initial moisture content (%)
W_v = end moisture content (%)
a = drying characteristic (its values can be seen on *figure 1.* and *figure 3.*)
n = during the 1st stage is 2, while in the 2nd stage is 1
T_a = current time of the drying (h)
T_k = starting point of the drying (its value is 0, or in the 2nd stage, in this case, is 23 h)

e.) At the end-stage of the drying process (T>38 h) [*see figure 4*] **back-moistening** of the cob can be well proved. Conclusion of the measurements and calculations is that, during this tage of the drying process, dewatering of corn takes place **conductively** in 90 % and **convectively** in 10 % extent.

f.) Average value of the **germinating power** in the lower and upper layers was 97.7 % alike, and the deviation was not more than 1 %.

g.) In that case if the lenght ot time of the drying process is decreased by 4-5 hours, **energy consumption** can be decreased by 8-10 %, and at the same time the qualitative features of the dried grain can be guaranteed more certainly.

References

1. CSERMELY J. - BELLUS Z. - HERDOVICS M. - KOMKA GY.: Heat and material transport process in drying of hybrid maize. Hungarian Agricultural Engineering 1994. Nº7

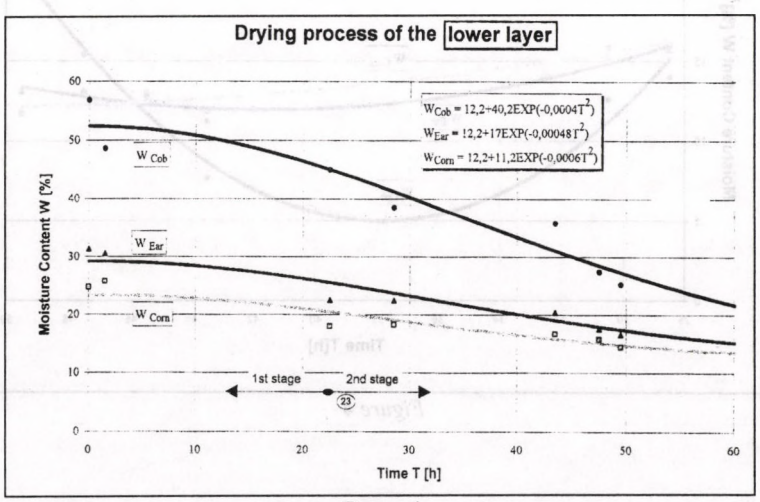

Figure 1

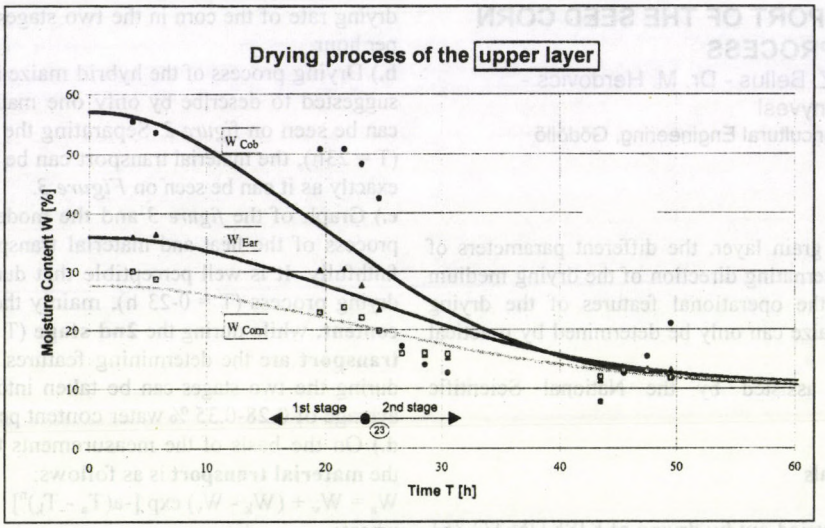

Figure 2

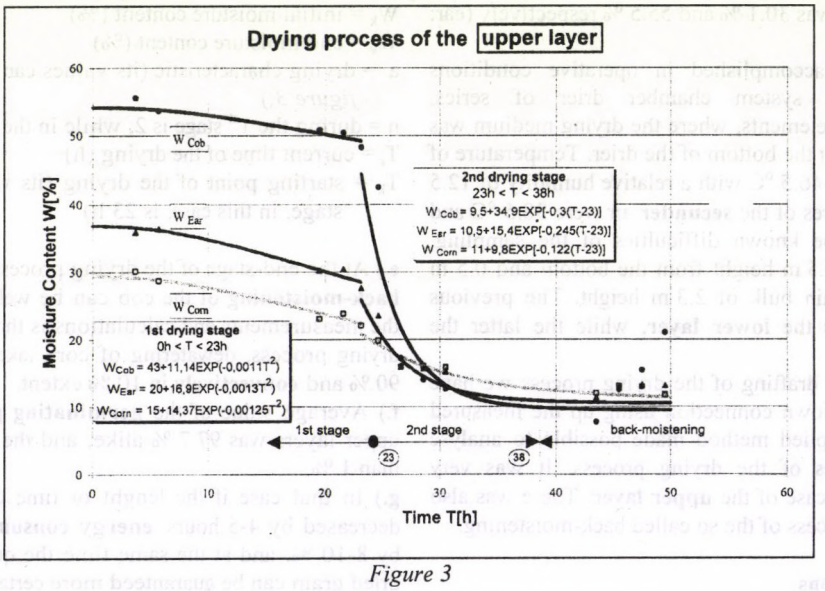

Figure 3

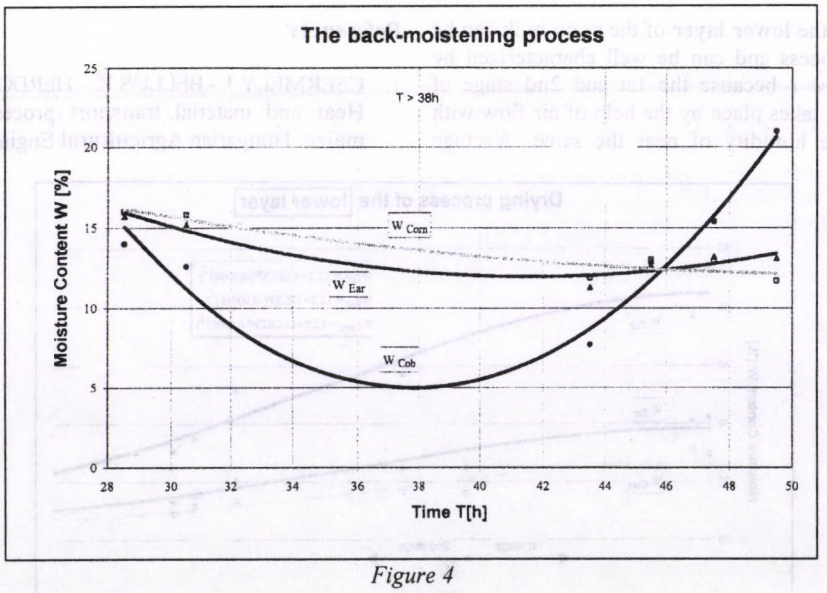

Figure 4

RELATIONSHIPS BETWEEN INDIVIDUAL AND AGGREGATION CHARACTERISTICS OF SOME AGRICULTURAL MATERIALS

Dr. L. Fenyvesi - Dr. Z. Bellus
Hungarian Institute of Agricultural Engineering, Gödöllő

Research field

Most of the agricultural materials are found as aggregations in different technologies and processes. These bulk materials are usually loaded on the whole (e.g. transport, storage etc.) and then loads are transformed in different ways. Loads on the individual parts are developed as a result of these processes and cause lasting deformations (e.g. fracture, damage etc.). While the load is mostly a form of stress on the aggregation (e.g. repeated load, flow etc.) damage is basically determined mainly by the individual features too. In the first part of our OTKA supported research program methods of the examinations are elaborated.

Goals

Goals of the research work were to characterize the response of the individual crop on the basis of the load of the coarse and grainy aggregations and to explore the relationships between the damage causing mechanical state and loads on individual cropps of the aggregation.

Method

i.) In the case of **coarse crops** where the minimum individual size of the crops were more than 30-40 mm, elements of the aggregation were tested one-by-one by the means of building up a pillar of apple (*figure 1*) and storage happened in bulk form using different kind of wrapping (*figure 2*). Loading of the fruit aggregations were carried out by using a hydraulic pulsator. Measured parameters were the accelerations in the aggregations, using an artifical apple developed in the HIAE, the exciting frequency (f), acceleration (a), and the mass of the damaged apple (V) respectively (*figure 3*).

ii.) For examining **grainy aggregations,** where the minimum measure of the individual grain varied between 5-30 mm, fodder pellets were chosen. In this case relationships between the main characteristics of the different compound feed (pellets) produced with almost the same technology were attempted to explore. Determination the mechanical effect, taking place inside the aggregations, results (PD index) carried out by the help of a special abrasion drum (Q-Tester) were used. Mechanical characterization of the individuals in the aggregation was carried out on the basis of characteristics of the radial crackling (F_k).

Results

i.) In the case of changes of the the rate of the damaged apple mass plotted against the loading time (t) at different loading levels are shown in (*figure 3*). Effect of the wrapping systems on different loading levels can be studied in (*figure 4*). In addition to these characteristics surface strength characteristics of the apples also were determined. Exploration the relationships between the individual and aggregation characteristics will be carried out in the second part of the research program.

ii.) In the case of **grainy aggregations** the PD index as the main feature of the fodder pellet was determined by means of different geometrical measures (l/d ratio) and the compositions of the compound feed. Results can be sin in (*figure 5*). Index of the resistance to rupture as the main feature of the individual parts in the aggregation was determined plotted against the above mentioned variables and it was presented by the help of the radial crumbling force (F_k) as it shown in (*figure 6*). Analysis of the relationships among the mechanical effects will be carried out in the following part of the program.

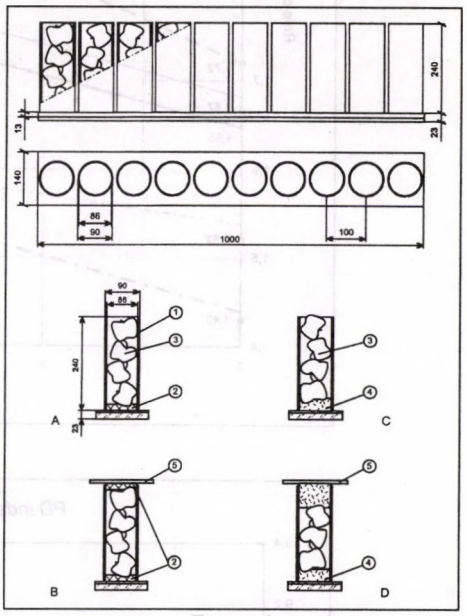

Figure 1
Rows of tubes and wrappings for testing apple pillars

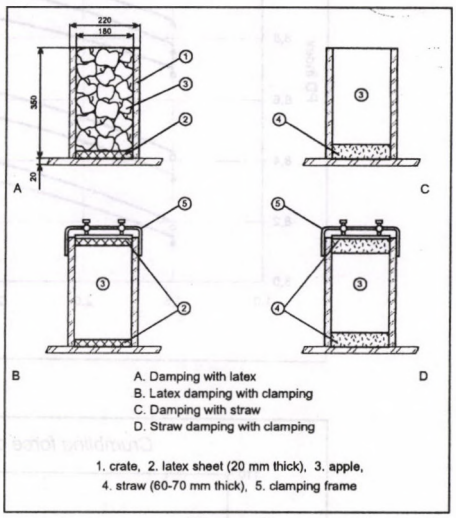

Figure 2
Wrapping solutions for apple stored in crate

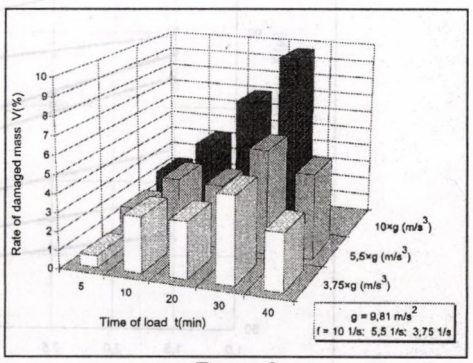

Figure 3
Change of rate of the damaged mass plotted against the load and time of load

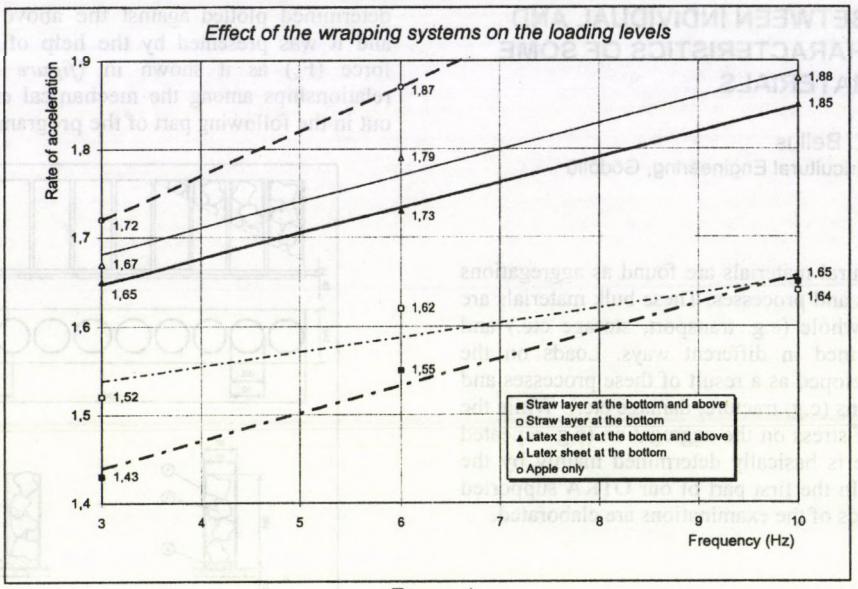

Figure 4

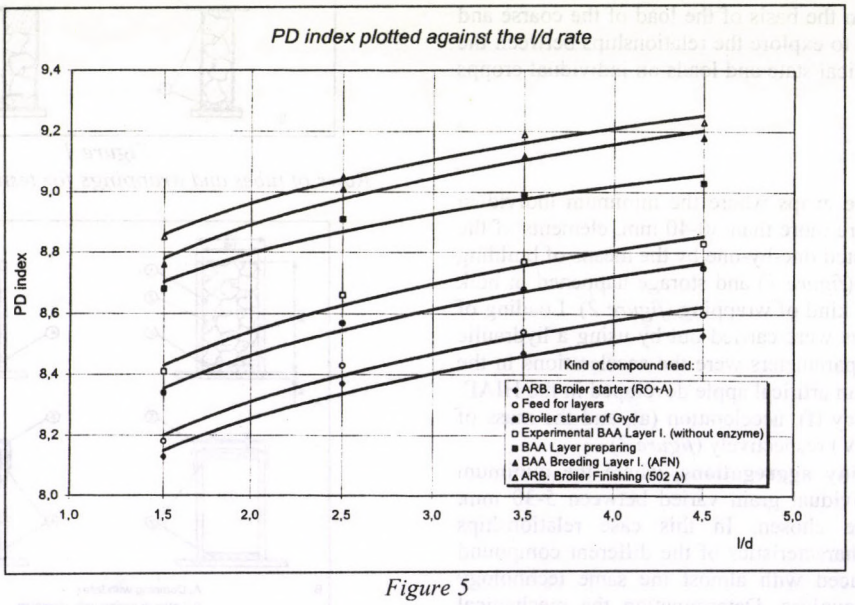

Figure 5

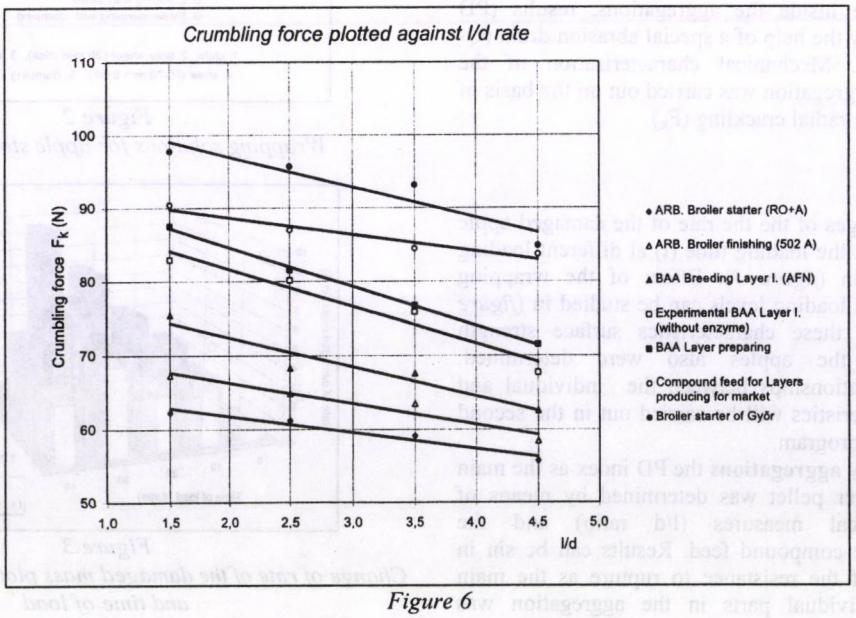

Figure 6

QUALITY, RELIABILITY, EFFICIENCY AND COMPROMISES IN THE PLANNING OF MILKING SYSTEMS

Dr. L. Tóth
University of Agricultural Sciences, Gödöllő
Dr. J. Bak
Hungarian Institute of Agricultural Engineering, Gödöllő

Abstract

There are two different trends at the design and the construction of milking equipment:

- In order to ensure the quality – because of the higher operational reliability –, the investment costs are extremely high and, this way, the energy and auxiliary consumptions will be increased as well.
- In order to avoid the oversizing the constructions, it is reasonable to make an effort to minimise the investment as low as possible which can result a save in energy and auxiliary requirement but at the same time the level of the necessary service will be higher and the immediate intervention will be needed if the parameters are not suitable to the quality standards.

Both solutions can be advantageous if they are synchronised with the real conditions correctly. In the case of a good infrastructure and service network, the rapid service can be available and its extra costs covered by the saving of the energy and auxiliary expenditures. Under more difficult conditions of infrastructure services, the oversizing is evidently advantageous which can provide a higher reliability. The subject and aim of the present paper is to analyse and evaluate these trends which can be recognised in Europe as well.

Preludes

In the past 35 years the requirement to the milk quality has been increasing and the cow stocks has been concentrated. The increasing milk yield and milk producing ability cow stocks are milked with higher flow rate milking devices. In our country, due to the large scale farming conditions (Holstein-Friesian herds, 4000-8000 litre/cow/year, average herds of 420 cows), the American, European and Hungarian milking device dimensioning principles had different effect on the quality, reliability and efficiency.

Method

Making use of milking device examination results and literature data of more decades modification of milking productivity is exposed, such as

- the transformation of the milk producing ability and milking rate of our cow stocks,
- the effect of the ISO, American and Hungarian dimensioning principles on air transport,
- the change of the milk tubes and collectors.

Results

Efficiency

In the past 35 years the productivity has increased significantly with the pipeline milking devices and milking platforms (*figure 1*).

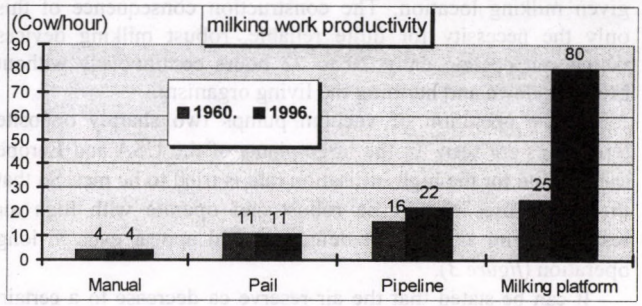

Figure 1
The efficiency of hand milking, pail and pipeline milking apparatuses

The efficiency increased also significantly. Whilst one person milked 4 to 5 cows in one hour, the pail milking devices made possible to milk 11 to 12 cows hourly. The today's milking efficiency is around 60-80 cows per hour for one person, which means at least 500 to 600 % increase brought by machine milking.

In the productivity the performance of the given milking device plays a role, but it is more significant how the shape, structure and automation of the apparatus is realised.

The advent and development of microelectronics and the automation made possible to carry out numerous machine operations what were unimaginable in the sixties. Such operations are udder preparation, separation of animals when driving in and out and the automatic getting off the milking device controlled by the milk flow.

Milking rate

That time milk production of the individual cows and mainly the performance of the milking devices is characterised by the average of 1.25 kg/minute and 2 kg/minute maximum milking rate achieved with Hungarian Spotted cow herds.

Those data of the 1960's years were the features of the milking devices rather than that of the herds.

The recent developments reached the 6 kg/minute maximum milking rate, and some cows can produce 9 kg/minute milk flow rate.

The evolution is better exhibited by the average milking rate, which increased to 3.8 kg minutely. Of course, those results can not be due to the milking devices. Meanwhile considerable breeding changes has happened and populations were selected for milk production (*figure 2*).

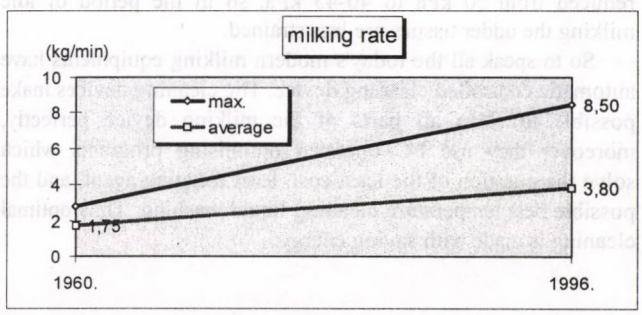

Figure 2
The change of milking rate in the past 30-40 years

Cost and energy saving

The main factor of raising investment efficiency is the extension of milking period i.e. the milking of more cows at a

given milking location. The construction consequence of this only the necessity for quite reliable, robust milking devices which can operate daily 20 to 22 hours continuously without breaking down and harming the living organism.

In the operation of vacuum pumps two sharply opposite tendencies are seen. In the large plants of the USA and Europe the demand for the high utilisation rate is tried to be met. So that the apparatuses should be robust and operate with high air reserve for no airtransport defects should appear even in long operation (*figure 3*).

It can be stated that the air reserve ca decrease to a certain extent and the vacuum pumps should be inspected and reinstated only then. In the case of ISO prescriptions only a few percent decrease is allowed in the air capacity, otherwise significant defects will occur. Thus those apparatuses need more frequent inspection and service by which the regular cost will increase.

In the most large equipments electronic control pulsators are used, at which the differences between the front and back udder quarter capacities are changed according to requirements of the herds.

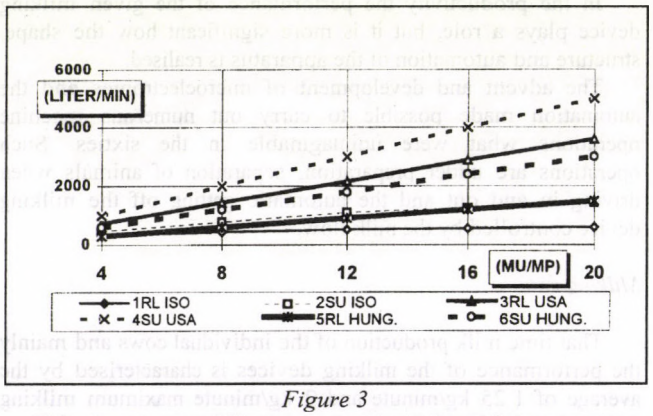

Figure 3
ISO, American and Hungarian prescriptions of air capacity (Differences in the air capacities - litre/min)
MU/MP = milking device/milking platform; 1RL ISO = Reserve ISO; 2SU ISO = Pump capacity ISO; 3RL USA = Reserve capacity USA; 4SU USA = Pump capacity USA; 5RL HUNG = Reserve capacity Hungary; 6SU HUNG = Pump capacity Hungary

With practically no exception lower building milk pipeline arrangements are used. Such way the milking devices became considerably simpler, while the milking vacuum level can be reduced from 50 kPa to 40-45 kPa, so in the period of idle milking the udder tissues are less strained.

So to speak all the today's modern milking equipments have automatic controlled cleaning device. The cleaning devices make possible to clean all parts of the milking device perfectly, moreover they use PC operated optimising programs which solve the question of the least cost, least cleaning agent, and the possible best temperature cleaning liquid washing. Thus optimal cleaning is made with saving energy.

Milk tubes and collectors

To follow the cows' milking ability increase the diameter of collectors and pipelines should (have) be(en) increased.
Both inner diameter of milk tubes (*figure 4*) and the milk reservoir volume of collectors (*figure 5*) and the diameter of main vacuum tube have been enlarged.

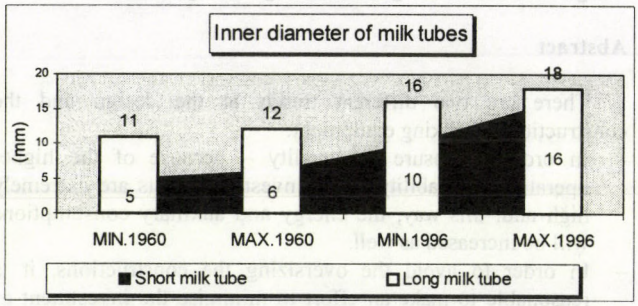

Figure 4
Evolution of inner diameter of milk tubes

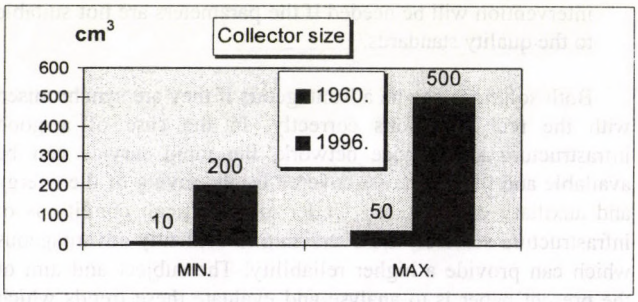

Figure 5
Evolution of milk reservoir volume of collectors

Conclusions

These days small volume working cylinders are applied at the milking device removers instead of large ones, so that the air consumption will be a fraction of the earlier value. In a milking platform the pulsators are operated in cascade system, thus the pulsation happens in different time at the milking devices, and not coinstantaneously.

Considering the whole milking platform the average air consumption for each milking unit is 25-30 % less nowadays. Thus the application of lower rate vacuum pumps is reasonable which need lower power supply by electric motors obviously. The result is reducing electric power requirement such way saving energy and cost.

The air reserve volume can be even reduced to 10 to 20 %. Of course, these equipments require the high precision operation and the continuous monitoring of the operation state during milking. Finally energy is saved by investing in

INSTRUMENTATION = SENSING, INDICATION & ALARM

TRANSMISSION OF RADIATION ON THE COVERING SURFACES OF GREENHOUSES

M. Szabó
University of Agricultural Sciences, Gödöllő

Introduction

Possibilities and importance of modelling of climate conditions in greenhouses were presented in my earlier publications. I pointed out the importance of examination of solar radiation which is the most important element of climate conditions in greenhouses.

Solar radiation respectively light are the fundamental factor of plant life conditions among the several factors being with each other in close connection which are determining the processes taking place in greenhouses. The characteristic of these is the timely determination by geographical base and climatic conditions.

Solar irradiance in greenhouses

The intensity of incoming radiation in greenhouses is determined first of all by the radiation on the Earth-surface and it is depending on solar-geometrical parameters and geographical latitude. The transmission of atmosphere is 70 % on average so the radiation intensity on the Earth- surface is maximal 1000 W/m^2 on average on a clear day. The construction and orientation of greenhouses influence considerably the forming of radiation coming into the greenhouse however covering materials and their condition have the most important role.

Method of research

The research of the measure of the radiation coming through the covering material of greenhouses was carried out by simulation models. I have determined the daily development of behaviour of 3 materials (glass, PE, PVC) in relation to radiation (their radiation transmission, reflection and absorption) for different periods by taking into consideration the physical characteristics and parameters of materials. These are summarised in *table 1.*

Table 1
Physical parameters of materials

	glass	PE	PVC
thickness (mm)	3 and 6 mm	1.5 and 3 mm	1.5 and 3 mm
index of refraction	1.526	1.54	1.46
extinction coefficient	0.0441	0.075	0.17

The outputs determined by simulation are specified to behaviour of materials against radiation:

- transmissivity
- reflectivity
- absorptivity.

The radiation coming on the material is 100 %. A part of radiation coming on to the material is absorbed and reflected by the material, and only a certain part of it is coming through the material. Transmissivity means the ratio of the radiation coming through the material and that of coming on to the material. The sum of these three components is 100 %, namely 1 at every time.

Result of the examination

The examination was carried out on new, unused, clear materials. The solar radiation and climate conditions in Hungary shown a yearly periodical change. For demonstration of the results I have selected two days of one year – 13 January, and 19 July (13^{th} and 200^{th} day of one year) with extreme climate conditions. The results are shown in the *figures 1, 2* and *3.*

It can be proved that the absorptivity is depending on the thickness of material, and the effect of radiation characteristics has not a significant role in it's developing. The glass and PE film have similar behaviour against radiation. Redoubling thickness of materials the transmissivity is reduced on average by 10 % each in both materials in summer and winter radiation conditions alike. The maximal value of radiation transmissivity in winter time is on average by 20 % less than that of in summer time independently of thickness, and it's period is less due to the shorter length of a day.

The physical parameters of PVC film differ from those of both previous materials. With double thickness of the PVC film the reduction of transmissivity was much more than in case of previous materials, moreover it had a change in values relating summer and winter periods as well. The reduction was 15 % in winter period and 17 % in summer period. The maximal value of radiation transmissivity of PVC film in winter time is on average by 18 % less than that of in summer time and it is independent of thickness as well.

It can be stated too that comparing materials with the same thickness (for example 3 mm) the radiation transmissivity of glass is the largest it is by 7 % smaller in case of PE film and by 23 % in PVC film in winter period (these values are 8 % and 26 % in summer period).

Conclusions

In the course of examinations it can be stated that there is not much difference between the characteristics of glass and PE film relating to the change of radiation transmissivity with double thickness of both materials however the transmissivity is reduced by 10 %. The reduction of transmissivity of PVC film is nevertheless 17 % in case of double thickness .

The measure of absorption is depending on the thickness of material, it is not influenced by radiation conditions (angle and intensity of incoming radiation).

Of the three materials the glass transmits the most light (radiation) by the same thickness the PE film transmits by nearly 7 % less radiation and the PVC film by 23 %.

Summarising the following conclusions can be drawn:

In the course of selection which covering material will by used taking into consideration of thickness of materials is important not only from the structural point of view (weight of material, fixing possibilities) but from the point of view of solar radiation transmissivity as well. The solar radiation transmissivity decreases considerably with the increase of thickness of materials and with that of absorption.

I tested the reduction of solar radiation transmission depending on thickness represents one of the characteristics of new, unused and clear materials. The physical quality of materials and its surface condition changes with using (ageing, getting dirty, condensation) and that can lead to further changes resulting in the solar radiation transmissivity. Further examinations are directed to determination of these.

Preferences

1. SZABÓ M., I. BARÓTFI.: Simulation possibilities of climate conditions in greenhouses. Hungarian Agricultural Engineering, 9/96 Gödöllő
2. SZABÓ, M.: 1996. Energetic Aspects of Condensation in Greenhouses. World Renewable Energy Congress IV. Denver, USA.
3. TAKAKURA, T.: 1983. Climate under Cover. Digital Simulation in Plant Bio-Engineering.

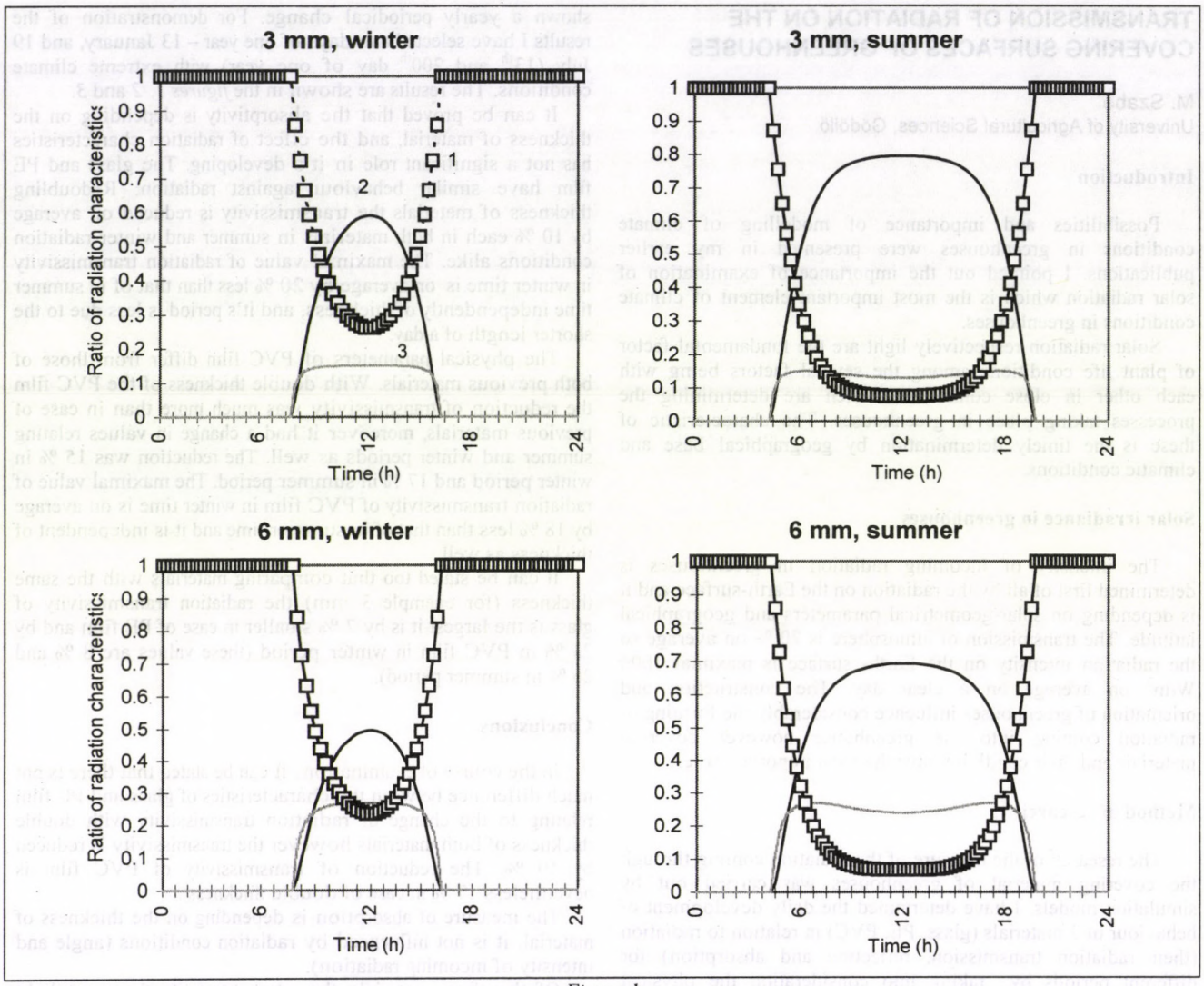

Figure 1

The change of radiation characteristic on glass with different thickness on different days (1 - reflectivity, 2 - transmissivity, 3 - absorptivity)

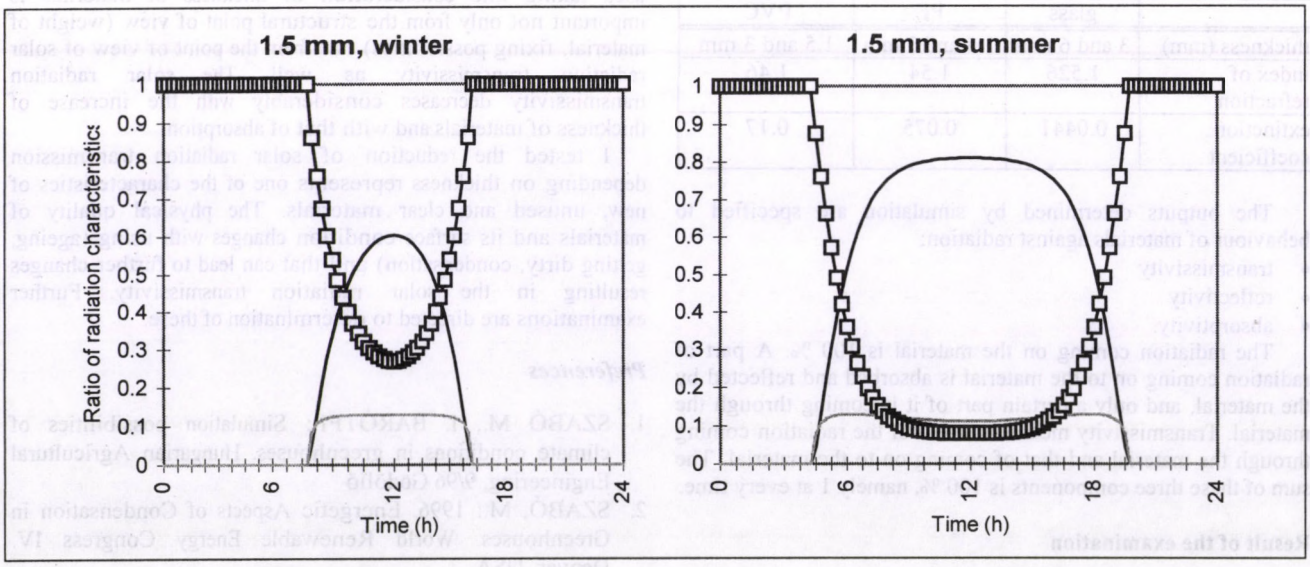

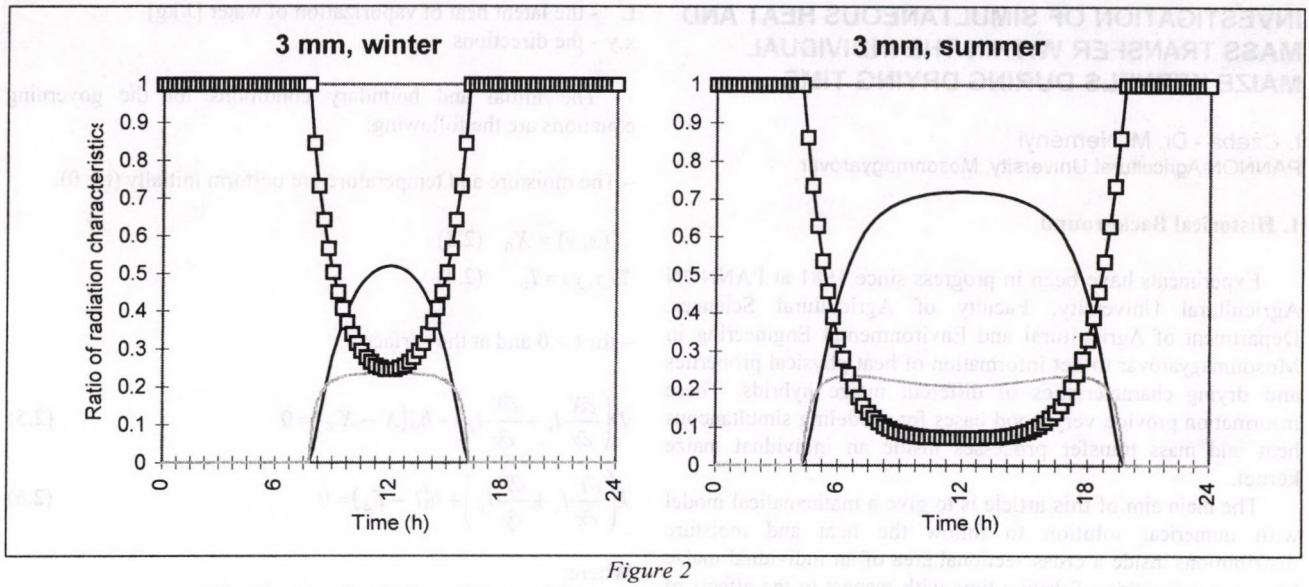

Figure 2

The change of radiation characteristic on PE film with different thickness on different days

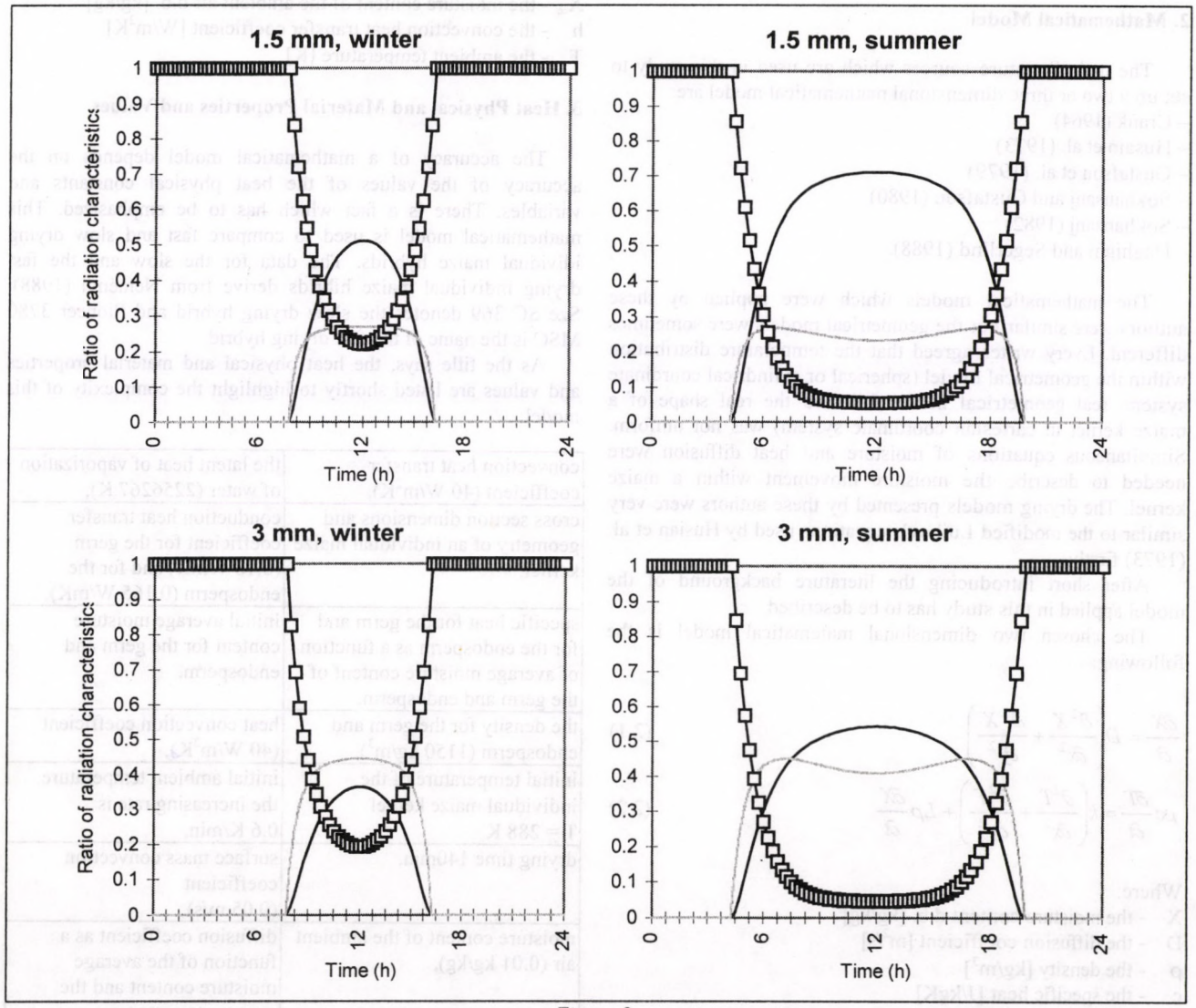

Figure 3

The change of radiation characteristic on PVC film with different thickness on different days

INVESTIGATION OF SIMULTANEOUS HEAT AND MASS TRANSFER WITHIN THE INDIVIDUAL MAIZE KERNELS DURING DRYING TIME

I. Czaba - Dr. M. Neményi
PANNON Agricultural University, Mosonmagyaróvár

1. Historical Background

Experiments have been in progress since 1981 at PANNON Agricultural University, Faculty of Agricultural Sciences, Department of Agricultural and Environmental Engineering in Mosonmagyaróvár to get information of heat physical properties and drying characteristics of different maize hybrids. These information provide very good bases for modeling simultaneous heat and mass transfer processes inside an individual maize kernel.

The main aim of this article is to give a mathematical model with numerical solution to follow the heat and moisture distributions inside a cross sectional area of an individual maize kernel as a function of drying time with respect to the effects of the coupled heat and mass transfer processes to be beyond the existing models and solutions published by literature sources.

2. Mathematical Model

The main literature sources which are used in this study to set up a two or three dimensional mathematical model are:
- Crank (1964)
- Husain et al. (1973)
- Gustafson et al. (1979)
- Sokhansanj and Gustafson (1980)
- Sokhansanj (1982)
- Haghighi and Segerlind (1988).

The mathematical models which were applied by these authors were similar but the geometrical models were sometimes different. Every writer agreed that the temperature distribution within the geometrical model (spherical or cylindrical coordinate system, real geometrical model followed the real shape of a maize kernel in cartesian coordinate system) was not uniform. Simultaneous equations of moisture and heat diffusion were needed to describe the moisture movement within a maize kernel. The drying models presented by these authors were very similar to the modified Luikov's equations used by Husian et al. (1973) firstly.

After short introducing the literature background of the model applied in this study has to be described.

The chosen two dimensional matematical model is the following:

$$\frac{\partial X}{\partial t} = D\left(\frac{\partial^2 X}{\partial x^2} + \frac{\partial^2 X}{\partial y^2}\right) \tag{2.1}$$

$$\rho c \frac{\partial T}{\partial t} = k\left(\frac{\partial^2 T}{\partial x^2} + \frac{\partial^2 T}{\partial y^2}\right) + L\rho \frac{\partial X}{\partial t} \tag{2.2}$$

Where:
X - the moisture content d.b. [kg/kg]
D - the diffusion coefficient [m^2/s]
ρ - the density [kg/m^3]
c - the specific heat [J/kgK]
T - the temperature [K]
t - the time [s]
k - the thermal conductivity [W/mK]
L - the latent heat of vaporization of water [J/kg]
x,y - the directions

The initial and boundary conditions for the governing equations are the following:

– The moisture and temperature are uniform initially (t = 0):

$$X(x,y) = X_0 \quad (2.3)$$

$$T(x,y) = T_0 \quad (2.4)$$

– for t > 0 and at the surface:

$$D\left(\frac{\partial X}{\partial x} l_x + \frac{\partial X}{\partial y} l_y\right) + h_m(X - X_\infty) = 0 \tag{2.5}$$

$$k\left(\frac{\partial T}{\partial x} l_x + \frac{\partial T}{\partial y} l_y\right) + h(T - T_\infty) = 0 \tag{2.6}$$

Where:
l_x, l_y - the direction cosines of the outward drawn normal to the boundary
h_m - the surface mass transfer coefficient [m/s]
X_∞ - the moisture content of the ambient air d.b. [kg/kg]
h - the convection heat transfer coefficient [W/m^2K]
T_∞ - the ambient temperature [K]

3. Heat Physical and Material Properties and Values

The accuracy of a mathematical model depends on the accuracy of the values of the heat physical constants and variables. There is a fact which has to be emphasized. This mathematical model is used to compare fast and slow drying idividual maize hybrids. The data for the slow and the fast drying individual maize hibrids derive from Neményi (1988). Sze SC 369 denotes the slow drying hybrid and Pioneer 3780 MSC is the name of the fast drying hybrid.

As the title says, the heat physical and material properties and values are listed shortly to highlight the complexity of this model:

convection heat transfer coefficient (40 W/m^2K),	the latent heat of vaporization of water (2256267 K),
cross section dimensions and geometry of an individual maize kernel,	conduction heat transfer coefficient for the germ (0.18 WmK) and for the endosperm (0.165 W/mK),
specific heat for the germ and for the endosperm as a function of average moisture content of the germ and endosperm,	initial average moisture content for the germ and endosperm,
the density for the germ and endosperm (1150 kg/m^3),	heat convection coefficient (40 W/m^2K),
initial temperature of the individual maize kernel T = 288 K,	initial ambient temperature, the increasing rate is 0.6 K/min,
drying time 140min,	surface mass convection coefficient (0.05 m/s),
moisture content of the ambient air (0.01 kg/kg),	diffusion coefficient as a function of the average moisture content and the average temperature,
shrinkage and deformation are not considered	

4. Solution Method

The HSTAR module of the COSMOS/M general finite element program package is used for the simulation. The geometrical model is drown by the GEOSTAR module. Finite element program package can be applied to solve transient heat transfer problems. Several tricks have to be figured out to enable the use of this general finite element program package for coupled heat and mass transfer problems.

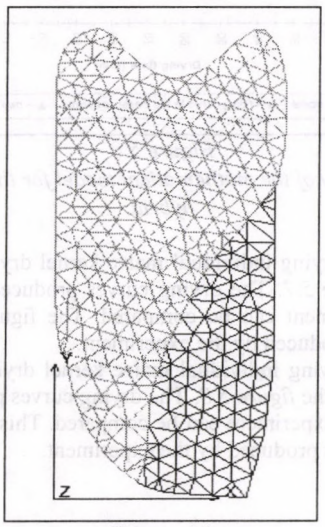

Figure 4.1
The FEM geometric model

The structure of the heat and moisture equation is similar so two identical geometrical models have to be used with this boundary and initial conditions for the heat and moisture equation respectively. *Figure 4.1* shows the cross sectional area of the individual maize hybrid. This area is divided into two parts namely the germ and endosperm. The applied finite element number of the germ is 197. The element number of the endospermium is 476 so the total element number of the cross sectional area is 673.

The effect of moisture evaporation can be taken into account by negativ heat sources for every element.

The running time is 140 min divided into 5 min element segments.

5. Results

Comparing drying characteristics of slow and fast drying individual maize kernel can help to understand the processes taken place during drying.

After five minute drying time there is not significant differences between the two type hybrids as *figure 5.1* shows. The moisture content of germs is higher than that of the endosperms that is reflected the initial parameters as well.

After seventy minute drying time there are significant differences between the moisture contents of the slow and fast drying hybrid. The slow drying hybrid contains more water than the fast drying hybrid. There are differences between the locations of the moistures too as *figure 5.2* represents.

After one hundred and forty-minute drying time the moisure differences increase between the slow and fast drying hybrid. The fast drying hybrid contains less water than slow drying hybrid. There are significant differences between the locations and distributions of the moisture profiles as well. These processes can be investigated in *figure 5.3.*

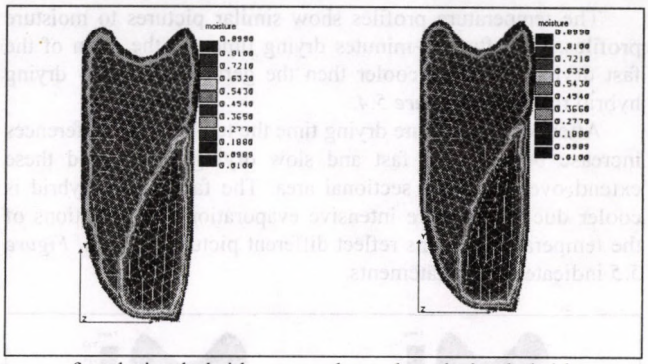

fast drying hybrid and slow drying hybrid

Figure 5.1
Moisture distributions after ten-minute drying time

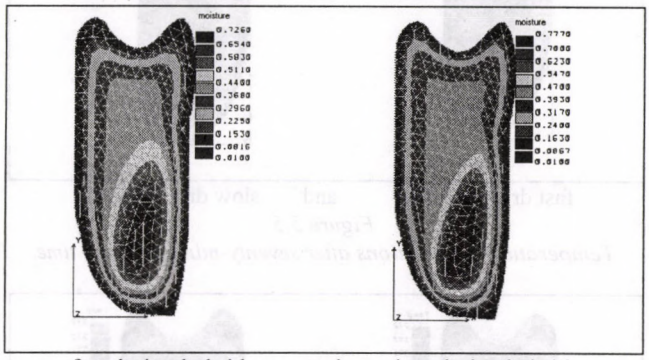

fast drying hybrid and slow drying hybrid

Figure 5.2
Moisture distributions after seventy-minute drying time

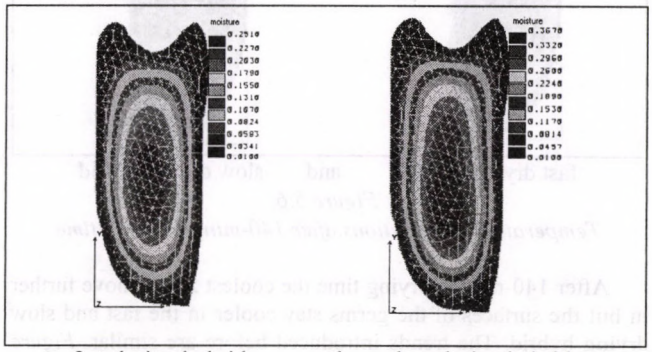

fast drying hybrid and slow drying hybrid

Figure 5.3
Moisture distributions after 140-minute drying time

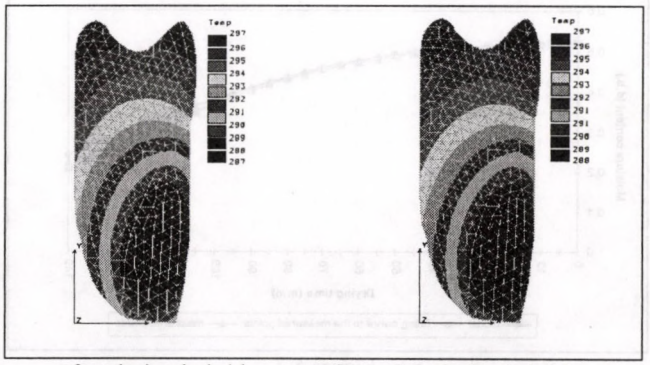

fast drying hybrid and slow drying hybrid

Figure 5.4
Temperature distributions after ten-minute drying time

The temperature profiles show similar pictures to moisture profiles. But after ten-minutes drying time the the germ of the fast drying hybrid is cooler then the germ of the slow drying hybrid reflected in *figure 5.4.*

After seventy-minute drying time the temperature differences increase between the fast and slow drying hybrid and these extend over the cross sectional area. The fast drying hybrid is cooler due to the more intensive evaporation. The locations of the temperature regions reflect different pictures as well. *Figure 5.5* indicates these statements.

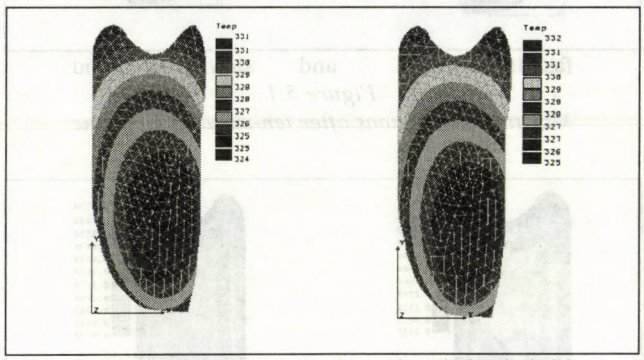

fast drying hybrid and slow drying hybrid

Figure 5.5

Temperature distributions after seventy-minute drying time

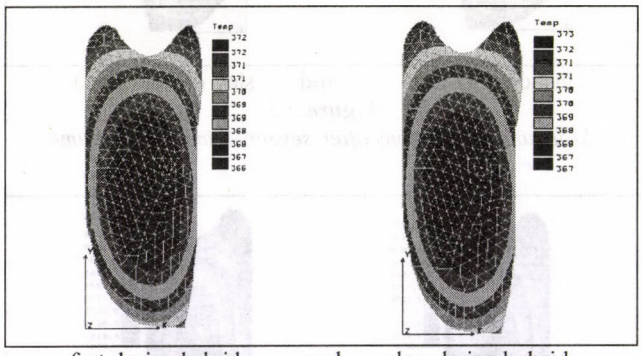

fast drying hybrid and slow drying hybrid

Figure 5.6

Temperature distributions after 140-minute drying time

After 140-minute drying time the coolest zones move further in but the surfaces of the germs stay cooler in the fast and slow drying hybrid. The trends introduced before are similar. *Figure 5.6* shows these tendencies.

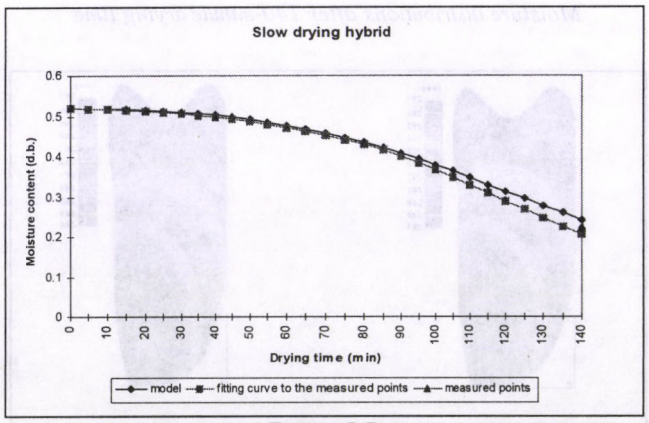

Figure 5.7

The accuracy of the mathematical model for the slow drying hybrid

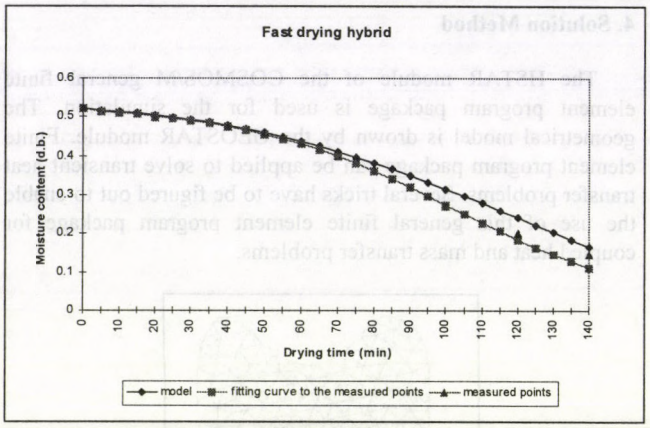

Figure 5.8

The accuracy of the mathematical model for the fast drying hybrid

The slow drying individual maize kernel drying data can be shown in *figure 5.7.* The drying curves produced by the model and the experiment can be compared. The figure contains the result points produced by the experiment.

The fast drying individual maize kernel drying data can be investigated in the *figure 5.8.* The drying curves produced by the model and the experiment can be compared. This figure contains the result points produced by the experiment.

6. Summary

This model can follow the drying processes very well. The mathemathical model with the boundary and initial conditions can reveal the differences between the fast and slow drying hybrids (Czaba, 1997). The temperature and moisture distributions inside the individual maize kernel produced by the model show more realistic picture than the results published before .

References

1. CZABA, I. (1977): Investigation of Coupled Heat and Mass Transfer Processes within the Individual Maize Hybrids during Drying Time. Mathematical Modelling and Simulation in Agricultural and Bio-Industries, IMACS/IFAC Second International Symposium, PhD Course.
2. CRANK, J. (1964): The Mathemathics of Diffusion. Oxford Press, NY.
3. GUSTAFSON. R.J. - THOMPSON, D.R. - SOKHANSANJ, S. (1979): Temperature and Stress Analysis of Corn Kernel - Finite Element Analysis. TRANSACTIONS of the ASAE, 22: 955-960.
4. HAGHIGHI, K. - SEGERLIND, L.J. (1988): Modeling Simultaneous Heat and Mass Transfer in an Isotropic Sphere - A Finite Element Approach. TRANSACTIONS of the ASAE, Vol. 31(2):March-April, 629-637.
5. HUSAIN, A. - CHEN, C.S. - CLAYTON, J.T. (1973): Simultaneous Heat and Mass Diffusion in Biological Materials. Journal of Agric. Engng. Res. 18, 343-354.
6. NEMÉNYI, M (1988): Energiatakarékosan szárítható kukoricahibridek jellemzői. Akadémiai Kiadó, Budapest.
7. SOKHANSANJ, S. (1982): Drying Induced Stresses in Food Grains - A Finite Element Approach. Drying '82 Edited by Mujumdar, A. S., McGrow-Hill International Book Company, 214-219.
8. SOKHANSANJ, S. - GUSTAFSON, R.J. (1980): Prediction of Heat and Mass Transfer within a Grain Kernel - A Finite Element Application. Drying '80 Volume2: Proceedings of the Second International Symposium, Edited by: Mujumdar, A. S., McGrow-Hill International Book Company, 229-232.

FINITE ELEMENT PREDICTION OF SOIL LOOSENING AND FORCES ACTING ON A MEDIUM-DEEP SUBSOILER

A. M. Mouazen - Dr. M. Neményi
PANNON Agricultural University, Mosonmagyaróvár

Abstract

The finite element method was used to study tillage of a sandy soil being externally loaded with medium-deep subsoiler. The numerical analysis was performed with three-dimensional models and COSMOS/M 1.71 software. The soil was considered as elastic-perfectly plastic material of nonlinear behavior. On the basis of the elastic-perfectly plastic material assumption, the Drucker-Prager material model was adopted. Soil loosening was estimated as soil volume change. The chisel and shank particular forces as well as the subsoiler total forces were calculated from the finite element model at the interface elements.

Introduction

Soil compaction owing to impact of the heavy agricultural machinery along with the cropping season is one of the most critical problems that negatively affects soil productivity and soil water content. However, layers of compacted soil can be built up by the action of tillage tools themselves, particularly where the same tool (mouldboard plough or heavy disc harrow) is used at the same cultivating depth in successive seasons (Trouse, 1985). This type of tillage practise creates the so-called hard pans. Hard pans, however, badly act in restriction of the gravitational water infiltration and vertical root growth. Subsoiling is a common tillage practise being used to loosen compacted deep layers.

The finite element method (FEM) is being used to study soil cutting and tillage. The strategy followed in this paper was to apply the FEM for investigation of a deep tillage system. On the basis of the Drucker-Prager material model, a commercially available COSMOS/M 1.71 FFM program was used to accomplish the analysis.

Objectives

The paper aims to:

1- develop three-dimensional, FEM model of sandy soil cutting by a medium-deep subsoiler,
2- introduce the FEM calculations of the draft and vertical force, and
3- demonstrate soil deformation as well as soil stress distribution of different types.

Materials and methods

Since agricultural soils, as bulk materials under external loads, suffer of plastic deformations in addition to the elastic ones, the Drucker-Prager elastic-perfectly plastic material model was used, whose the yield function can be expressed as follows:

$$f = 3\alpha\sigma_m + \overline{\sigma} - k = 0$$

where: α, k = material parameters, σ_m = mean principal stress, $\overline{\sigma}$ = effective stress.

Two sources of nonlinearity appear when a soil is being under external load, namely material and geometrical non-linearity. In order to deal with the material nonlinearity, an incremental analysis technique was used. The increment size was selected to be moderate in order to get as much as possible an accurate solution under an acceptable computational time. Inside each load step the Newton-Raphson iteration method was applied. While the geometrical nonlinearity was solved by employing the small strain assumption (COSMOS/M 1.71 FEM program, 1994).

Eight nodes, solid elements, were selected to represent the soil body. The subsoiler was determined as rigid body. The chisel and shank of the subsoiler enclosed 23, and 90 degree with the horizon, respectively. The chisel was 6 cm thick, whereas the shank was 3.6 cm thick.

Since the problem was symmetric about the central plane *ABCD* (*figure 1*), only one half of the total region was meshed and considered during the analysis.

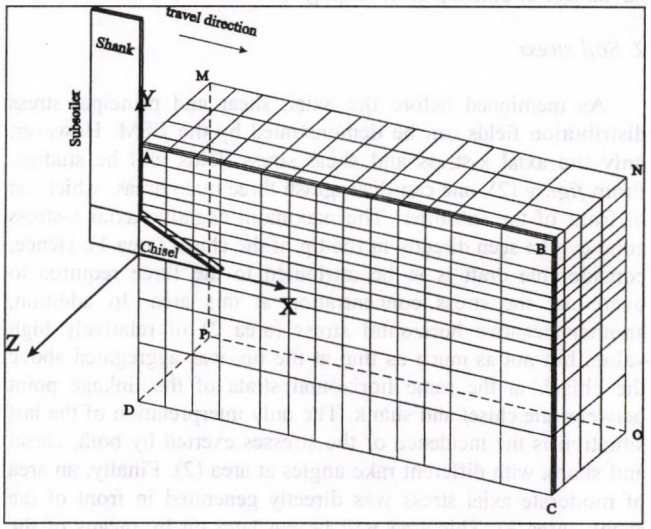

Figure 1
Three-dimensional FEM mesh of soil cutting with medium-deep subsoiler

The sideways surfaces *ABCD* and *MNOP* were constrained in the positive and negative (Z) directions, respectively. The vertical Y-displacement of the bottom surface *DPOC* was also constrained, whilst the surfaces *AMPD* and *BNOC* were transfixed against the positive negative and X-displacements, respectively. The upper surface *ANMB* was left free of any constraints.

The subsoiler was moved 10 cm in the positive X-direction as had been done by Araya and Gao (1995). This displacement was set at all interface nodes.

On the other hand, the effect of soil-tool interaction was taken into account by inserting two nodes, gap elements between the two bodies. The Coulomb's criterion of dry friction was specified to the interface elements.

The material parameters incorporated into the FFM analysis were given by previous study (Mouazen and Neményi, 1996).

Results and discussion

After 10 cm subsoiler movement in travel direction, upward soil displacement and soil stress distributions were investigated. On the other hand, the draft and vertical force were calculated for the chisel and shank separately, and the subsoiler total forces were then obtained from the summation of the chisel and shank particular forces.

1. Soil displacement

Since soil loosening by different subsoilers is of lifting the type, the maximum upward soil displacement is chosen as an

indicator of the quality of soil loosening. The maximum upward soil displacement predicted by the FEM model, was 11.4 cm. This number coincides well with the measured one (10 cm) (Araya and Gao, 1995). Araya and Gao performed subsoiling measurements with the same sandy soil. But their FEM model has predicted a maximum vertical soil displacement of 6.5 cm. This low prediction was attributed by them to the soil continuity, which decreased the upward movement of soil surface as it was connected to deeper layer. To overcome the disability of predicting an accurate vertical soil displacement, two nodes, soil-soil cutting elements were assigned directly in front of the subsoiler tip. Accordingly, the better estimation of the vertical soil displacement (11.4 cm) achieved herein, proved the advantage of utilising such cutting elements.

2. Soil stress

As mentioned before the axial, shear and principal stress distribution fields can be demonstrated by the EFM. However, only the axial x-stress and shear stress fields will be studied. From *figure* (2), one can distinguish three main areas, which sat in front of the subsoiler. The maximum negative axial x-stress zone can be seen directly at the tip of the chisel (area 1). Hence, considerable draft is to be attributed to the force required to overcome the stress concentration at this area. In addition, another negative horizontal stress (area 2) of relatively high value, but not as much as that at the tip, was aggregated above the chisel, at the same horizontal strata of the linkage point between the chisel and shank. The only interpretation of the last situation is the incidence of the stresses exerted by both, chisel and shank with different rake angles at area (2). Finally, an area of moderate axial stress was directly generated in front of the shank (area 3). This area will be cut later on by means of the subsoiler shank. However, the negative value of the whole stress contours corresponding to these three zones indicted that the whole area situated above the chisel was under compressive load.

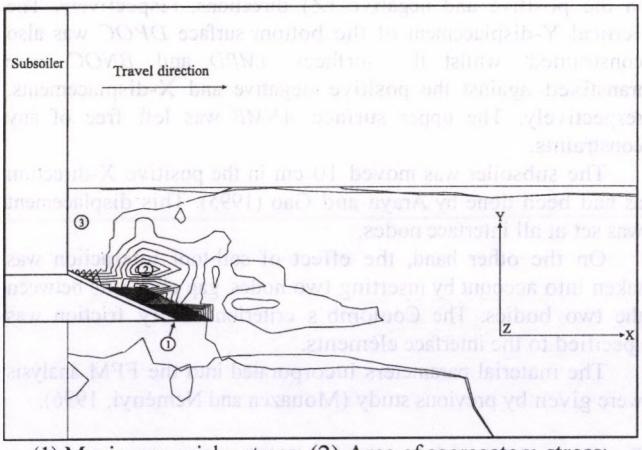

(1) Maximum axial x-stress; (2) Area of aggregate x-stress; (3) Slightly disturbed area

Figure 2

Illustrates the axial x-stress distribution throughout the central plane ABCD

On the other hand, two other stress zones of shear type can be distinguished (*figure 3*). The area (1) started from the tip of the chisel, extended toward the shank along the cutting edges of the chisel. This might explain the cutting of the sideways and front soils by the chisel edges and tip, respectively. Also, the extension of another high shear stress from the tip of the chisel upward the soil surface (area 2) explained occurring of another soil failure in shear along with a so called failure surface which extended from the tip upward the soil surface. In general, the highest soil shear stress concentration at the tip and the area surrounding the chisel body emphasised the necessity of subsoiling in disruption and breaking deep horizons at the chisel working depth, where hard pans are usually created by mouldboard ploughs or heavy disc harrows.

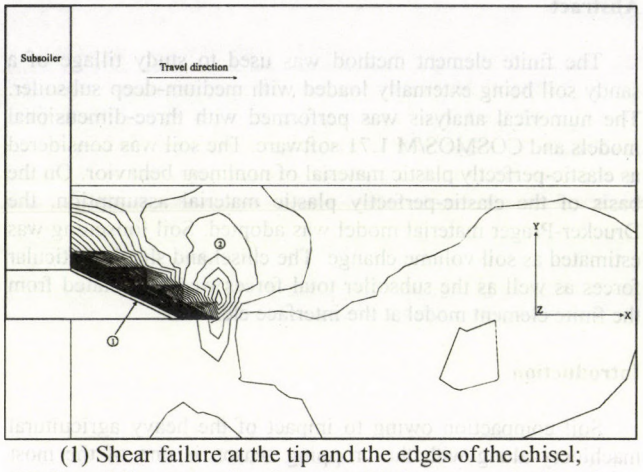

(1) Shear failure at the tip and the edges of the chisel; (2) shear failure extending from the chisel tip upward soil surface

Figure 3

The distribution of the shear τ_{xy} stress throughout the central plane

3. Draft and vertical force

At working depth of 34 cm, draft and vertical force were predicted from the forces acting on the interface elements. This was performed by the summation of the interface node forces. The horizontal and vertical components represented the draft and vertical force, respectively. Since only one half of the total region was considered in the analysis, the actual forces were twice the magnitude of the half model. *Figure* (4) shows the calculated draft from the FEM model of the chisel, shank and whole subsoiler (total draft). They had increased with the subsoiler progress in the travel direction till they achieved peak values of 3469 N, 4367 N and 7835 N of the shank, chisel and subsoiler, respectively. Moreover, the maximum draft occurred at 5 cm subsoiler displacement. Since the maximum draft refers to the force required for the failure of the soil block in front of cutting tool, soil failure has taken place at 5 cm subsoiler displacement. The total draft was compared with the measured one by Bánházi et al., (1984).

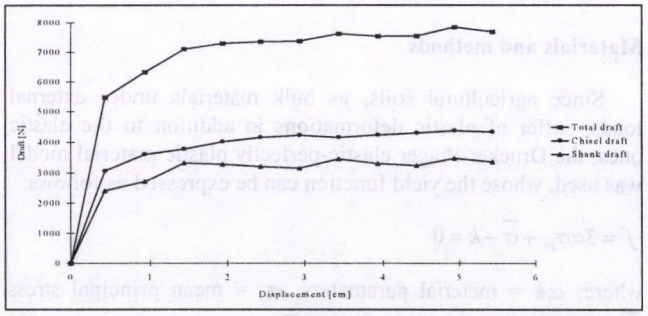

Figure 4

FE calculation of the draft as a function of subsoiler displacement

As shows in *table* (1), the estimated draft from the FE model was less than the measured one by nearly 2000 N.

Table 1
A comparison of measured and predicted draft (Resources are denoted under the table)

Reso-urces	Draft	Cultivating depth (cm)	Speed (m/s)	Draft value (N)
1	measured	40	0.55	9810
2	predicted 2-D	34	0.066	3142
3	predicted 3-D	34	0.066	7835

1- Bánházi et. al. (1984). 2- Mouazen and Neményi (1996).
3- The authors prediction of draft

The divergence of draft estimation might be attributed either to a deeper cultivating depth of 40 cm, or a higher speed of 0.55 m/s of the field subsoiling. Therefore, further study should be carried out to evaluate better draft by assuming equal cultivating depth and speed.

Mouazen and Neményi, (1996) have conducted two-dimensional FEM analysis of soil cutting by the subsoiler investigated in this paper, from which less draft force of 3142 N was calculated. They also utilised the same soil mechanical coefficients. The sideways soil reaction force taken into account at the three-dimensional FE models, increased the total draft up to 7835 N. This asserted the necessity of creating three-dimensional models when studying the soil cutting process by narrow tools, because the predicted force would agreed better with the measured in the field.

Likewise, the vertical force of the chisel, shank and subsoiler were estimated from the model *figure* (5). The vertical force of the shank was negative, while the total and chisel vertical forces were positive. The negative vertical force refers to the force tending to lift the shank upwards. However, the overall vertical force of the subsoiler was positive but less than the chisel positive vertical force. Hence, the resulted vertical force would push the subsoiler downwards. The magnitude of the vertical forces were 5922 N, - 909 N and 5013 N of the chisel, shank and subsoiler respectively.

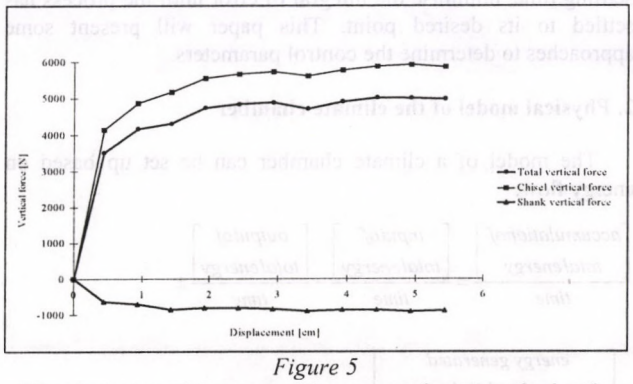

Figure 5
FE calculation of the vertical forces as a function of subsoiler displacement

A comparison of total draft and total vertical force is shown in *figure* (6). The total vertical force comprised 63% of the total draft.

Conclusions

1. A construction of satisfactory, non-linear, 3-dimensional finite element model of soil cutting by a medium-deep subsoiler was done. The model was able to overcome the complexity of assembly the chisel and shank of unequal rake angles. Soil-tool external friction was also taken into consideration in addition to soil shear strength.
2. Soil vertical displacement was higher than the measured one by 1.4 cm.
3. The demonstration of the soil shear stress and soil axial stress assured that most of the soil breaking occurred at the tip and around the whole chisel. This was because of the high shear stress concentrations at this area.
4. The draft predicted from the model was relatively in good agreement with that measured and reported in previous study. Further study should be done in order to get better prediction of draft by compromising the model hypothesises with the experimental circumstances so that the cultivating depth and speed should be equalised for both, the model and experiment (soil bin). However, the calculated total draft was 7835 N cutting at 34 cm depth, while the measured in the field was 9810 N cutting at 40 cm depth.

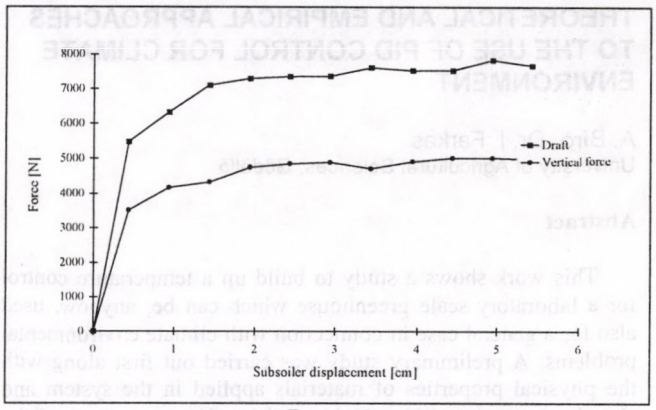

Figure 6
Total draft and vertical force with subsoiler displacement

References

1. ARAYA, K.; GAO, R., 1995. A non-linear three-dimensional finite element analysis of subsoiler cutting with pressurised air injection. Journal of Agricultural Engineering Research, 61, 115-128.
2. BÁNHÁZI, J., JÓRI, J.L. AND SOÓS, P., 1984. Investigation and Comparing of Soil Cultivation with Medium-Deep Subsoilers. (In Hungarian). Hungarian Academy of Science, Budapest, 74 pp.
3. CHEN, W.F.; MIZUNO, E., 1990. Nonlinear analysis in soil mechanics. Elsevier Science Publisher, Amsterdam, The Netherlands.
4. Cosmos/M Version 1.71., Finite Element Program., 1994. Advanced modules manual.
5. DUNCAN, J.; CHANG, C.Y. 1970. Nonlinear analysis of stress and strain in soils. Journal of Soil Mechanics and Foundation Division. American Society of Civil Engineering, 96 (sm5): 1629-1653.
6. MOUAZEN, A. M.; NEMÉNYI, M., 1996. Tow-dimensional finite element analysis of soil cutting by medium deep subsoiler. Hungarian Agricultural Engineering 9/96, 32-36.
7. TROUSE, A.C., 1985. Development of the controlled traffic concept. Proceeding of International Conference on Soil Dynamics. Auburn, Alabama. June 17-19, Vol. (5): 1112-1119.

THEORETICAL AND EMPIRICAL APPROACHES TO THE USE OF PID CONTROL FOR CLIMATE ENVIRONMENT

A. Bíró -Dr. I. Farkas
University of Agricultural Sciences, Gödöllő

Abstract

This work shows a study to build up a temperature control for a laboratory scale greenhouse which can be, anyhow, used also for a general case in connection with climate environmental problems. A preliminary study was carried out first along with the physical properties of materials applied in the system and also the governing differential equations. The parameters of the system were identified on the basis of measurements inputting with standard signals. The identification shows that heat capacity dependence on ventilation can not be ignored. The constants of PID controller were determined taking into consideration the calculated and the measured parameters. A trial was made to use an empirical approach to the determination of PID controller, as well.

1. Introduction

Respecting for the energy cost, the temperature in climate chambers, especially in greenhouse should keep around a desired level more precisely. Lower accuracy requires higher setpoint in temperature which results more energy consumption (Tantau, 1997). In the recent work it was aimed to control the inside temperature for a laboratory scale greenhouse – as climate chamber – using PID controlled electrical heater.

The laboratory size of greenhouse was developed inside the process control laboratory in the Department of Physics and Process Control. (*figure 1*). The greenhouse can be heated with solar preheated water or with electrical energy. The opening of top window can be controlled, while front windows open manually. The ventilation rate can be changed by two fans located on the bottom of the greenhouse. The light tubes are above the greenhouse. Extra light can be provided with temporarily mounted light sources inside the greenhouse.

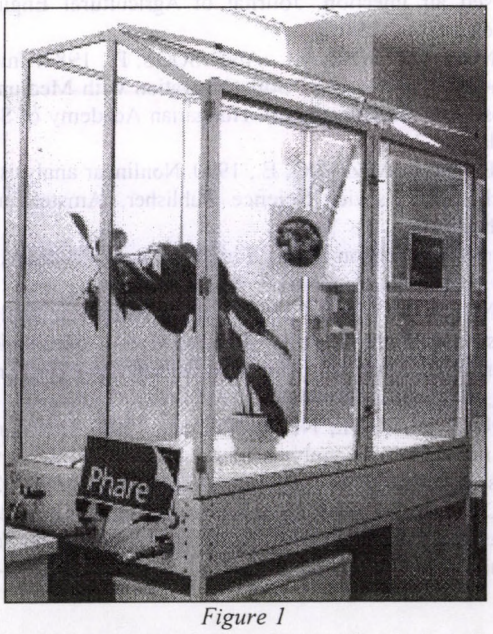

Figure 1
Sight of laboratory scale greenhouse after the installation (1996)

The continuous data logging and control system is based on ADAM 4000 series modules, while supplementary circuits and the software were individually designed and elaborated (Seres et al., 1997). The applied temperature sensors are standard Pt100 type. The area of 3 mm thick glass layer is 8.34 m^2, the mass of glass is about 60 kg, the mass of aluminium structure is about 60 kg. The maximal power of electrical heater is 2025 W.

The most commonly used feedback controller to a climate chamber is a PID one, the output of which can be given by

$$c(t) = P\varepsilon(t) + I\int_0^t \varepsilon(t)dt + D\frac{d\varepsilon(t)}{dt} + c_0\,, \qquad (1)$$

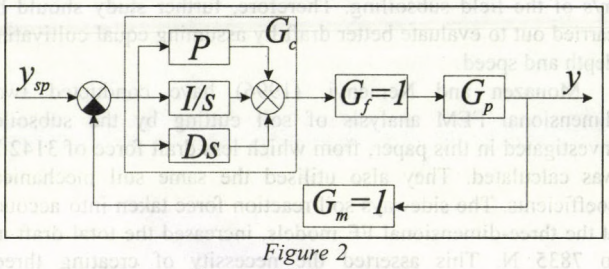

Figure 2
Sketch of PID controller

where $c(t)$ - controller output, $\varepsilon(t)$ - error between the desired and measured value , P - proportional gain, I - integral gain, D - derivative gain and c_0 - output of the controller when $\varepsilon = 0$ (constant zero). The sketch of PID feedback controller describing in Laplace domain can be seen in *figure 2*. P, I, D represent the constants, y_{sp} - setpoint, y - output of the process, G_c - transfer function of the controller, G_f - transfer function of the final control element, G_p - transfer function of the process and G_m - transfer function of the measurements.

There are several ways to determine the constants of such a controller considering the performance criterion, i.e., to keep maximum deviation (error) as small as possible, achieve a short settling time, minimise the integral of error until the process has settled to its desired point. This paper will present some approaches to determine the control parameters.

2. Physical model of the climate chamber

The model of a climate chamber can be set up based on energy flow:

$$\frac{\left[\begin{array}{c}accumulation of\\ total energy\end{array}\right]}{time} = \frac{\left[\begin{array}{c}input of\\ total energy\end{array}\right]}{time} - \frac{\left[\begin{array}{c}output of\\ total energy\end{array}\right]}{time} \pm$$

$$\pm\frac{\left[\begin{array}{c}energy\ generated/\\ consumed\ within\ the\ system\end{array}\right]}{time} \qquad (2)$$

For control purpose it is much more preferable to use a model which has only a few identified parameters. Instead of using a rather complicated model, in our case, the following simplified model was applied:

$$\frac{dx_t}{dt} = \frac{1}{C_q}\left[K_{out,air}\left(u_t - x_t\right) + u_H\right], \qquad (3)$$

where x_t - greenhouse temperature, C_q - greenhouse heat capacity, $K_{out,air}$ - heat transfer coefficient from greenhouse air to outside air, u_t - outside temperature, u_H - power of electrical heating. In this special case the outside air is identical to the laboratory air where the greenhouse is located in. The reason of

using the x and u notations is that in process control terminology x means the state variable and u means the input variable. The estimated values of parameters (C_q, $K_{out,air}$) can be calculated based on physical properties of materials from which the climate chamber is composed of. For C_q it yields:

$$C_q \approx \frac{1}{2}\sum_{i=1}^{n} c_i m_i = \frac{1}{2}\left(c_{AL} m_{AL} + c_{GL} m_{GL}\right) =$$

$$\frac{1}{2}\left(900 \cdot 60 + 840 \cdot 60\right) = 52200 \ \ [\mathrm{J\ K^{-1}}],$$

where 1/2 comes from the average temperature of greenhouse structure which is $(u_t+x_t)/2$. The n means the number of main components of the greenhouse, here those are aluminium (AL) and glass (GL). The c_i means the specific heat and m_i means the mass of ith material component. For $K_{out,air}$ the estimation yields:

$$K_{out,air} \approx k_{GL} A_{GL} = \frac{1}{\frac{1}{\alpha_{out,GL}} + \frac{d_{GL}}{\lambda_{GL}} + \frac{1}{\alpha_{GL,air}}} A_{GL} =$$

$$= \frac{1}{\frac{1}{15} + \frac{0.003}{0.8} + \frac{1}{8}} 8.34 = 43 \ \ [\mathrm{W\ K^{-1}}],$$

where k_{GL} - the specific heat transfer coefficient from greenhouse to outside, A_{GL} - surface area of glass, $\alpha_{out,GL}$ - specific heat transfer coefficient from glass to outside, d_{GL} - thickness of glass, λ_{GL} - specific heat conduction coefficient for glass, $\alpha_{GL,air}$ - specific heat transfer coefficient from greenhouse air to glass.

3. Identification of the model

Building the model of a process requires also the identification part. In the recent case there were eight experiments carried out with different heating and ventilation. The heating can be measured as the heating power (u_H), while the ventilation can be expressed as the percentage of the roof opening (r_w). The temperature in the laboratory was almost the same in each experiment, so difference was calculated between greenhouse and laboratory temperatures, and it was used as a temperature for greenhouse. Eq. (3) was fit to the numerical values of the measurements in order to identify the parameters C_q and $K_{out,air}$. *Figure 3* and *table 1* show the result of the identification.

Table 1
Result of parameter identification

No.	$x_{t,0}$ - $u_{t,0}$ [°C]	u_H [W]	r_w [%]	C_q [kJ K^{-1}]	$K_{out,air}$ [W K^{-1}]
1	0.0	2025	0	63.900	39.9
2	48.2	0	0	63.900	34.9
3	0.0	950	0	67.844	34.7
4	27.6	0	0	67.844	35.2
5	0.0	950	30	117.964	65.3
6	15.9	0	30	117.964	44.4
7	0.0	2025	100	216 609	163.9
8	12.8	0	100	216.609	117.0

The results show that the heat capacity (C_q) and heat transfer coefficient ($K_{out,air}$) are dependent on the roof opening. *Figures 4a* and *4b* show these relations for which a linear approximation is suggested to introduce. So it is proved that the window opening is not negligible in this sense. The parameters at r_w=100 % are more than three times higher than the case at r_w=0 %.

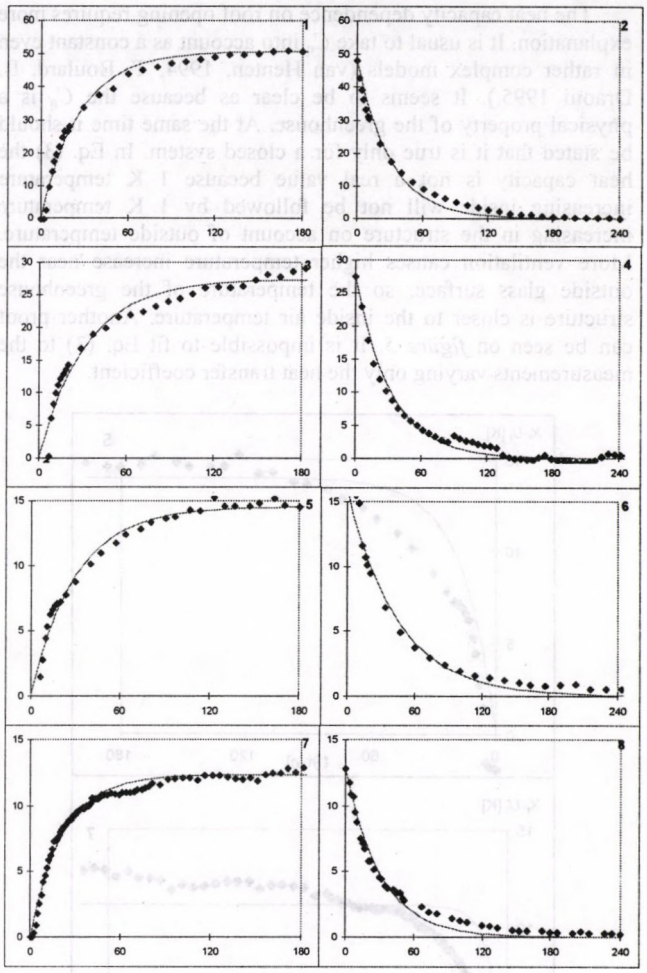

Figure 3
Measured (dots) and modelled (solid line) temperatures difference [°C] during the time [min]

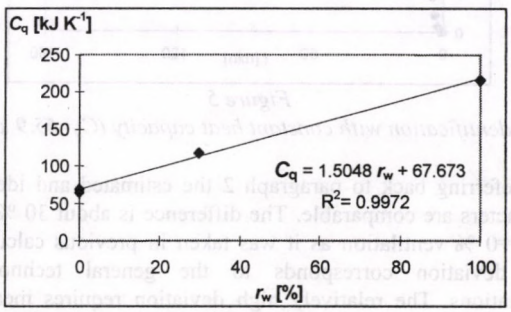

Figure 4a
C_q function of roof opening

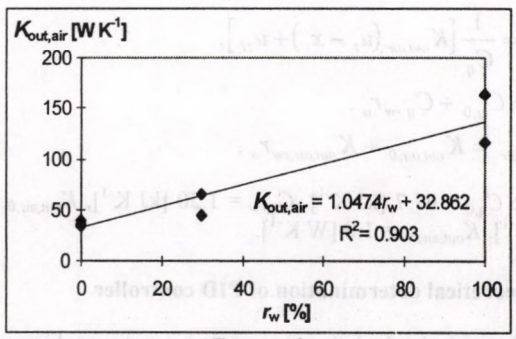

Figure 4b
$K_{out,air}$ function of roof opening

The heat capacity dependence on roof opening requires more explanation. It is usual to take C_q into account as a constant even in rather complex models (van Henten, 1994, T. Boulard, B. Draoui 1995.). It seems to be clear as because the C_q is a physical property of the greenhouse. At the same time it should be stated that it is true only for a closed system. In Eq. (3) the heat capacity is not a real value because 1 K temperature increasing inside will not be followed by 1 K temperature increasing in the structure on account of outside temperature. More ventilation causes higher temperature increase near the outside glass surface, so the temperature of the greenhouse structure is closer to the inside air temperature. Another proof can be seen on *figure 5*. It is impossible to fit Eq. (3) to the measurements varying only the heat transfer coefficient.

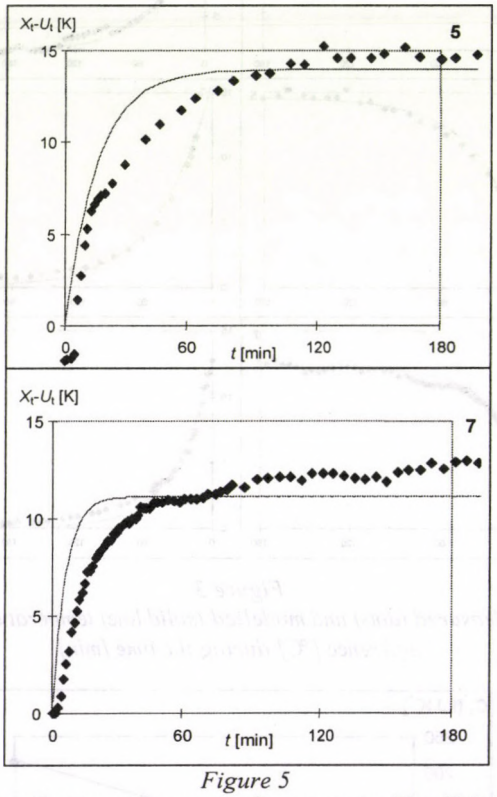

Figure 5
Identification with constant heat capacity (C_q=65.9 kJ)

Referring back to paragraph 2 the estimated and identified parameters are comparable. The difference is about 30 % based on r_w=0 % ventilation as it was taken in previous calculation. The deviation corresponds to the general technological calculations. The relatively high deviation requires measuring and identification for almost all control problems.

The identified model is as follows:

$$\frac{dx_t}{dt} = \frac{1}{C_q}\left[K_{out,air}(u_t - x_t) + u_H\right], \tag{4a}$$

$$C_q = C_{q,0} + C_{q,rw} r_w, \tag{4b}$$

$$K_{out,air} = K_{out,air,0} + K_{out,air,rw} r_w, \tag{4c}$$

where $C_{q,0}$ = 67.7 [kJ K^{-1}], $C_{q,rw}$ = 1.50 [kJ K^{-1}], $K_{out,air,0}$ = 32.9 [W K^{-1}], $K_{out,air,rw}$ = 1.0 [W K^{-1}].

4. Theoretical determination of PID controller

Theoretical calculation was carried out at a working point of r_w=50 %. Here $K_{out,air,rw}$ = 82.9 [W K^{-1}], $C_{q,50}$ = 142.7 [kJ K^{-1}].

The transfer function of the process can be derived from Eq. (3). Taking the Laplace transform of both sides of Eq. (3):

$$sX_t = \frac{1}{C_q}\left[K_{out,air}(U_t - X_t) + U_H\right], \tag{5}$$

where X_t, U_t and U_H note the Laplace transformation of x_t, u_t and u_H. Let us consider steady state and U_t =0, which means that outside temperature is supposed to be constant. Rearranging Eq. (5) yields:

$$X_t\left(s + \frac{K_{out,air}}{C_q}\right) = \frac{1}{C_q} U_H, \tag{6}$$

from which the transfer function of the process (relationship between input and output) comes as:

$$G_p = \frac{X_t}{U_H} = \frac{1}{C_q s + K_{out,air}}. \tag{7}$$

The transfer function of a PID controller is:

$$G_c = \frac{Ds^2 + Ps + I}{s}, \tag{8}$$

and so in the actual case the global transfer function, based on *figure 2*, is:

$$G = \frac{G_c G_p}{1 + G_c G_p} = \frac{Ds^2 + Ps + I}{Ds^2 + (P + C_q)s + I + K_{out,air}}. \tag{9}$$

The goal is now to find the „best" controller setting with no overshoot and minimum integral error. The objective function to be minimised can be:

$$J = \left(1 + t_{over}/t_f\right)\int_0^{t_f} \left|X_t - X_{t,\infty}\right| dt, \tag{10}$$

where t_{over} - time while the system $X_t > X_{t,\infty}$ is in overshot state, t_f - final time when the system is in steady state again and $X_{t,\infty}$ - the new steady state. The minimisation was carried out with a MATLAB program which uses functions of Control Toolbox and it can be found in the Appendix. The final results of the determination of the parameters of the PID controller are as follows:

P = 285.4 [W K^{-1}], I = 0.1678 [W K^{-1} min^{-1}], D = 16214 [W K^{-1} min].

5. Empirical determination of PID controller

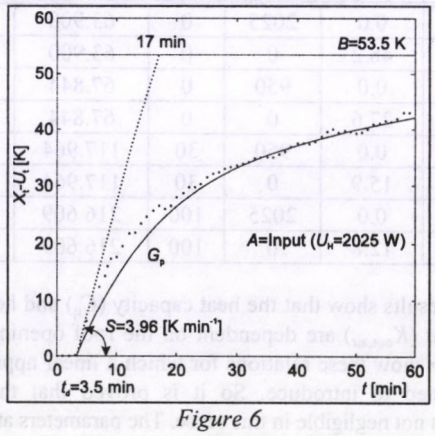

Figure 6
Calculation of the PID constants based on Cohen and Coon method

There are several ways to tune the PID control parameters based on different performance criteria. Cohen and Coon (1953) observed that the response of most processing unit to an input change had sigmodial shape. The response can be approximated by the response of a first order system with dead time:

$$G_p = \frac{Ke^{-t_d s}}{\tau s + 1}. \qquad (11)$$

Figure 6 shows the first hour of the measurements. In the experiment the heat power was a step function from 0 to 2025 W and the roof was closed. The laboratory temperature was constant so the temperature difference was calculated between the laboratory and greenhouse temperatures. In such a way the „empirical" parameters in Eq. (11) can be calculated as:

$$K = \frac{output at steady state}{input at steady state} = \frac{B}{A} = \frac{53.5}{2025} = 0.0264\ [\mathrm{K\ W^{-1}}],$$

$$\tau = \frac{output at steady state}{slope at inflection point} = \frac{B}{S} = \frac{53.5}{3.96} = 13.5\ [\mathrm{min}],$$

$$t_d = time elapsed until the system responded = 3.5\ [\mathrm{min}].$$

After all, the „best" controller setting with one-quarter decay ratio, minimum offset and minimum integral square error is as follows:

$$P = \frac{1}{K}\frac{\tau}{\tau_d}\left(\frac{4}{3} + \frac{t_d}{4\tau}\right) = \frac{1}{0.0264}\frac{13.5}{3.5}\left(\frac{4}{3} + \frac{3.5}{4 \cdot 13.5}\right) = 204.3\ [\mathrm{W\ K^{-1}}],$$

$$I = \frac{P}{\tau_d}\frac{13 + 8\frac{t_d}{\tau}}{32 + 6\frac{t_d}{\tau}} = \frac{204.3}{3.5}\frac{13 + 8 \cdot (3.5/13.5)}{32 + 6 \cdot (3.5/13.5)} = 26.22\ [\mathrm{W\ K^{-1}\ min^{-1}}],$$

$$D = P\tau_d \frac{4}{11 + 2\frac{t_d}{\tau}} = 204.3 \cdot 3.5 \frac{4}{11 + 2 \cdot (3.5/13.5)} = 248.3\ [\mathrm{W\ K^{-1}\ min}].$$

6. Conclusions

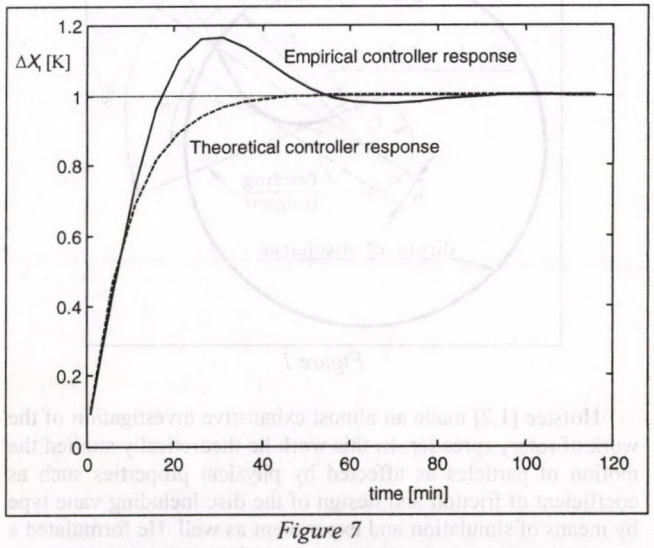

Figure 7
Responses of different controllers to stepwise input

The empirical methods for tuning of controllers found in the literature are easy to use for control climate chambers. The only disadvantage of such methods is that the general performance criteria is not suitable for all cases.

In the actual case the controller was designed on the basis of theoretical considerations for the critically damped response. This kind of controller requires a bit less energy because it has not any overshoot.

The simulation results for the examined two PID controllers can be seen in *figure 7* 1 K temperature rise in the setpoint has different responses for different controllers.

The parameter identification has shown that heat capacity dependence on ventilation can not be ignored neither for modelling nor for the designing controller.

Acknowledgements

This work was supported by the projects of Hungarian Academy of Sciences No. F-325-95. and OTKA No. F 024046.

Appendix

MATLAB program and its functions for solving Eqs (9-10) are given furthermore:

```
function [num, den] = pidfn(k,C, P,I,D)
% calculate the resulting transfer function
Gcn = [D P I]; Gcd = [0 1 0];     % transfer function of control
Gpn = [0 1];   Gpd =   [C k];     % transfer function of process
[num1 den1] = series(Gcn, Gcd, Gpn, Gpd);
[num den] = feedback(num1, den1, [1],[1], -1);
```

```
function [f] = pidob(x,K,C)          % objective function
P = x(1);                            % trial of P, I, D constants
I = x(2);                            %
D = x(3);                            %
[num den] = pidfn(K,C, P,I,D);       % feedback transfer function
[y x t] = step(num, den);            % calculate step response
k = dcgain(num, den);                % steady state gain
a = sum(y>k)/length(y);              % overshoot ratio
b = sum( abs(k-y) );                 % integral of error
f = (a+1)*b;                         % value to be minimised
```

```
% pid1.m program determination of P, I, D constants
P = 204;                             % initial values
I = 26/60;
D = 248*60;
K = 32.9+1.0*50;                     % heat transfer coefficient
C = (67.7+1.5*50)*1e3;               % heat capacity
x = fmins('pidob',[P I D],[],[],K,C);
P = x(1);                            % solution
I = x(2);
D = x(3);
```

References

1. BOULARD, T. - DRAOUI, B.: In-situ calibration of greenhouse climate control including sensible heat, water vapour and CO_2 balances, M²SABI'95 IMACS/IFAC Symposium, Brussels, Belgium, 1995.
2. COHEN, G.H. - COON, G.A.: Theoretical consideration of retarded control, *Trans. ASME 75,* 827. 1953.
3. VAN HENTEN, E.J.: Greenhouse climate management: an optimal control approach, Thesis Wageningen, The Netherlands, 1994.
4. NYBRANT, T.: Modelling and control of grain dryers, UPTEC 8625 R, Uppsala University, Sweden, 1986.
5. SERES, E.E. - FARKAS, I. - BIRÓ, A. - BUZÁS, J. - LÁGYMÁNYOSI, A.: Data logging and monitoring tools used for simulation and modelling of a solar system, M²SABI'97 IMACS/IFAC Symposium, Budapest, Hungary, 1997.
6. STEPHANOPOULOS, G.: Chemical process control: An introduction to theory and practice, Prentice-Hall Inc. Englewood Cliffs, New Jersey, USA, 1984.
7. NISE, N.S.: Control System Engineering: The Benjamin /Cummings Publishing Company Inc., Redwood City, California, USA, 1995.
8. TANTAU, H. J.: Energy saving potential of greenhouse climate control, M²SABI'97 IMACS/IFAC Symposium, Budapest, Hungary, 1997.

SIMULATION OF FERTILIZER DISCHARGE CHARACTERISTICS AS EFFECTED BY DISC AND VANE DESIGN PARAMETERS AND THE PARTICLE MOTION ON THE DISC

A. Soleymangoli - Dr. F. Kasza
University of Agricultural Sciences, Gödöllő

Abstract

The spinning disc fertilizer spreader is the most widely used tool of spreading fertilizer to the ground. A well designed machine should produce the uniform distribution as well as the desired working width. Our research focused on the comparison of different feeding radii, vane shapes and orientation. Computer simulation was applied in order to qualify and optimize vane designs with flat disc. The discharge direction, the absolute discharge velocity and the time of the duration on the disk were the output parameters. The approximate equation of vane shape, the equation of forces acting on the particle and the numerical integration formulae are considered as governing relationships. For straight radial vanes the effect of (1*) feeding and discharge radius on the target values were calculated and plotted. In the other groups of simulation experiments the mutual effect of (2*) pitch angle and friction coefficient, (3*) the feed and discharge angles as well as (4*) pitch angle and curve height of near circular shaped vane. In some cases mathematical optimum was found, but in all cases the results can be used for design and adjustment purposes.

*The numbers refers to the groups of simulation completed.

1. Introduction

Optimal application of fertilizer, minimization of its spoilage, improvement of existing and development of possible new application techniques, all require a thorough knowledge of the processes and the factors that affect the spreading of fertilizer.

Particle motion on disc and in air is the important feature of the rotary fertilizer spreader construction and is calculated on the bases of mechanical and physical properties and parameters using laws of mechanics and physics. In general exact calculations are not possible to obtain. Instead of them it is normal to use approximate numeric methods, which still supply more reliable and accurate results in the overwhelming number of cases.

Basically, the spreading of granulated fertilizer is influenced by three groups of factors: *(a)* physical properties of fertilizer, *(b)* the fertilizer spreader (disc and vane) design, *(c)* external factors (power machine, soil, wind, etc.).

Fertilizer parameters affecting spreading quality are the particle size and distribution, particle shape, roundness, rolling and sliding factors (friction coefficient), collision characteristics, air resistance of particle, as well as other properties (moisture content, strength, etc.).

Characteristic parameters of spreader design are spinning disc axis orientation (angle to vertical direction), speed of disc rotation, feeding radius on the disc, disc shape (e.g. cone parameters), vane shapes (forward or backward pitched vanes, radial, straight or curved, flat or twisted shapes, etc.), surface quality of the disc and vane (roughness, elasticity, painting or coverage quality etc.).

The most important external factors are motion characteristics of the power machine transferred to the implement. (motion speed, vibrations, etc.); unevenness of the soil surface, clogs, etc.; weather characteristics (wind, humidity).

One tries to use only most important factors which has the major affect. All the other characters should be kept standard.

Simulation preliminaries (literature review)

In an earlier study Mennel and Reece [3] dealt with designs of vane with respect to the discharge direction in the vertical plane. They concluded that (a) The air resistance cannot be neglected in the computation of the trajectory of even the largest fertilizer particles and (b) Unless the blades are specially shaped, a centrifugal distributor will project material at quite large angles to the plane of the disc. This will result in large variation of range.

Cunningham [5] provided analytic solutions for a flat disc with forward or backward pitched vanes, a cone shaped disc with straight radial vanes, and a flat disc with a vane meeting a logarithmic spiral. Situations for which α or β are not equal to zero or where the vanes are not straight have to be solved by numerical methods since no analytical solutions exist for most situations. The advantage of a forward curved vane is that a greater acceleration and a more positive action near the centre can be developed than with forward pitched vanes.

Cunningham and Chao [5] described the equation for a composite vane, starting with a curved section (circular), and followed by a straight radial section. The advantage of such a vane should be that it can pick up the fertilizer flowing from the delivery opening smoothly without impact. Impact at an early stage will usually result in scattering of the particles over the disc.

Brinsfield and Hummel [6] derived a similar equation for a disc with tubes instead of vanes. The first tube region has a constant radial radius and the second tube region is radial. The advantage of this vane type is that it should also reduce the random motion inherent in most conventional distributor disc designs.

Galili and Shteingauz [7] and Galili et al. [8] developed equations for a vertical disc. The vertical disc produces a linear distribution pattern instead of a horizontal circular pattern.

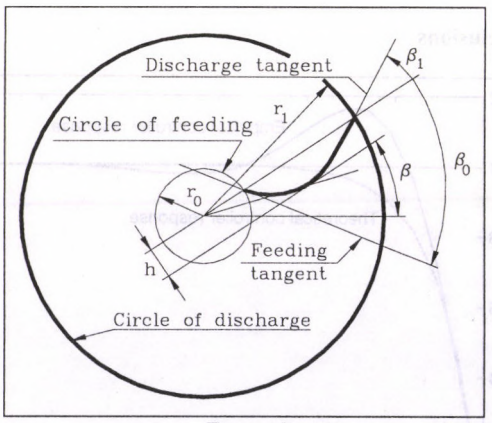

Figure 1

Hofstee [1,2] made an almost exhaustive investigation of the work of rotary spreader. In this work he theoretically studied the motion of particles as affected by physical properties such as coefficient of friction and design of the disc including vane type by means of simulation and experiment as well. He formulated a general equation governing equation of the particle motion on the disc and the vane. He collected also the formulae for straight radial and pitched vanes with flat and conical discs, and for curved circular and spiral vanes. He showed the results for different design characteristics. In this work a thorough collection of references is included.

Csizmazia, Kasza and Polyák [9,10,11] developed general numerical approximation equations of particle motion on a vane of general shape. This work is a continuation and development of that study.

As compared to the above references results of the present paper claims apply and develop the previous references. A different approach is used compared to that of Hofstee. The most important difference lays upon using a general polynomial vane shape which can approximate any vane type described by one curve. Compared to the earlier developed three dimensional statement [9,10,11], the concrete simulation results are evaluated restricted to flat disc and two dimensional vane shape.

Equations of simulation

Among many other effects the three major factors that influence the fertilizer distribution pattern are discharge angle, discharge velocity and particle duration of stay on disc. Although it is not possible to neglect the effect of the particle motion in the air on the distribution pattern, our investigations on that topic are not included in this paper, because the vane design can be completely characterized on the used basis.

There are three fundamental equation of the simulation used by us:

- Equation of vane shape
- Equation of forces acting on a particle while moving on the disc and along the vane
- Numerical integration equations

Equation of vane shape

The curve of grain path along the vane is by polynomial curve. The general form of arc length ($s=r\varphi$) function used by us contains four constants (ψ_i) and the general form is

$$s=\sum_{i=1}^{n}\psi_i r^i \text{ or } s=\psi_0+\psi_1 r+\psi_2 r^2+\psi_3 r^3 \quad (1)$$

because we used third order function in order to introduce four characteristics which are polar co-ordinates of feed and discharge points (r_0,0 and r_1,s_1), feed and discharge angles (β_0 and β_1). in some cases other conditions are introduced to the approximate shape on this basis. The curve geometry and the parameters are shown in *figure 1.*

To formulate the kinetic equation of motion one applies the general expression of the tangent direction and the value of curvature in an arbitrary point.

The equation of tangent is

$$\beta=\frac{s}{r}+\arctan s'$$

while the curvature value is

$$\frac{1}{\rho}=\cos(\arctan s')\frac{d}{dr}(\arctan s')$$

and after applying differentiation:

$$\frac{1}{\rho}=\cos(\arctan s')\frac{s''}{1+s'^2}$$

Skipping the mathematical details it is only mentioned that the above equations supply the sufficient formulae to simulate any case considered.

Equation of forces acting between the particle, vane and disc while moving

The particle is accelerated on the horizontal flat disc along the vane by the force expressed as follows

$$F_t=F_{cf}\left[\cos(\beta-\vartheta)-\mu_v\sin(\beta-\vartheta)\right]-(F_{pn}+F_C)\mu_v-G\mu_d \quad (1)$$

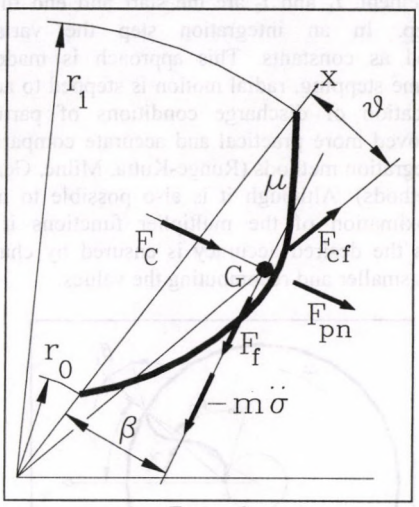

Figure 2

Going through the expression from left to right the formula consists of terms corresponding to the centrifugal force component tangential to the vane, the friction force part on the vane due to the centrifugal force, the friction forces on the vane generated by the normal load originated from rotational inertia force and the Coriolis inertia force and the friction force on the disc from the weight. The forces and angles can be identified in *figure 2.* The total of the friction force on the disc and vane is denoted by F_f in the figure. To identify the figure better it is noted that in the case shown in the figure β is positive and ϑ is negative because they are measured counter-clockwise from x axis fixed to the disc.

The expressions of the forces:

Centrifugal force: $F_{cf}=mr\omega^2$,

where m is the mass of particle, r is the off-centre radial position of particle ω is the angle rotation speed.

Rotational inertia force normal to the curved vane: $F_{pn}=m\frac{\dot{\sigma}^2}{\rho}$,

where $\dot{\sigma}$ is the relative particle velocity along the vane and ρ is the vane radius of curvature.

Coriolis inertia force: $F_C=2m\omega\dot{\sigma}$

Using the driving force expression (1) the equation of motion will be

$$\ddot{\sigma}=F_t/m \quad (2)$$

The combination (1) and (2) relationships are used in the simulation.

Equations of numerical integration

The governing equation of the particle motion can be interpreted as

$$A(t)\ddot{\sigma}+B(t)\dot{\sigma}+C(t)\sigma+D(t)=0 \quad (3)$$

where A,B,C and D are time functions.

Using weighted residual formulation to (3) with weight function $w(t)$ and using integration by parts twice [11], the differential equation is replaced by the integral equation

$$A\left[\dot{\sigma}w-\sigma\dot{w}\right]_{t_1}^{t_2}+B\left[\sigma w\right]_{t_1}^{t_2}+\int_{t_1}^{t_2}(A\sigma\ddot{w}-B\sigma\dot{w}+C\sigma w)dt=-\int_{t_1}^{t_2}Dwdt \quad (4)$$

The weight functions we need are the homogeneous solutions to the differential equation inside the left hand side integral statement. t_1 and t_2 are the start and end times of an integral step. In an integration step the variables are approximated as constants. This approach is made because instead of time stepping, radial motion is stepped to achieve the exact application of discharge conditions of particle. This approach proved more practical and accurate comparing to the standard integration methods (Runge-Kutta, Milne, Gear, Adams or other methods). Although it is also possible to use higher order approximation of the multiplier functions it was not necessary as the desired accuracy is ensured by changing the motion steps smaller and recomputing the values.

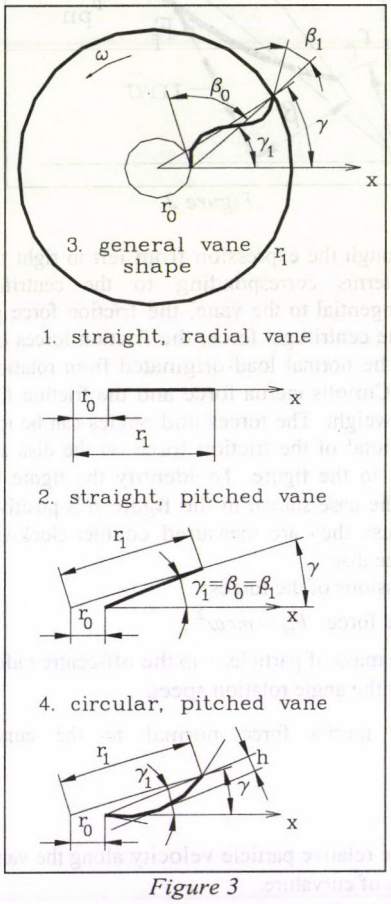

Figure 3

Describing simulations and evaluation of results:

The influence of different design parameters on discharge angle, discharge velocity and duration of stay on disc are investigated in four groups. Only flat disc is considered in this stage of our simulation research. In the *first group* the above mentioned characteristics are calculated as functions of feed radius and discharge radius. The vane is straight and radial. The *second group* of simulation discovers the effect of the vane pitching on the particle motion and the three target values. The *third group* deals with the feed angle and discharge angle as geometry parameter of vane. In the *fourth group* arc shaped vane was examined with changing height and pitch angle. The examined vane shape parameters are shown in *figure 3* according to the simulation groups.

Simulation group 1

The effect of changing feed and disc radii values on the target values were searched. Four types of fertilizer with four different disc surface materials (of 16 friction coefficient values) were examined. The *figures 4, 5, 6* are illustrations of discharge angle, discharge velocity and duration of stay for Nitrate with painted steel material.

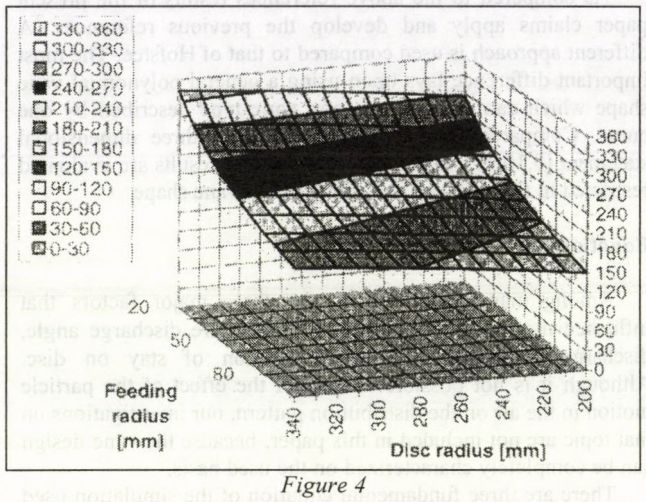

Figure 4
Effect of variation of feed and disc radius on particle discharge angle (Nitrate – Painted pate)

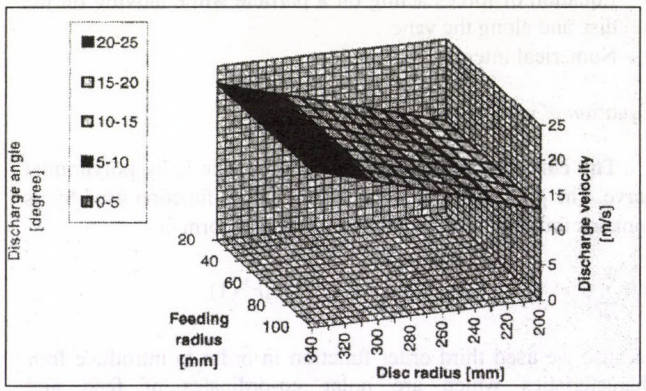

Figure 5
Discharge velocity as affected by the changes of feed and disc radius (Nitrate – Painted pate)

In the simulation example shown, the vane was straight and radial. The examination parameters are:

Feed radius:

$20mm \le r_0 \le 100mm$

Discharge radius:

$200mm \le r_1 \le 340mm$

As one can find out from the simulation equations it was necessary to apply other parameters kept constant in the simulation. The fixed parameters in this group are

Friction coefficient: $\mu = 0.45$ (nitrate with painted disk, as we measured.

Speed of angle rotation: $\omega = 56\,\text{radian/s}$

According to the *Figure 4*, increasing the discharge radius i.e. vane length, will proportionally increase the discharge angle, while an increase of the feed radius will decrease that in a decreasing rate.

Figure 5 shows a double linear relationship of discharge velocity versus disc radius (or vane length) and feeding radius.

Comparing *figure 6* to *figure 4* one can recognise that the shape of the duration of stay surface is the same as that of the discharge angle. (That is why this type of diagram will not be shown in this paper any more.)

Simulation group 2

In this group the effect of pitch angle and coefficient of friction on the discharge angle, discharge velocity and duration of stay were investigated. The most important results are presented in *figures 7 and 8*.

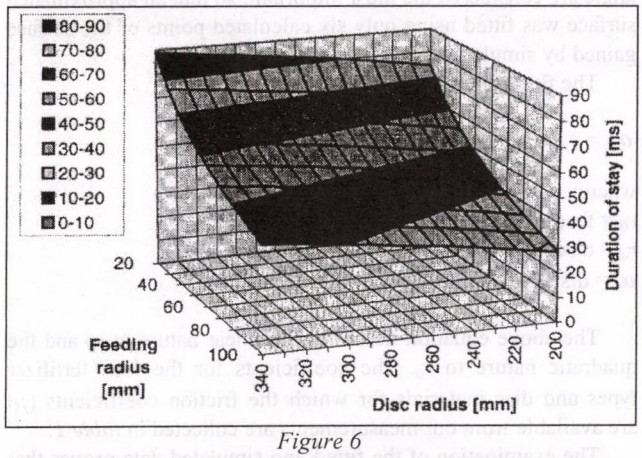

Figure 6
Particle duration of stay affected by changes on feed and disc radius (Nitrate – Painted pate)

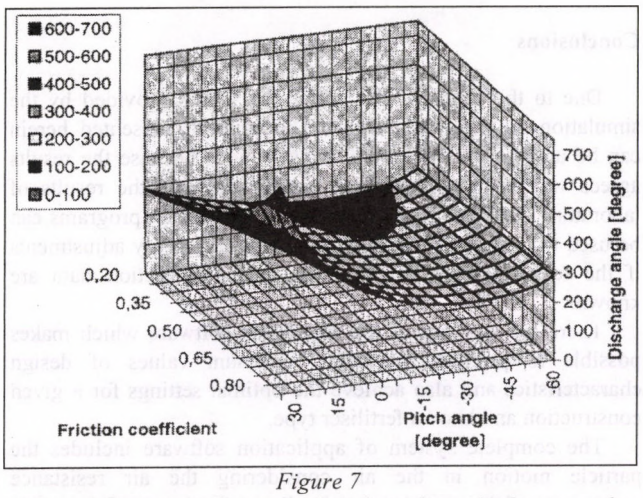

Figure 7
Effect of friction coefficient and pitch angle on discharge angle (Nitrate – Painted pate)

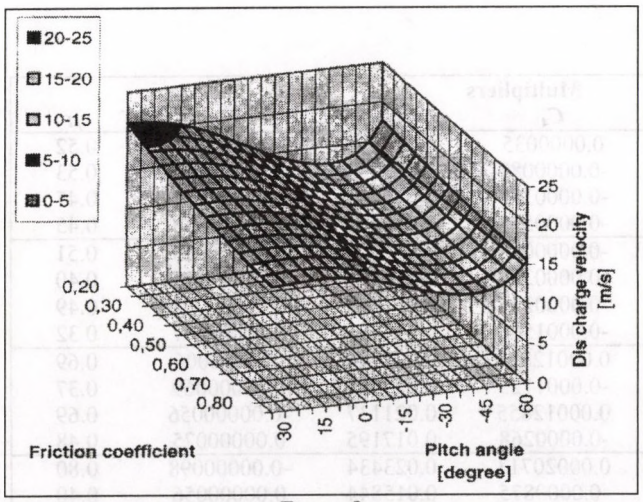

Figure 8
Effect of friction coefficient and pitch angle on discharge velocity (Nitrate – Painted pate)

The discharge angle surface has a minimum area related to the pitch angle. The is the optimum for the orientation of the vane. The optimum value slightly changes with the coefficient of friction.

It is important that the target value is almost constant around the minimum offering stable conditions for the fertiliser distribution pattern. The stability comes to the fact that the surface is not steep and the deviance of the material properties and design imperfectness will not influence the discharge angle considerably.

The discharge velocity surface has two extreme areas: a minimum and a maximum. Selecting the neighbourhood of the maximum gives the possible largest working width (corresponding to the highest discharge velocity) but the discharge angle will not be as stable as if the minimum area is selected. The cause of instability occurs because the deviations of the friction coefficient or other factors have greater influence on the target value.

The simulation results presented in *figures 7* and *8* completely support the practical experiences by which the forward pitched vane result in larger working width through the higher value of discharge velocity and worse distribution pattern due to the instability of discharge angle. At the same time backward pitched vanes are favourable for even distribution and inadvantageous for large working width.

Simulation group 3

The investigated factors were the feeding and discharge (tangent) angles of the vane aligned radial. The result are shown in *figure 9*.

There are two important findings given by this simulation group:

- The discharge characteristics are practically independent of the angle of particle entering the vane.
- The discharge angle has a minimum if the discharge tangent of the vane is varied.

It is also shown that the behaving of discharge velocity is very similar to what was found for pitched straight vane.

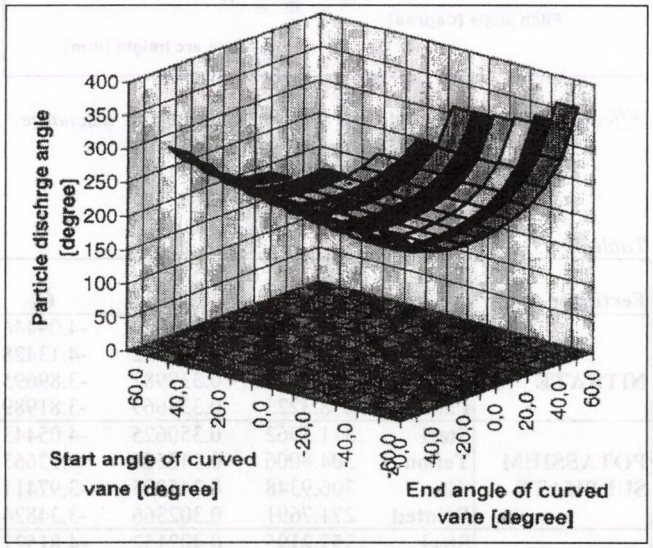

Figure 9
Effect of start and end tangent of vane curve on particle discharge angle (Nitrate – Painted pate)

Simulation group 4

According to the simulation experiments the effect of the pitch angle and the arc height of an approximately circular arc

shaped vane and the pitch angle are the input parameters. The *figures 10 and 11* suggests that the effect of negative arc height generates similar effect as the forward pitching. The positive and increasing arc height has also similar effect as that of backward pitching. This group of simulation needs still some more quantitative examinations.

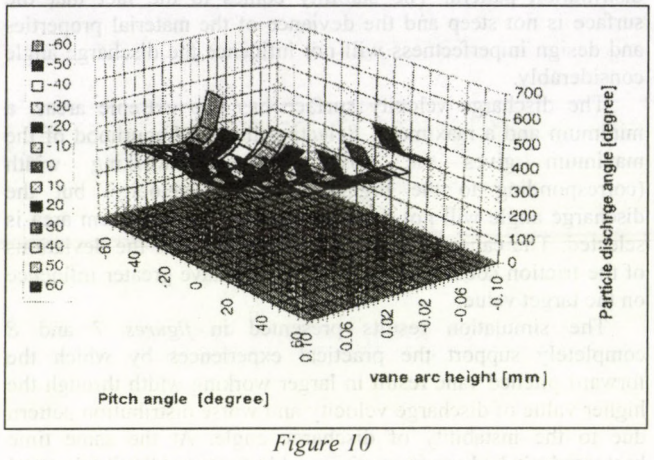

Figure 10
Effect of curved pitch and vane arc height on particle discharge angle (Nitrate – Painted pate)

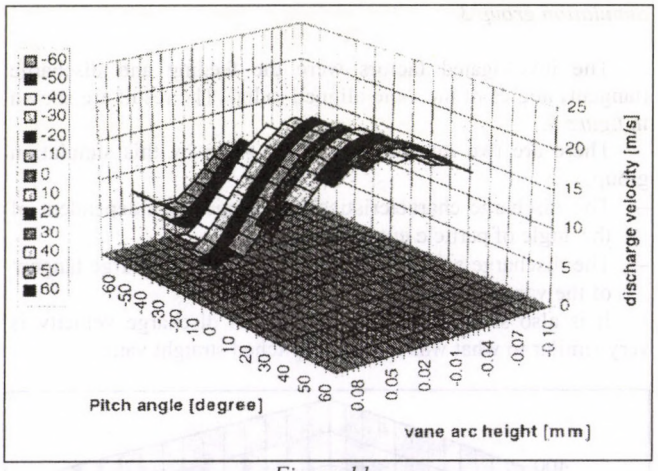

Figure 11
Effect of curved pitch and vane arc height on particle discharge velocity (Nitrate – Painted pate)

Evaluation of simulation results

For practical application the simulation diagrams can be replaced by approximate equations which allows a quick determination of the optimal parameters. Only an example of this is shown here. The simulation results concerning discharge angle are considered the most important, so that an approximated surface was fitted using only six calculated points of the surface gained by simulation.

The fitted equation is

$$\alpha_d = c_1 + c_2 r_d + c_3 r_0 + c_4 r_0 r_d + c_5 r_0^{\,2} + c_6 r_d r_0^{\,2}$$

where:
r_0 = feed radius
r_d = discharge radius
α_d = discharge angle

The above equation describes the linear nature to r_d and the quadratic nature to r_0. The coefficients for the four fertilizer types and disc materials for which the friction coefficients (μ) are available from our measurements are collected in *table 1*.

The examination of the fitted and simulated data proves that the highest related difference between the values are below 0.5 %.

Conclusions

Due to the limits of this paper the values provided by the simulation are only flashed up. The methods presented herein can be used to determine real constructions because the results agrees well with the practical experiences and the results of laboratory and field machine tests. The simulation programs can be used to evaluate constructions and the necessary adjustments if the relevant physical properties and construction data are known.

There are versions of the simulation software which makes possible to produce theoretical optimum values of design characteristics and also achieve the optimal settings for a given construction and known fertiliser type.

The complete system of application software includes the particle motion in the air considering the air resistance parameters of the particles, but its discussion is out of the scope of this paper.

Table 1.

Fertilizer		Multipliers						
		C_1	C_2	C_3	C_4	C_5	C_6	μ
NITRATE	Steel	313.5743	0.353322	-4.09446	0.0000035	0.017898	0.00000009	0.52
	Teflon	315.7846	0.356152	-4.13428	-0.0000089	0.018074	0.00000007	0.53
	Zinc	302.5985	0.339982	-3.89695	-0.0000375	0.017012	0.00000031	0.47
	Painted	298.3223	0.334669	-3.81989	-0.0000518	0.016671	0.00000038	0.45
POTASSIUM SULPHATE	Steel	311.3562	0.350625	-4.05443	-0.0000054	0.017720	0.00000013	0.51
	Teflon	304.8006	0.342509	-3.93663	-0.0000268	0.017195	0.00000025	0.40
	Zinc	306.9348	0.345295	-3.97411	-0.0000232	0.017354	0.00000024	0.49
	Painted	271.7691	0.302366	-3.34824	-0.0001500	0.014582	0.00000087	0.32
COMPLEX	Steel	353.2195	0.402152	-4.81521	0.00012855	0.021136	-0.0000006	0.69
	Teflon	281.7070	0.314402	-3.52374	-0.0001125	0.015355	0.00000069	0.37
	Zinc	353.2195	0.402152	-4.81521	0.00012855	0.021137	-0.00000056	0.69
	Painted	304.8006	0.342509	-3.93664	-0.0000268	0.017195	0.00000025	0.48
PHOSPHATE	Steel	380.7442	0.436179	-5.32167	0.00020713	0.023434	-0.00000098	0.80
	Teflon	287.8548	0.321813	-3.63349	-0.0000875	0.015844	0.00000056	0.40
	Zinc	375.6627	0.429786	-5.22757	0.00019285	0.023004	-0.00000089	0.78
	Painted	355.6706	0.405134	-4.86025	0.00013748	0.021339	-0.0000006	0.70

Acknowledgement

The authors express thanks to Professor Zoltán Csizmazia (Debrecen University of Agricultural Sciences) for his help to the Ph.D. research and to Seki Ei research student from the Tokyo University of Agriculture and Technology who contributed the computer simulation with programming and computing work. The research results includes also the benefits of OTKA T6136. The research is also supported under the contract OTKA T022408.

References

1. HOFSTEE, J. W.: Handling and spreading of fertilizers Part 1: Physical properties of fertilizer in Rational to particle motion. Journal of Agricultural Engineering Research, 1990 (47), 213-234
2. HOFSTEE, J. W.: Handling and spreading of fertilizers Part 4B: The spinning Disc Type Fertilizer Spreader. Journal of Agricultural Engineering Research *[submitted]*
3. MENNEL, R. M. - REECE, A. R.: The theory of the centrifugal distributor, III: particle trajectories. Journal of Agricultural Engineering Research, 1963, 8(1): 78-84
4. GUNNINGHAM, F. M.: Performance characteristics of bulk spreader for granular fertilizer. Transactions of the American Society of Agricultural Engineers. 1963, 6(2): 108-114
5. GUNNINGHAM, F. M. - CHAO, E. Y. S.: Design relationships of bulk spreaders for centrifugal distributors. Transactions of the American Society of Agricultural Engineers. 1967, 10(1): 91-95
6. BRINSFIELD, R. B. - HUMMEL, J. W.: Simulation of a new centrifugal distributor design. Transactions of the American Society of Agricultural Engineers, 1975, 18(2): 213-216, 220
7. GALILI, N. - SHTEINGAUZ, G.: Wide-swath vertical spreader material. Transactions of the American Society of Agricultural Engineers, 1982, 25(5): 1195-1203
8. CSIZMAZIA, Z. - KASZA, F. - NAGYNÉ POLYÁK, I.: Műtrágyaszóró tárcsa lapátkialakítás optimalizálása számítógépes szimulációval, Mezőgazdasági és Élelmiszeripari Géptervezők Országos Konferenciája, Gödöllő, 1994. pp. 45-52.
9. CSIZMAZIA, Z. - NAGYNÉ POLYÁK, I. - KASZA, F.: Műtrágyaszóró tárcsa-lapát kialakításának optimalizálása számítógépes szimulációval, A Debreceni Agrártudományi Egyetem Tudományos Közleményei, Debrecen, 1995. Vol. 31. pp. 383-394
10. KASZA, F. - CSIZMAZIA, Z. - NAGYNÉ POLYÁK, I.: A General Approach to Computer Simulation of Fertiliser Particle Motion on Spreader Disc and Vane of Arbitrary Shape, Agricultural and Biological Engineering Conference, New Horizons, New Challenges, Newcastle, 1995.
11. KASZA, F. - CSIZMAZIA, Z. - NAGYNÉ POLYÁK, I.: Simulation of fertilizer spreading using a new general approach to vane and disc design, The First International Conference on Engineering Computation and Computer Simulation - Theory and Applications, Changsha, China, 27-29. November 1995.

TECHNOLOGY OF TOMATO PRODUCTION ON SUPPORT SYSTEM

J. Dimény - Gy. Varga
University of Agricultural Sciences, Gödöllő
M. Gaál
University of Horticulture and Food Industry, Budapest

The vegetable cultivation method on support system causes crop quality improvement of freshly consumed vegetables and increasing of yield quantity per area unit. The arrangement of this intensive cultivation method is made possible partly by technical development (spreading of production and application of drip irrigation systems, water soluble multicomponent fertilisers, soil cover materials) and partly by increased labour employment.

At the Horticultural Department of University of Agricultural Sciences in Gödöllő were investigated in 1995-1996 the agrotechnical elements of this cultivation method and the varieties, being able to produce using this system. Our results and experiences are summarised as follows.

Establishment of support system

On our experimental farm wooden poles in twin row planting system with a row distance of 1,8 m were established in the row spacing of 4 m. The method of stretching the supporting wires, having drawn 2 m high on the top of wooden poles, and fixing of fmal poles were similar to practical method, being used in vineyards.

Preparation of soil, basic dressing

In the autumn 5 kg/m^2 decayed cow manure was spread and was ploughed into the soil by deep ploughing. On this sandy soil, susceptible to consistence, manuring was completed in the spring by application of 0,06 kg/m^2 "Cropcare 3" fertiliser and had been ploughed into the soil by a shallow ploughing.

Choosing of varieties

In order to support the vegetable production in the practise, organise agricultural extension courses and demonstrations comparative variety testing was established using 10 different varieties together with OMMI (Institute of Agricultural Quality Control). The plant habit of most varieties was indeterminate - expecting one of them that belonged to medium-determinate variety group.

Growing of nursery plants

For better utilisation of growing season and for getting higher amount of yield should be planted nursery plants, grown in feed blocks. The seeds were sown only on 18 of March because they were delivered later than usual. In the practise earlier sowing time is recommended. The small plants were pricked out into 6 x6 cm size feed blocks on 1 of April and were grown in a glasshouse. It is very important to provide for the permanent water supply, the leaf dressing and - if required - the plant protection of small plants. The light demand of continuously growing nursery plants (after closing of their foliage) should be assured by putting them in a distance of 12-15 cm; only in this way can be produced compact plants that grow well even after planting out.

Planting out

Planting out was made on 7 of May. Ground covering with plastic foil was planned against occasional ground frosts - but finally it was not necessary.

Spacing of plants

In twin rows with a row distance of 140+40 cm nursery plants were planted out in triangle planting design where plant to plant distance was 30 cm and 40 cm. Higher amount of yield was observed at closer planting.

Water supply and nutrient supply

Providing for water supply and nutrient supply of plants drip irrigation system was established on the experimental fields. Its pipes were put at the edge of twin rows. Nutrient supply was promoted by fertiliser solving system that was directly connected to irrigation equipment.

Application of black coloured soil cover material in twin rows and in wide rows promoted warming of soil surface and hindered the ground surface evaporation and growth of weeds too.

Plant cultivation

The growth control of continuously developing plants' main stems were assisted by a string, tied up between the base of stems and the supporting wires, drawn on the top of wooden poles. Growth of plants was continuously controlled by winding their main stems around the strings and simultaneously by breaking the lateral stems. (When leaving only one main stem of tomato plant higher amount of early yield can be harvested.)

Number of irrigations depended on weather conditions (it could be arranged dailyif it was required). At the same time top dressing was made applicating "Ferticare III" fertiliser, this was later followed by "Ferticare I" and "Ferticare II" fertilisers and during crop ripening they were completed by KNO_3 application. Yellowing of foliage was stopped by leaf dressing with "Sequestren 330 FE".

Because of significant costs of investment, labour input and significant production value must be brought great care to bear upon plant protection. The condition of our plant population, being nicer and healthier than the average, showed the success of these plant protection works. Against different kind of diseases and pests was sprayed on the fields 11 times between 8 of May and 16 of August.

Harvesting was arranged between 12 of July and 15 of October once in a week - all together 14 times.

The quantity of early crops, harvested in July, is showed on *figure 1*. It can be observed that closer planting is favourable to crop earliness.

The process of ripening is influenced by weather conditions - especially by temperature. It shows the *figure 2*: The considerable temperature decrease in September significantly slowed the ripening process, even almost stopped it.

Most of the fruits belonged to the I. class quality category (see *figure 3*). Only a small amount of crops were out of these quality categories.

The fruits of some varieties cracked because of one missed picking during OMÉK (National Exhibition of Agriculture and Food Industry) and because of quite a lot of rainfall that time. During late pickings some diseases, decreasing quality of fruits, were observed too.

On 6 of August a practical demonstration was organised for the producers of Gödöllő-Jászság region. That time it seemed to be possible to get 20 kg/m^2 average yield but later its realisation was detained by extremely cold and wet weather conditions. (In spite of these bad circumstances whole crop quantity of some varieties was quite close to this average.)

On the basis of visitors' opinions and crop results tomato production on support system can be considered successful. The arrangement of this experiment was supported by financial assistance of Ministry of Agriculture, by drip irrigation system of Company KITE, by fertilisers of Company KEMIRA Kft. and by soil cover material of Company TISZATEXTIL.

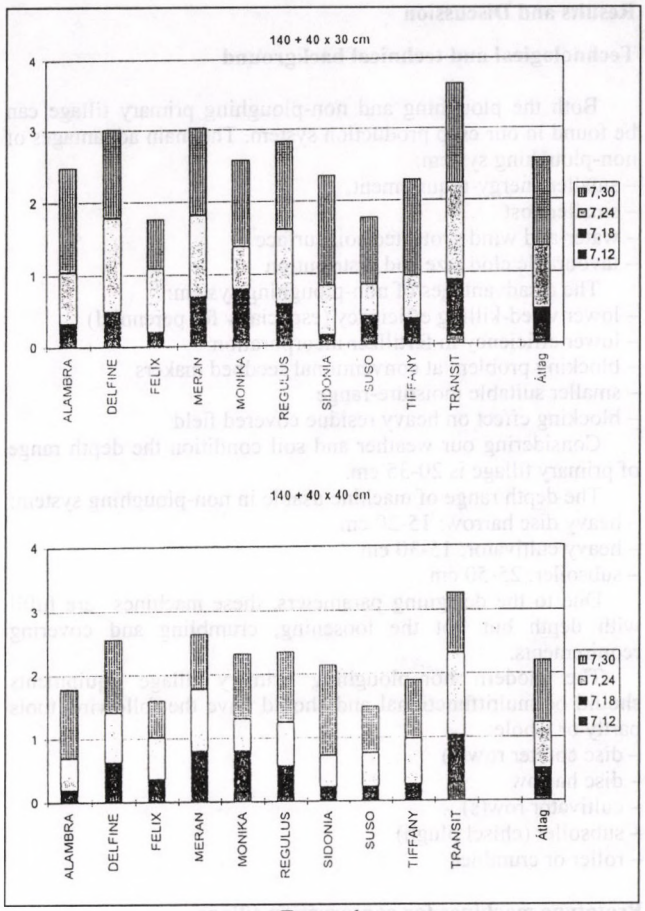

Figure 1

Amount of early yield (harvested until 30 of June) kg/m²

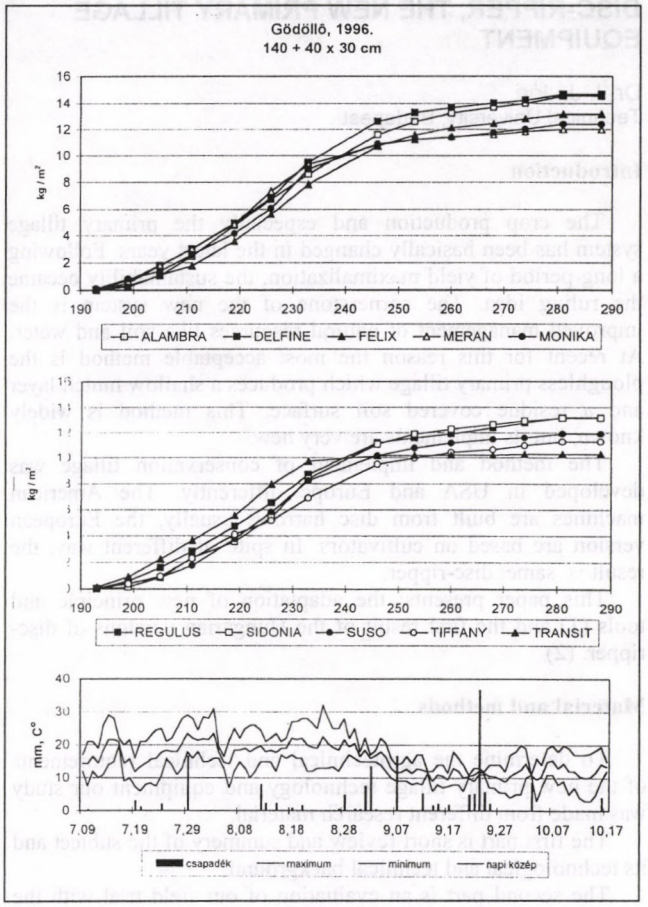

Figure 2

Ripening process of different tomato varieties, Gödöllő 1996

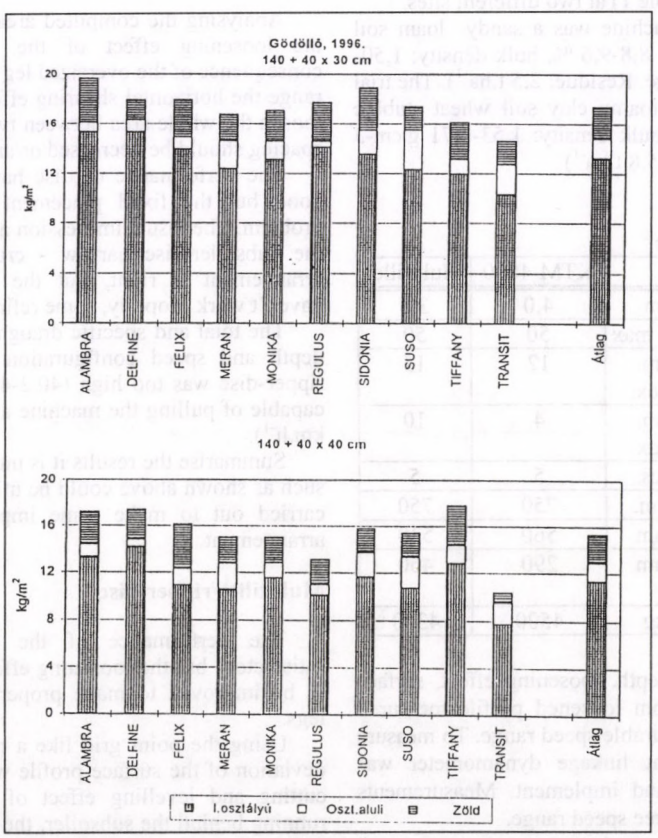

Figure 3

Whole amount of tomato yield, Gödöllő 1996

DISC-RIPPER, THE NEW PRIMARY TILLAGE EQUIPMENT

Dr. I. J. Jóri
Technical University, Budapest

Introduction

The crop production and especially the primary tillage system has been basically changed in the latest years. Following a long period of yield maximalization, the sustainability became the ruling idea. The cornerstone of the new system is the improved management of natural resources like soil and water. At recent for this reason the most acceptable method is the ploughless primary tillage which produces a shallow mulch layer and a residue covered soil surface. This method is widely known, but its implements are very new.

The method and implement of conservation tillage was developed in USA and Europe differently. The American machines are built from disc harrows usually, the European version are based on cultivators. In spite of different way, the result is same: disc-ripper.

This paper presents: the adaptation of new principle and tools (1) and the first result of the Hungarian versions of disc-ripper. (2)

Material and methods

To determine the agrotechnical and technical requirements of the new primary tillage technology and equipment our study was made from different research material.

The first part is short review and summery of the subject and its technological and technical background.

The second part is an evaluation of our field trial with the first two prototype machines. The field experiment was carried out with KTM-4000 (KAPOSGÉP Co.) and Multitiller (AGRIKON Co.) chisel-disc (Table 1) at two different sites.

The site of KTM-4000 machine was a sandy loam soil wheat stubble (Moisture content: 8,8-9,6 %, bulk density: 1,50-1,62 $g.cm^{-3}$ at 5-40 cm depth range. Residue: 2,5 $t.ha^{-1}$). The trial site of Multitiller machine was loamy clay soil wheat stubble (Moisture content: 12,2-15,1%, bulk density: 1,53-1,71 g.cm-3 at 5-40 cm depth range. Residue: 5,8 $t.ha^{-1}$)

Table 1
Main specifications of implements

Type		KTM-4000	Multitiller
Working width	m	4,0	3,8
Depth of subsoiler	cm, max	50	50
Depth of disc harrow	cm, max.	12	15
Depth of crumbler or star wheel	cm, max.	4	10
Number of legs	pcs.	5	5
Space of legs	mm.	750	750
Diameter of blade	mm	560	530
Diameter of crumbler or star wheel	mm	290	460
Weight	kg	4500	4300

The machine performance (depth, loosening effect, surface eveness etc.) was determined from loosened profile measured with a point grid at the most favourable speed range. To measure implement draught a three-point linkage dynamometer was connected between the tractor and implement. Measurements were taken from two depth and three speed range.

The third part is a machine review from most accepted American and European disc- rippers.

Results and Discussion

Technological and technical background

Both the ploughing and non-ploughing primary tillage can be found in our crop production system. The main advantages of non-ploughing system:
– smaller energy-requirement
– smaller cost
– water-and wind protected soil surface
– favourable clod size and distribution

The disadvantages of non-ploughing system:
– lower weed-killing efficiency (especially for perennial)
– lower efficiency in fertilizer incorporation
– blocking problem at conventional seedbed makers
– smaller suitable moisture-range
– blocking effect on heavy residue covered field

Considering our weather and soil condition the depth range of primary tillage is 20-35 cm.

The depth range of machine usable in non-ploughing system:
– heavy disc harrow: 15-20 cm
– heavy cultivator: 15-30 cm
– subsoiler: 25-50 cm

Due to the designing parameters, these machines are fulfil with depth but not the loosening, crumbling and covering requirements.

The modern non-ploughing primary tillage equipments should be multitfunctional and should have the following tools partly or whole:
– disc coulter row(s)
– disc harrow
– cultivator row(s)
– subsoiler (chisel plugh)
– roller or crumbler

Prototype machines for conservation tillage

KTM-4000 ripper-disc

Analysing the computed area of the profiles was found that the loosening effect of the implement is insufficient in consequence of the oversized leg spacing. At the 30-50 cm depth range the horizontal shearing effect of the rake is not enough to loosen the whole area between two legs. For better result the leg spacing should be decreased or/and the rake should be widened.

The performance of disc harrow behind the subsoiler was good but the fixed placement of disc gangs caused depth problem. The visual impression and the analysis of interaction of the subsoiler-disc harrow - crumbler parts showed that the arrangement is right, but the control and adjustment tools haven't work properly, some refinements could still be made.

The total and specific draught force was calculated for each depth and speed configuration. The draught requirement of ripper-disc was too high (40,2-48,7 kN) so the tractor was not capable of pulling the machine at the desired speed range (8-10 $km.h^{-1}$).

Summarise the results it is intended, that a machine designed such as shown above could be utilised, but further work is being carried out to make some improvement for the proper tool arrangement.

Multitiller ripper-disc

The performance of the machine at both sites was satisfactory but the loosening effect of the subsoiler part needed to be improved to make proper work between the neighbour legs.

Using the point grid like a micro relief meter the standard deviation of the surface profile was measured. Due to the good cutting and levelling effect of disc harrow and star wheel, running behind the subsoiler, the eveness of the soil surface was slightly better than the separate tool. In spite the good performance some modification could still be made. In the case

of summer stubble work the star wheel part of machine should be substitute for a crumbler or roller.

The total draught force of the machine at two depth range has also been measured. At 30 cm depth and 4,3-6,8 km.h^{-1} speed range the average draught force varied between 48,9-53,2 kN. Increased the depth to 37 cm the tractor was able to pull the machine with 4,3 km.h^{-1} only because the 77,6 kN very high draught force.

The findings presented here indicate that the main problems are the same on both prototype conservation tillage machines: the unproper leg spacing and the very high power requirement. Due to these unfavourable results and other designing problems the machine development for conservation tillage was finished for a long period.

Foreign machinery review

There is two different way of the conservation tillage machine development. The first is the American style which came from the Corn-Belt area where the corn-soybean crop rotation mostly used and where the disc harrow was the most popular tillage implement. The second is the European style coming from the wheat production region where the primary tillage system based on plough and cultivator.

USA machinery review

Before the disc-ripper combination was invented the disc coulter-disc harrow machines were very popular (see: JD mulch-tiller, I.H Conser-till, Glencoe soilsaver etc). These are the right implements for average situation but in some special case like heavy residue covered field or field with hard-pan under tilth-layer a deeper primary tillage tool is needed.

Formerly the single subsoiler was the medicine for this problem, but due to its poor performance and high cost the farmers try to find a better method and implement. Combining the subsoiler (chisel plough) and disc harrow seems to be the best solution because it is bringing together the advantages of the separate implements.

There are two different way to create the new conservation tillage machine. The first is very simple and could be home made when two single, serial manufactured implement are coupled behind each other. The Sunflower 4311 Disc-Ripper and the Landoll Model 2200 Weatherproofer is the best example to show this style. These machines are usable separate or coupled form depend on the local requirement. This system has advantages but unfavourable condition these combinations left undiserable large ridges that require at least one additional pass to level them out for secondary tillage.

The second way resulted an absolutely new conservation tillage implement. Setting the chisel plough (subsoiler) between the rows of disc harrow is an excellent idea. The benefits of the new machine, called disc-ripper, are

- most effective at sizing and incorporating heavy residue,
- eliminates both surface and deep compaction for improved water infiltration
- provides thorough mixing of fertiliser, manure,
- kills, weakens wide range of weeds
- leaves surface level for improved seedbed finishing and chemical incorporation.

Due to these capabilities using the new implements we are able to reduce soil erosion and surface runoff while maintaining soil productivity, water quality and profitability.

European machinery review

Analysing the European situation can't be found a clear and definitive picture. Despite of some very early research, the disc-ripper combination is not widely-known by European farmers. It can be found a few example only. The Mulcheur machine of Razol company try to follow the implement coupling method. The disc harrow-chisel plough combination has the same problem as the American version. The Kverneland spring cultivator-disc harrow-crumbler combination seems to be a good construction for winter wheat stubble only but not field covered heavy residue. The best European answer for the conservation tillage challenge is the Discordon disc-ripper made by Gregoire-Besson company. The trailed type machine has a cultivator between the rows of disc harrow like the American "brothers" and has some extras too.

The spiral roller behind the disc harrow eliminates the small ridges and "closed" the surface. The three-point linkage on the rear end of the frame gives an option to couple a drilling machine to the disc-ripper. This capability means a step ahead to the one-pass cultivation-drilling system.

Conclusions

Evaluating the foreign development process and the home R+D results the following conclusions can be drawn:

- the conventional (clear) tillage system (usually it includes a mouldboard plough but can also be done with other tools such as chisels and disc) should be changed however it remains beneficial on flat heavy, poorly drained soils that offer special problem for conservation tillage systems,
- the new conservation tillage system are no-till ridge-till and mulch-till. This paper highlighted mulch-till system and its machines because it is the most widely accepted in our region,
- the mulch-till system use full-width tillage tools while leaving high levels of erosion- controlling residue on the soil surface,
- the primary tillage implements for mulch-till are the combination of the following tools: disc coulter, disc harrow, subsoiler or chisel plough, roller or crumbler,
- considering to the site-specification and the crop rotation two different basic implement types were created. The subsoiler (chisel) part of the machine was developed for fall primary tillage is setting just behind the disc harrow or between the rows of disc harrow. The subsoiler (chisel) part of the machine was developed for summer primary tillage is setting between the rows of disc harrow always and behind the rear row of disc harrow a "closing" tool (roller or crumbler) should be attached,
- the results of the investigated prototype implements (KTM-4000, Multitiller ripper-disc), indicate that a machine designed such a way was shown, could be utilised but further developments still be made for the proper tool arrangement,
- based on the results of study and research the KL-4 disc-ripper was developed (*figure 1*).

References

1. JÓRI J.I.: 1996. Talajvédő és környezetkímélő talajművelési technológiák (Report in hungarian) FMMI, Gödöllő 29 p.
2. 1994: Conservation cropping systems: JD. Moline USA 49p

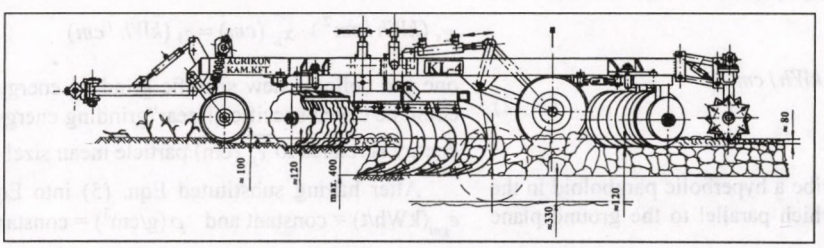

Figure 1

MATHEMATICAL MODELLING OF THE RELATION OF SPECIFIC SUPERFICIAL GRINDING ENERGY REQUIREMENT VS. GRIT FINENESS

Dr. I. Bölöni - Dr. Z. Bellus
Hungarian Institute of Agricultural Engineering, Gödöllő

Our activity carried out in the project (OTKA T 5392 and OTKA T 016124) sponsored by the National Fund for Scientific Research of Hungary made clear the utmost importance of the relation between the specific grinding energy requirements and the grit fineness characteristics. Examinations in the projects were implanted by means of a conventional hammermill (Hungarian made, type of D-24F having 19 kW power input) grinding feed grains (barley and corn).

The goal of the theoretical analysis done in 1996 was to develop a mathematical model, – on the basis of the superficial theory (Rittinger, 1867), – which describes the correlation between the most important grinding energy demands like

e_{gm} (kWh/t) = specific grinding energy consumption related to mass unit,
e_{gv} (kWh/cm^3) = specific grinding energy demand related to unit of volume,
e_s (kWh/cm^2) = specific grinding energy requirement related to surface unit,
e_l (kWh/cm) = specific grinding energy consumption related to the particle mean size and the grit fineness characteristics:
$\overline{a_g}$ (cm^2/g) = average specific surface of the ground material i.e. grit,
Δa_g (cm^2/g) = $\overline{a_g} - \overline{a_o}$ = grit specific surface increase during size reduction whereas,
$\overline{a_o}$ (cm^2/g) = specific surface of the whole grain kernels before grinding,
$\overline{x_g}$ = grit particles mean size.

According the our former analysis of the basic energetic relationship between specific grinding energy requirement vs. grit fineness – starts out of Rittinger's 130 years old superficial theory – had shown [1] that here we have not a one-variable function as Rittinger and his followers thought but a two-variable correlation exists:

$$e_{gm}(kWh/t) = 10^6\ (g/t) \cdot e_s\ (kWh/cm^2) \cdot \Delta a_g\ (cm^2/g) \quad (1)$$

where the meanings of the symbols were defined above.

As it is to be seen the dependent variable is e_{gm} (kWh/t) and the independent ones are: Δa_g (cm^2/g) grit specific surface increase and e_g (kWh/cm^2) specific superficial grinding energy demand that seems to be a physical criterion of the ground feed grain.

Substituting $\Delta a_g = \overline{a_g} - \overline{a_o}$ specific surface increase into Eqn. (1) is received

$$e_{gm}(kWh/t) = 10^6\ (g/t) \cdot e_s\ (kWh/cm^2) \cdot \left[\overline{a_g}\ (cm^2/g) - \overline{a_o}\ (cm^2/g)\right] \quad (2)$$

Above two functions describe a hyperbolic paraboloid in the space, the cross sections of which parallel to the ground plane (e_s, $\overline{a_g}$) – while e_{gm}(kWh/t) = constant – are first grade hyperboles (*figure 1 /a/*) and the sections of e_s(kWh/cm^2) = constant and $\overline{a_g}$ (cm^2/g) or Δa_g (cm^2/g) = constant are straight lines (*figure 1 /b/*).

Further on our research (Bölöni, 1994) proved that the grit specific surface can not be calculated simply from the cube or sphere shape of the individual particles, because of the particle mean size $\overline{x_g}$ and the specific surface $\overline{a_g}$ are not compatible characteristics of particle set since the distribution is askewed being log-normal distribution in general. A coefficient of skewness (c.s.) should be introduced that is always bigger than 1.0. This way the correct relation is:

$$\overline{x_g}(cm) = \frac{6 \cdot (c.s.)}{\rho\ (g/cm^3) \cdot \overline{a_g}\ (cm^2/g)} \quad (3)$$

where ρ (g/cm^3) = true density of feed grain.

Substituting Eqn. (3) into Eqn. (2)

$$e_{gm}(kWh/t) = 10^6\ (g/t) \cdot \frac{6}{\rho\ (g/cm^3)} \cdot e_s\ (kWh/cm^2) \cdot \left[\frac{c.s.}{\overline{x_g}\ (cm)} - \frac{1}{\overline{x_o}\ (cm)}\right] \quad (4)$$

Here should be mentioned that the particle size distribution of the whole grain kernels in Gaussian normal distribution yet so that $\overline{x_o}$ (cm) and $\overline{a_o}$ (cm^2/g) are compatible and in this special case *c.s.* = 1.0 .

Eqn. (4) is a further development of the old Rittinger law that is very commonly used in the grinding literature and can be rewritten as

$$e_{gm}(kWh/t) = 10^6\ (g/t) \cdot \frac{6}{\rho\ (g/cm^3)} \cdot e_s\ (kWh/cm^2) \cdot \frac{\overline{x_o}\ (cm) \cdot (c.s.)\ \overline{x_g}\ (cm)}{\overline{x_o}\ (cm) \cdot \overline{x_g}\ (cm)} \quad (5)$$

Deduction of the curve of this function, if e_S(kWh/cm^2) = constant, can be seen in *figure 2*. It is out utmost importance that this relation is a little bit more complicated than Rittinger's first grade hyperbole and the curve crosses the horisontal coordinate axis not by the value $\overline{x_o}$ (cm) but by (*c.s.*) · $\overline{x_o}$ (cm)!! According to the data of sieve analysis of barley grits the coefficient of skewness (*c.s.*) varied within the range 1.5 to 2.0 .

From Eqn. (5) the relation of e_S(kWh/cm^2) *vs* · $\overline{x_g}$ (cm) particle mean size can be transformed, if e_{gm}(kWh/t) = constant and it is illustrated in *figure 3*.

Analyzing the $e_S/\overline{x_g}/$ correlation we reached at an interesting recognition from Fig. 3. Namely by multiplying the two variables

$$e_s\ (kWh/cm^2) \cdot \overline{x_g}\ (cm) = e_l\ (kWh/cm) \quad (6)$$

one can define a new specific grinding energy requirement that could be called specific „linear"grinding energy demand whereas energy is related to $\overline{x_g}$ (cm) particle mean size!

After having substituted Eqn. (5) into Eqn. (6) in case of e_{gm}(kWh/t) = constant and ρ (g/cm^3) = constant one gets

$$e_1(kWh/t) = constant \cdot (kWh/cm^3) \cdot \frac{\overline{x_o}(cm) \cdot \overline{x_g^2}(cm)}{(c.s.) \cdot \overline{x_o}(cm) - \overline{x_g}(cm)} \quad (7)$$

a non-excepted quadratic-hyperbolic relationship having the interpretation range $|0, (c.s.) \cdot \overline{x_o}|$ were $(c.s.) \cdot \overline{x_o}$ is the perpendicular asymptote (*figure 4*).

Taking into consideration that the specific grinding energy requirement is four-fold

e_{gm}(kWh/t); e_{gv}(kWh/cm^3); e_s(kWh/cm^2); e_l(kWh/cm)

and the grit fineness is three-fold to be determined all together 4.3 = 12 different specific energy equation are to be deduced (*table 1*). This equation system is the mathematical model that was searched for and which makes connections between all specific grinding energy demands and grit finenesses.

Whatever can be found in *table 1* that is a two variable function of a grit fineness characteristic and of another specific grinding energy requirement else.

References

1. v. RITTINGER: Lehrbuch der Aufbereitungskunde, Berlin, 1867.
2. BÖLÖNI, I.: Analysis of Grinding's Basic Energetic Relationship (OTKA T 016124), Hungarian Agrar Eng.; Hungarian Institute of Agricultural Engineering, Gödöllő, 1996, No 9.
3. BÖLÖNI, I.: Report on Determination of the Decimal Efficiency of Hammermill (in Hungarian); (OTKA T 5392); Hungarian Agrar Eng.; Hungarian Institute of Agricultural Engineering, Gödöllő, 1994, 1-59 pp.

Table 1
Mathematical model of grinding's specific energy consumption in function of grit fineness as an equation-system consisting of 12 different relations

Sign	Equation	Remarks
1.	$e_{gm_1}(kWh/t) = 10^6\ (g/t) \cdot e_s\ (kWh/cm^2) \cdot \Delta a_g\ (cm^2/g)$	See *figure 1 /a/* and *figure 1 /b/*
2.	$e_{gm_2}(kWh/t) = 10^6\ (g/t) \cdot e_s\ (kWh/cm^2) \cdot (\overline{a_g} - \overline{a_o})\ (cm^2/g)$	
3.	$e_{gv_1}(kWh/cm^3) = 10^{-6}\ (m^3/cm^3) \cdot \rho\ (t/m^3) \cdot e_{gm_1}\ (kWh/t)$	These presentations differ just in coefficients from Eqn.(1) and Eqn. (2)
4.	$e_{gv2}(kWh/cm^3) = 10^{-6}\ (m^3/cm^3) \cdot \rho\ (t/m^3) \cdot e_{gm2}\ (kWh/t)$	
5.	$e_{gv2}(kWh/cm^3) = 10^{-6}\ (m^3/cm^3) \cdot \rho\ (t/m^3) \cdot e_{gm2}\ (kWh/t) =$ $= 10^{-6}\ (m^3/cm^3) \cdot \rho\ (t/m^3) \cdot 10^6\ (g/t) \cdot e_s\ (kWh/m^2 \frac{6}{\rho\ (g/cm^3)} \cdot \left[\frac{(c.s.)}{\overline{x_g}(cm)} - \frac{1}{x_o(cm)}\right]$ $e_{gv_2}(kWh/cm^3) = 6 \cdot e_s\ (kWh/cm^2) \cdot \left[\frac{(c.s.)}{\overline{x_g}(cm)} - \frac{1}{\overline{x_o}(cm)}\right]$	Eqn.(5) and (6) differ in coefficient 10^6 and ρ true density only: e_{gv} (kWh/m^3) = ρ (t/m^3)·e_{gm} (kWh/t)
6.	$e_{gm_2}(kWh/t) = 6 \cdot 10^6\ (g/t) \cdot \frac{e_s(kWh/cm^2)}{\rho\ (g/cm^3)} \cdot \left[\frac{c.s.}{\overline{x_g}(cm)} - \frac{1}{x_o(cm)}\right]$	In *figure 2* Eqn. (6) is to be seen after having reduced the two fractions to a common denominator
7.	$e_s(kWh/cm^2) = 10^{-6}(t/g) \cdot \frac{e_{gm}(kWh/t)}{\Delta a_g(cm^2/g)}$	
8.	$e_s(kWh/cm^2) = 10^{-6}(t/g) \cdot \frac{e_{gm}(kWh/t)}{\overline{a_g}(cm^2/g) + \overline{a_o}(cm^2/g)}$	
9.	$e_s(kWh/cm^2) = e_{gv_2}(kWh/cm^3) \cdot \frac{1}{6} \cdot \left[\frac{\overline{x_o}(cm) \cdot \overline{x_g}(cm)}{(c.s.) \cdot \overline{x_o}(cm) - \overline{x_g}(cm)}\right]$	See *figure 3*, if e_{gv} (kWh/cm^3) = constant
10.	$e_1(kWh/cm) = e_s\ (kWh/cm^2) \cdot \frac{6 \cdot (c.s.)}{\rho(g/cm^3)} \cdot \frac{1}{a_g(cm^2/g)}$	
11.	$e_1(kWh/cm) = e_s\ (kWh/cm^2) \cdot \frac{6 \cdot (c.s.)}{\rho(g/cm^3)} \cdot \frac{1}{\Delta a_g(cm^2/g) + \overline{a_o}(cm^2/g)}$	
12.	$e_1(kWh/cm) = e_s\ (kWh/cm^2) \cdot \overline{x_g}(cm) = e_{gv_2}(kWh/cm^3) \cdot \frac{1}{6} \cdot \frac{\overline{x_o}(cm) \cdot \overline{x_g^2}(cm)}{(c.s.) \cdot \overline{x_g}(cm) - \overline{x_g}(cm)}$	See *figure 4*, if e_{gv} (kWh/cm^3) = constant

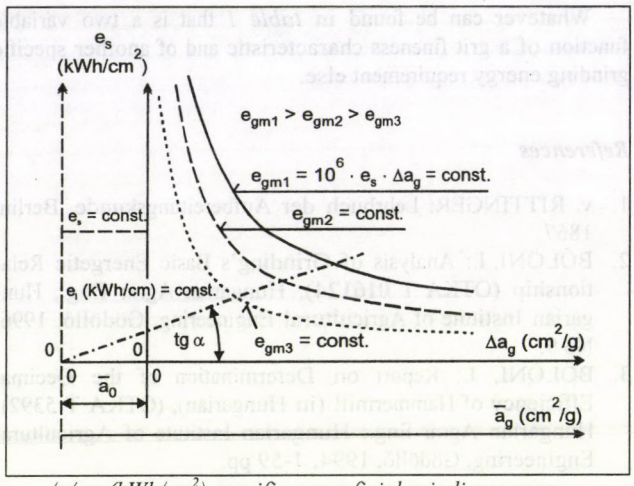

/a/: e_s(kWh/cm^2) specific superficial grinding energy requirement vs. $\Delta\, a_g$ (cm^2/g) grit specific surface increase, $\overline{a_g}$ (cm^2/g) grit specific surface, if e_{gm} (kWh/t) = constant

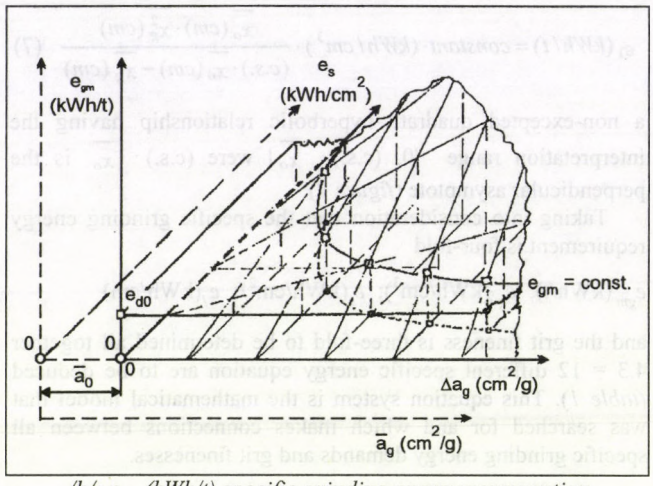

/b/: e_{gm} (kWh/t) specific grinding energy consumption vs. e_s(kWh/cm^2) specific superficial grinding energy demand and vs. $\Delta\, a_g$ (cm^2/g) grit specific surface increase or/and vs. $\overline{a_g}$ (cm^2/g)) grit specific surface illustrated in spatial form

Figure 1

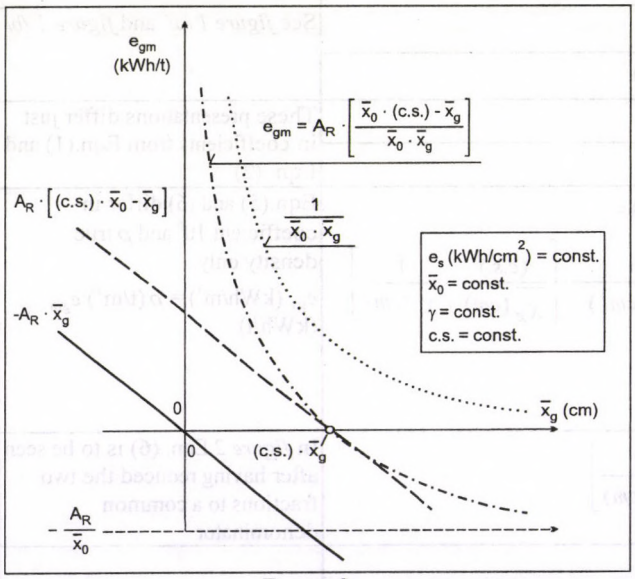

Figure 2

e_{gm} (kWh/t) specific grinding energy requirement vs. $\overline{x_g}$ (cm) grit particle mean size, if e_s(kWh/cm^2) = constant and $\overline{x_o}$ (cm) ρ (g/cm^3) and (c.s.) are also constant

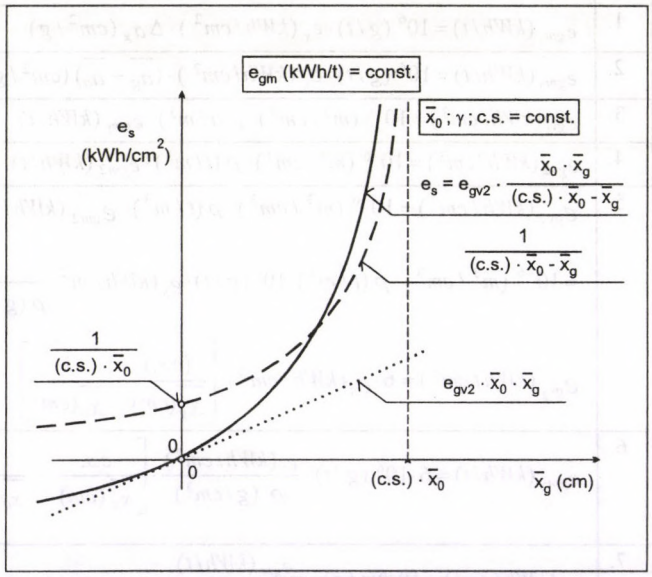

Figure 3

e_s(kWh/cm^2) specific superficial grinding energy consumption vs. $\overline{x_g}$ (cm) particle mean size, if e_{gm} (kWh/t) = constant and $\overline{x_o}$ (cm); ρ (g/cm^3) and (c.s.) are constant, too

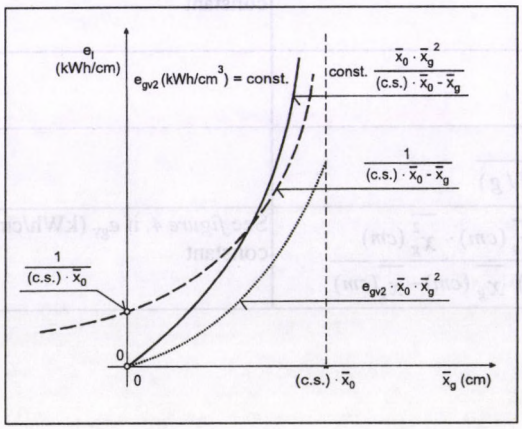

Figure 4

e_l(kWh/cm) specific "linear" grinding energy demand vs. $\overline{x_g}$ (cm) grit particle mean size, if e_{gv} (kWh/cm^3) = constant and $\overline{x_o}$ (cm); ρ (g/cm^3) and (c.s.) are also constant

UP-TO-DATE HIGH-STRENGTH PLASTICS IN THE MACHINE SERVICING

Dr. I. Pálinkás - Dr. G. Kalácska - L. Szabadi - G. Fledrich
University of Agricultural Sciences, Gödöllő

The term „technical plastics" is used widely and defined in several ways. A most frequent interpretation is as follows:

The technical plastics are polymers having excellent mechanical properties including strength resistance to creep, impact, fatigue and wearing in a wide range of the temperature. Due to these they can be used as construction materials in certain circumstances and they can replace the metals advantageously. In addition to the excellent mechanical characteristics they have good chemical resistance and electric insulation property.

The technical plastics can be favourite in the original manufacturing processes and in the maintenance and reparation.

It is a quite significant aspect in the maintenance and the reparation concerning technical plastics, that they overcome the metals in the tribological properties i.e. they have

- low friction and
- enduring

properties.

It is well known that a high percentage of failures, breakdowns are caused by the friction and abrasion processes. A fundamental job of the experts dealing with maintenance and reparation is to reduce the damages resulted by abrasion processes - even by suitable material selection after reconstruction design.

From the point of view of thermal resistance, mechanical properties and chemical stability general purpose and high performance materials (HPM) are differentiated. The material pyramid shows the everyday, general technical and the high performance materials of most important types and technology level.

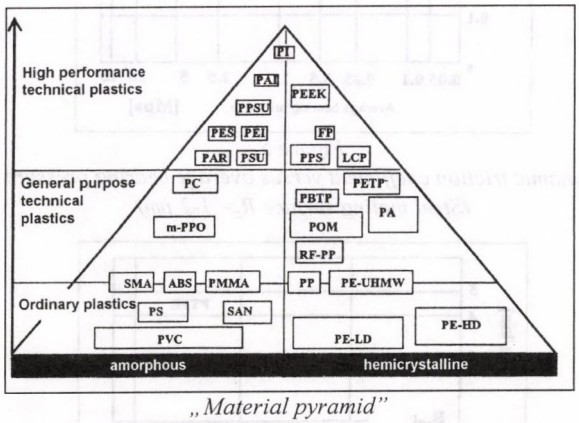

„Material pyramid"

Within the research projects of the Department of Machine manufacturing and Reparation Technology applicability examinations are conducted for built in plastic machine parts in several industrial companies, such as Gardénia Rt., Kühne Rt., Pharmavit Rt., Szabolcs Volán Rt., etc. Results concerning those parts built in during maintenance proved the applicability and the advantageous properties of theirs definitely. The main groups of the machine parts constructed and built in are as follows:

- sleeve bearings
- gearwheels
- sliding guideways
- rollers

In the following part several very important properties of technical plastics are discussed.

In *figure 1* the tension strain characteristics of plastics are compared to that of carbon steel.

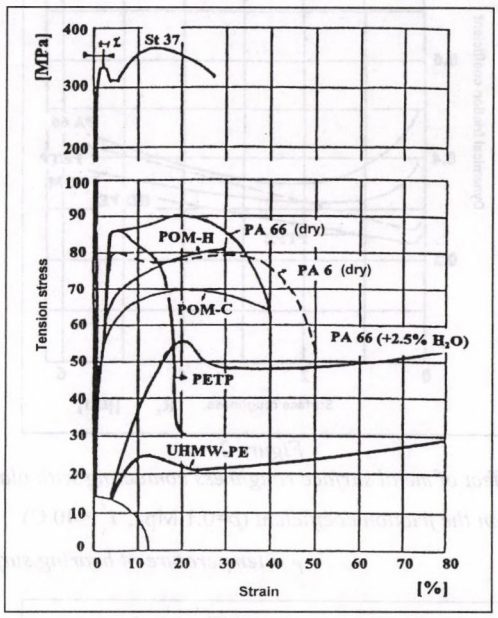

Figure 1
Tension stress versus strain characteristics of a few plastics compared to that of St37 carbon steel

One can see that the strength of the plastics are lower compared to the steel, however, their toughness is better in the most case if the toughness is characterised by the breaking strain value.

Actually the area under the stress-strain curve is the integral of the force versus deformation curve. Therefore the area under the curve characterise the energy absorbing capability of the material. From this aspect the plastics have favourable behaviour.

Tribology properties

The friction and wearing properties of the thermoplastics are so complex that it is impossible to define general acceptable values of the friction coefficient or of the wearing factor. The main factor having considerable effect from the point of view of tribology are as follows:

- bearing pressure (at slide bearings),
- relative sliding velocity,
- geometry of the contacting parts,
- temperarture,
- environment, surface roughness, hardness of the contacting surface,
- total operation time,
- the properties of the medium fluid, (water, lubrication material, abrasive particles).

Figure 2-7 show the effect of different factors, such as roughness of the mating surface, average bearing pressure, surface temperature, on the friction and wearing characteristics.

Note: The terms wearing and abrasion is declared as follows.

Wearing: material separation (transfer) occurring during motion between two relatively smooth surfaces moving relatively to each other (axial and radial bearings), without the presence of hard abrasive parts between the surfaces.

Abrasion: material separation from the material surface, the effect of abrasive particles moving on the surface (e.g. sand, cement, material slides of coal powder stores covered by UHMW PE.)

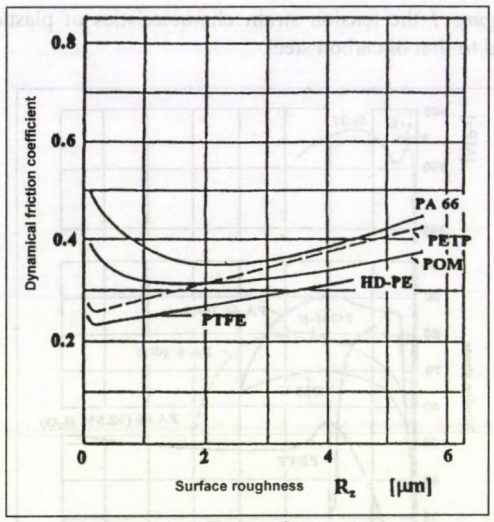

Figure 2

The effect of metal surface roughness contacting with plastic on the friction coefficient (p=0.1 Mpa, t_s° <40 C)

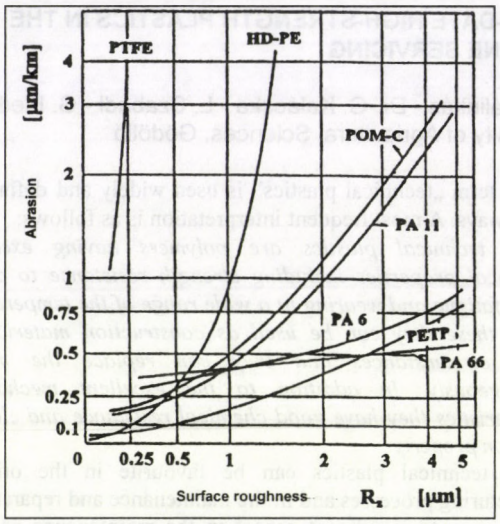

Figure 3

Abrasion versus roughness of the contacting surface (p=0.1 Mpa, t_s° <40 C)

t_s° = *temperature of bearing surface;* p = *average bearing pressure;* $R_z \approx 4\ R_a$

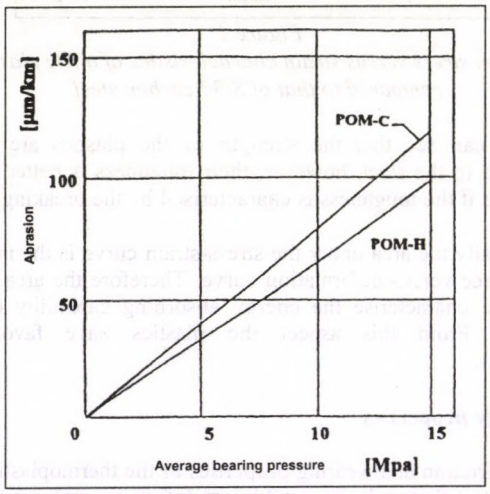

Figure 4

Abrasion versus average bearing pressure (Steel mating surface R_z= 1-2 μm)

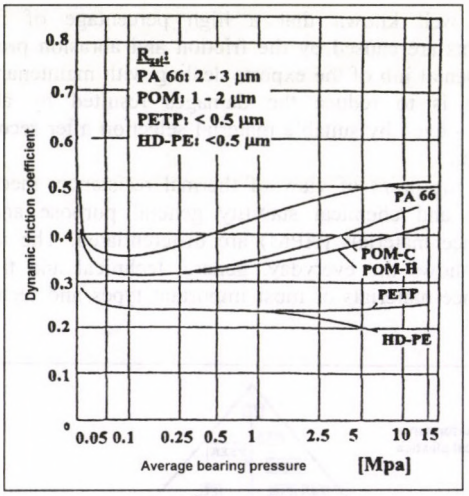

Figure 5

Dynamic friction coefficient versus average bearing pressure (Steel mating surface R_z= 1-2 μm)

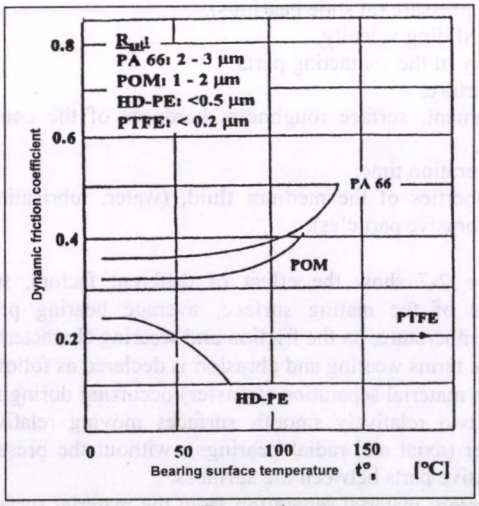

Figure 6

Dynamic friction coefficient versus surface temperature (Steel mating surface, P=0.1 MPa)

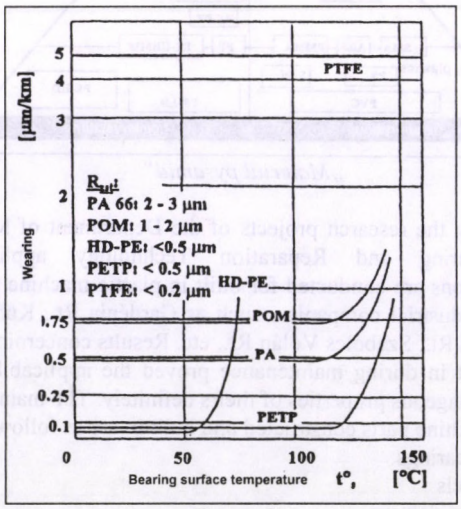

Figure 7

Wearing versus surface temperature (Steel mating surface, P=0.1 MPa)

R_{zst}: *The roughness of the steel contacting surface measured perpendicularly to the machining flutes*

OPTIMISATION OF THE ENVIRONMENT OF INDOOR POTATO STORES

Dr. M. Neményi - I. Czaba
PANNON Agricultural University, Mosonmagyaróvár
Z. Chalabi - W. Zhou
Silsoe Research Institute, Silsoe, Bedford, United Kingdom

I. Introduction

The environment of indoor potato store is complex. It is governed by the heat and moisture transfer processes between the potato and the indoor environment. Maintaining the potato under strict temperature and humidity conditions is important for the safe upkeep of potato.

The long term objective of this study is to develop mathematical methods for optimising the environment of potato stores. The work will focus on bulk storage of potatoes in piles. In this type of storage, there is a need to ventilate the store in order to remove heat due to respiration and to decrease the temperature of the tubers. On one hand excessive ventilation rates are detrimental because they remove water and thus dry out the potato and cause weight and quality losses. On the other hand, low ventilation rates would rise the temperature of the tuber and could cause inadequate mixing of the air and thus including significant spatial gradients in temperature and moisture content within the potato pile. There is therefore a need to optimise environmental conditions within the store. This could be achieved eighter by optimising the design of the store (e.g. ducts, inlet points and fan positions), ventilation equipment (e.g. fan capacity) or air speed rate at inlet points.

The first step towards achieving this long term objective is to develop a mathematical model to describe the environment of indoor potato stores. The purpose of this initial study is to formulate the set of equations which describe the heat and mass transfer processes in a potato store which is exposed to forced ventilation.

2. Model development

A non-equlibrium model describing the heat and mass transfer processes in an elemental thin-layer of potato of unit cross sectional area is developed (*figure 1*). The development and the underlying assumption of this model is similar to those of other non-equlibrium models of heat and mass transfer processes in biological materials (e.g. Sun et al., 1995).

2.1 Mass and energy balance equations

Let T(x.t), θ (x,t), H (x,t) and M (x,t) denote respectively the temperature of air [°C], the temperature of potato [°C], the absolute humidity of air [kg/kg, dry air] and the moisture content of potato [kg/kg] at position x in the potato pile (measured from the air inlet) and at time t.

The mass of potato in thin element of width δx is:

$m_E = \rho_\rho (1- \varepsilon)\delta x$

Where :
m_E - mass of potato in the element [kg]
ρ_ρ - density of potato [kg/m^3]
ε - void fraction

The mass of air passing through the element in time δt is:

$m_A = v_a \rho_a \delta t = G\delta t$

Where:
m_A - mass of air [kg]
ρ_a - density of air (kg/m^3)
δt - time interval (h)
v_a - average interstitial velocity of air [m/h]
G - the mass flow rate of air per unit cross-section of bed [kg/m^{2}h]

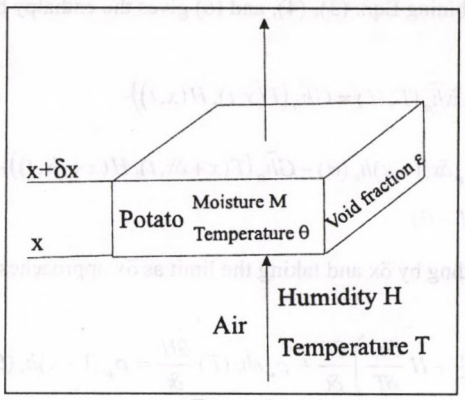

Figure 1
Elemental thin-layer of potato pile

2.1.1 Total water balance

The total water balance over the element is given by:

$$GH(x,t)\delta t - GH(x+\delta x,t)\delta t = \frac{\vartheta}{\vartheta_t}\left[\rho_\rho (1-\varepsilon)\delta x H\right]\delta t \qquad (1)$$

Where:
H - absolute humidity of air [kg/kg, dry air]
M - moisture content of potato [kg/kg, dry basis])

Dividing Eqn. (1) by δx and taking the limit as δx approaches zero, gives:

$$-G\frac{\vartheta H}{\vartheta x} = \rho_\rho (1-\varepsilon)\frac{\vartheta M}{\vartheta t} + \rho_a \varepsilon \frac{\vartheta H}{\vartheta t} \qquad (2)$$

2.1.2 *Energy balance on the air*

The total enthalpy flow entering the gas phase of the element leads to:

$$G\tilde{h}_a\left(T(x,t),H(x,t)\right) - \frac{\vartheta M}{\vartheta t}\rho_\rho \delta x(1-\varepsilon)h_v(\theta) \qquad (3)$$

Where:
$\tilde{h}_a$ - specific enthalpy of wet air at temperature T and humidity H [J/kg]
h_v - specific enthalpy of water vapor at temperature θ [J/kg]

The total enthalpy flow leaving the gas phase of element is:

$$G\tilde{h}_a\left(T(x+x,t),H(x+\delta x,t)\right) + Ua\delta x(T-\theta) \qquad (4)$$

Where:
U - convective heat transfer coefficient [J/hm^2°C]
a - specific surface area [m^2/m^3]

Assuming that wet air behaves as an ideal mixture, than

$$\tilde{h}_a(T,H) = h_a(T) + Hh_v(T) \qquad (5)$$

Where:

$\tilde{h}_a$ - specific enthalpy of dry air at temperature T [J/kg]

h_v - specific enthalpy of water vapor at temperature T [J/kg]

The energy accumulation in the gas phase is:

$$\frac{\partial}{\partial t}(\rho_a \varepsilon \delta x \tilde{h}_a(T,H)) \tag{6}$$

Combining Eqn. (3), (4), and (6) gives the enthalpy balance on air:

$$\frac{\vartheta}{\vartheta t}\left(\rho_a \varepsilon \delta x \tilde{h}_a(T,H) = G\tilde{h}_a\left(T(x,t),H(x,t)\right)\right)-$$
$$-\frac{\vartheta M}{\vartheta t}\rho_\rho \delta x(1-\varepsilon)h_v(\theta) - G\tilde{h}_a\left(T(x+\delta x,t),H(x+\delta x,t)\right)- \tag{7}$$
$$-Ua\delta x(T-\theta)$$

Dividing by δx and taking the limit as δx approaches zero, yields:

$$\rho_a \varepsilon\left(\frac{\delta h_a}{\delta T}+H\frac{\delta h_v}{\delta T}\right)\frac{\delta T}{\delta t}+\rho_a \varepsilon h_v(T)\frac{\vartheta H}{\delta t}=\rho_\rho(1-\varepsilon)h_v(\theta)-$$
$$-G\left(\frac{\vartheta h_a}{\vartheta T}+H\frac{\vartheta h_v}{\vartheta T}\right)\frac{\delta T}{\delta x}-Gh_v(T)\frac{\delta H}{\delta x}-Ua(T-\theta) \tag{8}$$

Where Eqn. (5) has been used to eliminate the wet air specific enthalpy.

Assuming constant heat capacities,

$$\frac{\delta h_a}{\delta T}=C_a \qquad \frac{\delta h_v}{\delta T}=C_v \tag{9}$$

Where:

G_a - specific heat capacity of dry air [J/kg°C]

C_v - specific heat capacity of water vapor [J/kg°C]

Combining Eqn. (2) with (8), and using Eqn. (9) to express

$$h_v(T)-h_v(\theta)=C_v(T-\theta) \tag{10}$$

finally gives:

$$\rho_a \varepsilon(C_a+HC_v)\frac{\vartheta T}{\delta t}=\frac{\vartheta M}{\vartheta t}\rho_\rho(1-\varepsilon)C_v(T-\theta)-$$
$$-G(C_a+HC_v)\frac{\vartheta T}{\vartheta x}-Ua(T-\theta) \tag{11}$$

2.1.3 *Energy balance on potato*

It is assumed that potato loses water vapor at its temperature θ. This yields the following equation:

$$\frac{\vartheta}{\vartheta t}\left(\rho_\rho(1-\varepsilon)\delta x\tilde{h}_p(\theta,M)\right)=\frac{\vartheta M}{\vartheta t}\rho_\rho(1-\varepsilon)\delta x h_v(\theta)+$$
$$+Ua(T-\theta)\delta x+Q\rho_\rho(1-\varepsilon)\delta x \tag{12}$$

Where :

$\tilde{h}_p$ - specific enthalpy of wet potato at temperature θ and moisture M [J/kg]

Q - heat generation rate (respiration) [J/kg]

Assuming that:

$$\tilde{h}_p(\theta,M)=h_\rho(\theta)+Mh_w(\theta) \tag{13}$$

Where:

h_p - specific enthalpy of dry potato [J/kg]

h_w - specific enthalpy of water absorbed on potato [J/kg]

Then Eqn. (12) can be written as:

$$\rho_\rho(1-\varepsilon)\left[\frac{\vartheta h_\rho}{\vartheta\theta}+M\frac{\vartheta h_w}{\vartheta\theta}\right]\frac{\vartheta\theta}{\vartheta t}+\rho_\rho(1-\varepsilon)h_w(\theta)\frac{\vartheta M}{\vartheta t}=$$
$$=\frac{\vartheta M}{\vartheta t}\rho_\rho(1-\varepsilon)h_v(\theta)+Ua(T-\theta)+Q\rho_\rho(1-\varepsilon) \tag{14}$$

Assuming constant heat capacities,

$$\frac{\vartheta h_\rho}{\vartheta\theta}=C_\rho \qquad \frac{\vartheta h_w}{\vartheta\theta}=C_w \tag{15}$$

Where :

C_p - specific heat of dry potato [J/kg°C]

C_w - specific heat of water [J/kg°C]

and noting that the heat desorption is:

$$\Delta H(\theta)\equiv h_v(\theta)-h_w(\theta) \tag{16}$$

gives:

$$\rho_\rho(1-\varepsilon)\left[C_\rho+MC_w\right]\frac{\vartheta\theta}{\vartheta t}=\frac{\vartheta M}{\vartheta t}\rho_\rho(1-\varepsilon)\Delta H+$$
$$+Ua(T-\theta)+Q\rho_\rho(1-\varepsilon) \tag{17}$$

2.1.4 *Drying rate equation*

The empirical drying rate equation is:

$$\frac{\vartheta M}{\vartheta t}=\frac{m_\rho}{\rho_\rho \%m_{dry}} \tag{18}$$

Where:

m_p - water evaporation rate of potato [kg/hm^3]

$\%m_{dry}$ - dry matter of potato

The water evaporation rate of potato is given by (Villa and Backer-Arkema (1974), Lerew (1978)):

$$m_\rho=-\frac{U_w D_{wa}}{r\delta U_D+D_{wa}}\gamma a(VPD) \tag{19}$$

Where:

U_w -.convective mass transfer coefficient [kg/Nh]

D_{wa} - molecular diffusivity of water vapor [m^2/h]

$r\delta$ - skin parameter [m]

U_D - convective mass transfer coefficient [m/h]

γ - fractional area which behaves as a permeable membrane

VPD - vapor pressure deficit [N/m^2]

The % dry matter of potato is given by (Burton (1966)):

$$\%m_{dry}=24.182+211.04\left(\frac{\rho_\rho}{\rho_w}-1.0988\right) \tag{20}$$

Where:

ρ_w - density of water [kg/m^3]

2.2 *Auxiliary equations*

A number of auxiliary equations are required in order to characterize various quantities appearing in the model equations.

2.2.1 *Heat generation rate (respiration) Q*

The model uses Misner and Shove's (1976) linear equation to compute the heat generation rate of potato in the temperature range 4.5 °C – 21 °C:

$$Q = 6.99\theta - 17.7 \quad (21)$$

2.2.2 *Convective heat transfer coefficient U*

The model uses Ophuis's (1957) equation to determine the overall convective heat transfer coefficient:

$$U = 20934 + 3.95v_a \quad (22)$$

2.2.3 Specific surface area a

The specific surface area is given by (Schumann (1929)):

$$a = \frac{A}{V}(1-\varepsilon) \quad (23)$$

Where:
A - average potato surface area [m^2]
V - average potato volume [m^3]

2.2.4 Heat of desorption of water ΔH

The heat desorption of water is given by (Gallaher (1951)):

$$DH = L(1.0 + a_1 e^{a2M}) \quad (24)$$

Where:
L - latent heat of vaporization [J/kg]
a1, a2 - coefficients

3. Summary

A mathematical model describing the heat and moisture transfer processes in a potato pile subject to forced ventilation has been developed for a one dimensional potato pile. The model is described by a set of nonlinear partial differential equations defined in the four variables: temperature of air, temperature of potato, absolute humidity of air and moisture content of air. The second step is to simulate the model equations using appropriate initial and boundary conditions.

Acknowledgement

This study was partially funded by the EU TEMPUS project S_JEP_09709_95. The autors are grateful to Professor Istvan Farkas for his support and to Dr Young Xu for his technical advice throughout this study.

References

1. BURTON W. G. (1966): The Potato. Second Edition. H. Veenman and Zonen N. V., Wageningen, Holland. GALLAHER G. L. (1951): A method of determining the latent heat of agricultural crops. J. Agric. Res. 21. pp. 263-272.
2. LEREW L. E. (1978): Development of a temperature-weight loss model fot bulk stored potatoes. PhD. theses, Michigen State University.
3. MISENER G. C. AND SHOVE G. C. (1976): Simulated cooling of potatoes. Trans. ASAE. 19. pp. 954-957, 961.
4. OPHUIS B. G. (1957): The effect of ventilation capacity on weight losses in ventilated potato stores. Netherlands Journal of Agricultural Science. 5. pp. 180-194.
5. SCHUMANN T. E. W. (1929): Heat transfer: A liquid flowing through a porous prism. Journal of Franklin Institute 208. pp. 405-416.
6. SUN Y., PANTELIDES C.C. AND CHALABI Z. S. (1995): Mathematical modelling and simulation of near-ambient grain drying. Computers and Elektronics in Agriculture 13. pp. 243-271.
7. VILLA L. G. AND BAKKER-ARKEMA F. W. (1974): Moisture losses from potatoes during storage. ASAE Paper No. 74-6510.

Contents of N° 10/1997

Contents of the "Mezőgazdasági Technika" periodical of the year 1997.

MEZŐGAZDASÁGI TECHNIKA
2100 GÖDÖLLŐ, TESSEDIK S.U.4.

N° 1.

N° 2.

N° 3.

N° 4.

N° 5.

N° 6.

N° 7.

N° 8.

N° 9.

N° 10.

N° 11.

N° 12.